Improved Diagnostics for Sleeping Sickness

Clemens Kremer

Submitted in fulfilment of the requirements for the degree of PhD

School of Engineering

College of Science and Engineering

University of Glasgow

August 2013

Abstract

The aim of this work was to explore an alternative to existing methods of detection for Human African Trypanosomiasis (also known as sleeping sickness). A new approach to diagnostics for sleeping sickness is needed, since the existing methods of detection employed in the field have significant shortcomings in terms of sensitivity, cost or ease of operation.

In this work, the enrichment of trypanosomes from blood using travelling electric fields and the selective lysis of cells using optoelectronic tweezers will be presented. Both techniques allow for the enrichment of trypanosomes from blood samples but the first is more suited for an application as a point-of-care device, while the latter is also applicable to other cell types and offers greater flexibility.

Besides demonstrating and quantifying the experimental results the work includes simulations to further explain the phenomena and investigate the underlying mechanisms.

The results presented here offer a new method to enrich trypanosomes, a central step in any potential diagnostic tool. They open up the possibility to develop a new solution to the challenges posed by sleeping sickness diagnostics and allow for miniaturisation and automation of the process.

Table of Contents

List of Figures

List of Tables

Acknowledgements

I would like to thank Prof. Jon Cooper for giving me the opportunity to pursue this interesting project. Despite being the busiest person I know, he managed to find time for me when I needed it. His supervision and guidance as well as his trust in me are much appreciated!

I would also like to thank Prof. Mike Barrett for co-supervising my work. He helped me find my way around the wonderful world of parasites. I have learned much, translating 'Engineer' into 'Biologist' and always enjoyed the discussions we had.

My sincere thanks go to the Kelvin Smith Scholarship, which funded my PhD.

I am grateful to the wonderful members of both the Cooper and the Barrett group for making me feel welcome in Glasgow and the invaluable help they have given me. I would like to especially thank Niall, Chris and Alasdair for their friendship.

I am grateful to both Steve and Anoop for their help with my work. Especially Anoop, who has been extremely supportive and helped me wrap my head around dielectrophoresis.

Last but not least, I would like to thank my family. My parents, without whom I would not have gotten to this point. My wife, for her love and support. Our son Jann, who was born shortly after we started our PhDs, and our daughter Johanna, who was born shortly before we finished them. You two are without a doubt our best experimental results!

Author's Declaration

All the work presented in this thesis, unless noted in the text, was conducted by the author. It has not previously been submitted for a degree or diploma at this university or any other institution.

Abbreviations

a:Si	Amorphous Silicon
AC	Alternating Current
CATT	Card Agglutination Test for Trypanosomiasis
CM	Clausius-Mossotti
CNS	Central Nervous System
DC	Direct Current
DEP	Dielectrophoresis
DIC	Differential Interference Contrast
F_{DEP}	Total Dielectrophoretic Force
F_{cDEP}	Component of the Dielectrophoretic Force
F_{twDEP}	Travelling Wave Component of the Dielectrophoretic Force
HAT	Human African Trypanosomiasis
ITO	Indium Tin Oxide
mAEC	Mini Anion Exchange Column
OET	Optoelectronic Tweezers
PBS	Phosphate Buffered Saline
QBC	Quantitative Buffy Coat
RBC	Red Blood Cell
T. brucei	*Trypanosoma brucei*
T. cyclops	*Trypanosoma cyclops*
TMP	Transmembrane Potential
TW-DEP	Travelling Wave Dielectrophoresis
VSG	Variant Surface Glycoprotein
WBC	White Blood Cell

Chapter 1: Theory and Background

1.0 Abstract

In this Chapter the theoretical framework for dielectrophoresis and electrically induced lysis will be discussed and a short literature review on these subjects presented.

1.1 Dielectrophoresis review of theory

Dielectrophoresis (DEP) describes the movement of particles in non-uniform electric fields. In this work, only the key equations will be presented and discussed, without the mathematical derivation. Several authors have provided an excellent literature on the subject [1-3] and the theory behind DEP and the reader is advised to seek them out for further understanding of the subject.

The central idea behind DEP is that an electric field induces a dipole in a particle which in turn interacts with the electric field. Because of spatial inhomogeneity of the electric field, a net force arises, which then moves that particle. This movement is directed along the gradient of the field and not along the field itself (see Figure 1-1). The movement will be either towards regions of high field (positive DEP) or away from regions of high field (negative DEP).

In this work the author will make use of an idea that is commonly employed to determine the governing equations for the dielectrophoretic forces, that of the effective dipole moment. It means in essence that a complex particle such as a cell, when interacting with an electric field, can be treated mathematically like a single dipole of a certain strength at a certain location. This idea is similar by analogy to using the centre of mass for calculation of the gravitational force acting on a particle. While determining the effective dipole moment has its limitations (when the inhomogeneity of the field is of similar order of magnitude as the particle, especially for particle-particle interactions), it is a valuable tool in determining valid, predictable results in many important cases.
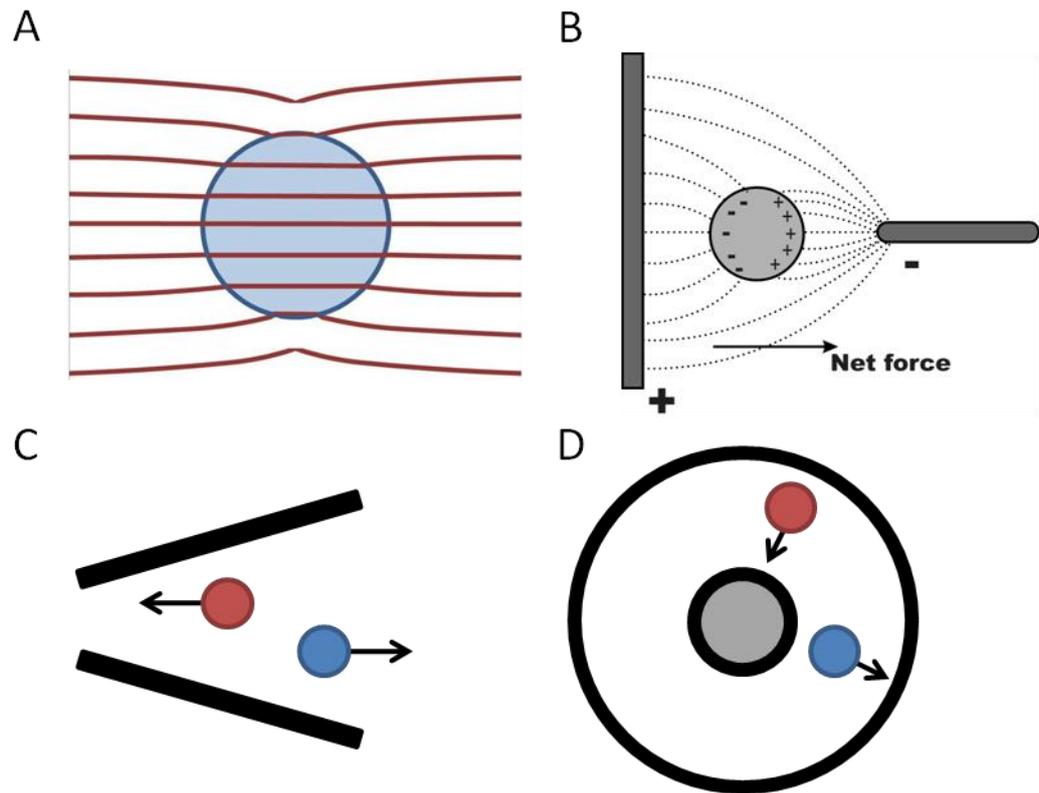
Figure 1-1: A) Spherical particle (blue) in an electric field (red lines). The field is created by parallel electrodes and is distorted locally by the presence of the cell (in this case the cell has a higher polarisability than the surrounding medium). The particle undergoes Maxwell Wagner polarisation. **B)** Spherical particle (with higher polarisability than the surrounding medium) in a non-uniform electric field. In this case the force acting on one end of the dipole is unequal to the force acting on the other end. Thus a net force arises, called the dielectrophoretic force (image modified from ref [1]). **C,D)** Examples of positive and negative DEP. Particles are represented as coloured circles (the direction of force is stated by the arrow) and electrodes as black lines (image recreated from ref [1]). **C)** Positive (red) and negative (blue) DEP forces on particles with the field lines being perpendicular to the gradient of the field. **D)** Positive (red) and negative (blue) DEP forces on particles with field lines being parallel to the field gradient.

The force acting on an infinitesimal dipole is given by [1]:

$$\bar{F}_{Dipole} = (\bar{p} \cdot \nabla)\bar{E} \qquad \text{[Eq. 1.1-1]}$$

Here F is the force, p the dipole moment and ∇E is the gradient of the electric field. This equation was derived (see e.g. [1]) by adding the forces acting on each charge of the dipole and performing a Taylor series expansion (which introduces the gradient), while ignoring second or higher order terms. Equation 1.1-1 already shows that the force is zero if the field is uniform. It should be noted that this equation only accounts for cases where the higher order terms can be ignored.

An important stepping stone in further determining the equations necessary to describe DEP is the effective dipole moment of a dielectric sphere in a dielectric medium (at a DC voltage). This is a common approach taken in the literature [1, 2]. Using the solutions for the potential inside and outside of the cell and the two boundary conditions (continuous electrostatic potential and continuous normal component of the displacement flux vector at the fluid-particle boundary) an expression for the effective dipole moment, p_{eff}, can be found as [1]:

$$\bar{P}_{eff} = 4\pi\varepsilon_m(CM)r^3\bar{E} \qquad \text{[Eq.1.1-2]}$$

Where ε_m is the permittivity of the medium, r is the radius of the particle and CM is the Clausius-Mossotti factor with ε_p being the permittivity of the particle.

$$CM(\varepsilon_m\varepsilon_p) = \frac{\varepsilon_p - \varepsilon_m}{\varepsilon_p + 2\varepsilon_m} \qquad \text{[Eq. 1.1-3]}$$

Permittivity is the intrinsic property of a particle or substance to polarise in the presence of an electric field. It is determined by the tendency of the atomic charges in the material to be distorted by said electric field and is a function of frequency.

It can be seen from Equation 1.1-2 and Equation 1.1-3 that the CM factor governs the direction of the effective dipole moment and limits the magnitude. The value of CM is thus limited by -0.5 ≤ CM ≤ 1.0 regardless of the values of the permittivity. A positive CM factor ($\varepsilon_p > \varepsilon_m$) means that P_{eff} is parallel to the electric field while a negative CM factor ($\varepsilon_p < \varepsilon_p$) indicates that the effective moment is antiparallel to the field.

In the case of a purely conducting sphere, in a conducting medium, a similar formula for the CM factor can be found:

$$CM(\sigma_m\sigma_p) = \frac{\sigma_p - \sigma_m}{\sigma_p + 2\sigma_m} \qquad \text{[Eq. 1.1-4]}$$

where σ_p and σ_m are the conductivity of the particle and the medium respectively.

In reality, a particle will usually be neither a pure dielectric nor a perfect conductor but will experience some form of loss instead. This loss (caused by energy dissipation mechanisms) will cause the dipole moment to experience a phase lag in a sinusoidal (AC) electrical field.

After assuming a sinusoidal electric field a simple phasor expression for the CM factor can be found as:

$$\underline{CM}\left(\underline{\varepsilon}_m\underline{\varepsilon}_p\right) = \frac{\underline{\varepsilon}_p - \underline{\varepsilon}_m}{\underline{\varepsilon}_p + 2\underline{\varepsilon}_m} \qquad \text{[Eq. 1.1-5]}$$

where the underlined quantities are complex. Complex permittivity is given by:

$$\underline{\varepsilon} = \varepsilon + \frac{\sigma}{j\omega} \qquad \text{[Eq. 1.1-6]}$$

The complex permittivity has two components which can be thought of as representing the two responses of the particle to the applied electric field. The first part is the instantaneous, permittive component that represents the forming and orientation of the dipoles of the atoms and or molecules in the medium. Meanwhile the second part represents the polarisation caused by the movement of atoms or molecules in the medium. This conductive part is not instantaneous and responds with a phase lag compared to the electric field.

When the permittive part dominates (that is, $|\varepsilon| \gg |\sigma/j\omega|$) Equation 1.1-5 naturally reverts to Equation 1.1-3. This is the case when σ is zero (which was our assumption for Equation 1.1-3, a pure dielectric) or when the frequency is very high. This is due to the fact that the ions can no longer respond to the field and are unable to move a significant distance before the polarity switches directions.

Equation 1.1-5 will consequently revert to Equation 1.1-4 in case the conductive part dominates ($|\varepsilon| \ll |\sigma/j\omega|$), since the frequency dependency is cancelled out of the equation. This limit corresponds to very low frequencies acting on the particle in question (the movement of ions becomes the dominating factor), agreeing with our assumption for Equation 1.1-4 of a DC field acting on a particle with finite conductivity.

It should be noted that the CM factor in these two cases (domination of the permittive or conductive part) is purely real. However for all circumstances in

between, the CM factor is a complex number. This complex number has both a magnitude and a phase, the latter of which describes the phase lag of the dipole with respect to the electric field.

In Equation 1.1-1 the only the part of the dipole moment that is in phase with the electric field will be contributing to the force. Consequently only the real part of the CM factor needs to be taken into account when calculating the DEP force. On the other hand, the imaginary part of the CM is responsible for the torque acting on the particle.

Combining Equations 1.1-1, 1.1-2 and 1.1-5 and taking the time average yields the Equation commonly used to describe traditional DEP:

$$\langle \bar{F}_{DEP}(t) \rangle = 2\pi\varepsilon_m r^3 RE\big[\underline{CM}(\omega)\big]\nabla\bar{E}_{rms}^2 \qquad \text{[Eq.1.1-7]}$$

where E_{rms} is the root mean square, ε_m is real (it is part of P_{eff} and not the CM factor) and r is the radius of the spherical particle.

As outlined above, the CM factor is a complex number, with the real part contributing to the DEP force. The CM factor is a function of frequency and can be plotted against frequency in order to gain a better understanding of the force response and the frequency regime required for separation of two different particles.

Figure 1-2 , taken from ref [2], shows both the real and imaginary part of the CM factor as a function of frequency. Figure 1-2 describes the case of a particle with lower conductivity and higher permittivity than the surrounding medium. The imaginary part is zero at the extreme high and low values of the frequency (the CM factor is completely real) and has a maximum value in between the two responses.
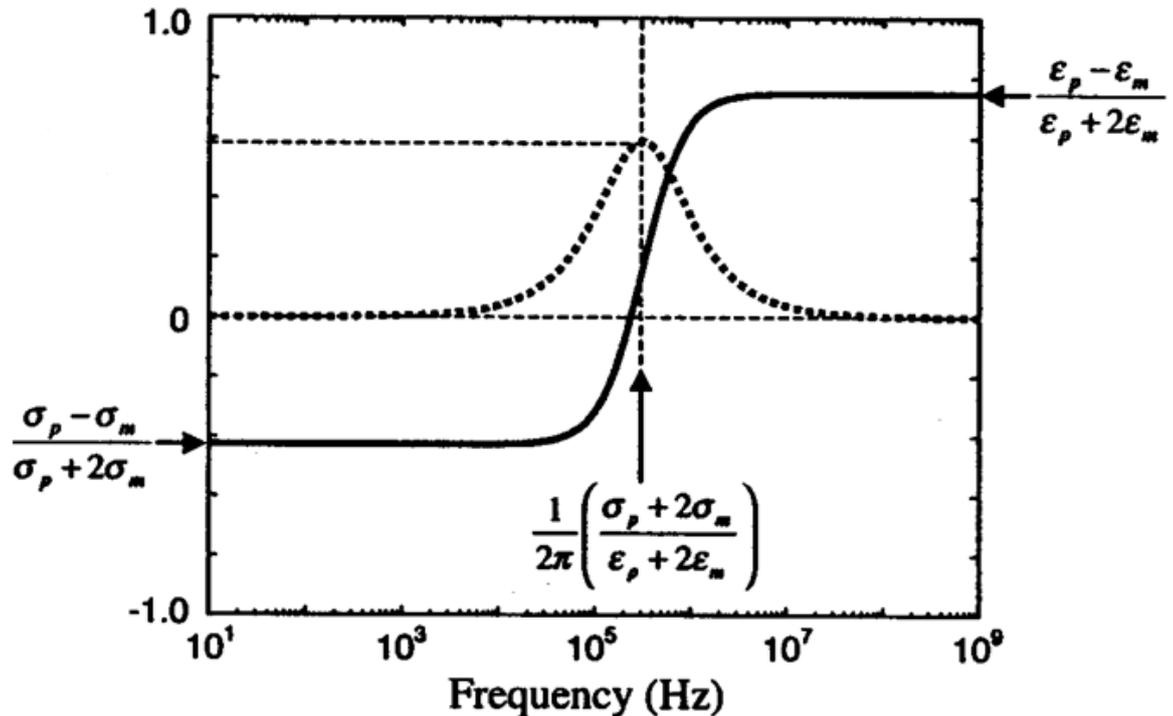
Figure 1-2: Real (solid line) and imaginary (dashed line) parts of the CM factor for a particle with $\sigma_p < \sigma_m$ and $\varepsilon_p > \varepsilon_m$ (image modified from ref [2]).

The Frequency where the real part of the CM factor is zero is called the crossover frequency and marks the point where no net force is acting on the particle. The sigmoid shape of the real part of the CM factor is only applicable for a spherical particle made up of a homogenous substance.

A homogenous sphere is, however, a poor model for a biological cell. The cell is formed by a lipid bilayer that acts as a near perfect insulator. As a consequence, a cell is often modelled as a sphere surrounded by a single shell with properties of the intracellular medium and the cell membrane respectively (e.g. [4]). In reality, cells have organelles and compartments and more complex (multi-shell) models have been developed (e.g. [5]). For a single shell, the additional interface causes the CM factor to take on an additional state (with the imaginary part now showing two peaks).

Further modifications to the CM factor need to be made if the particle in question shows a non-spherical geometry. An example of a model of the CM factor of an ellipsoidal cell is given in Figure 1-3. The exact details of the equation used for the CM factor for this model are detailed in Chapter Four.
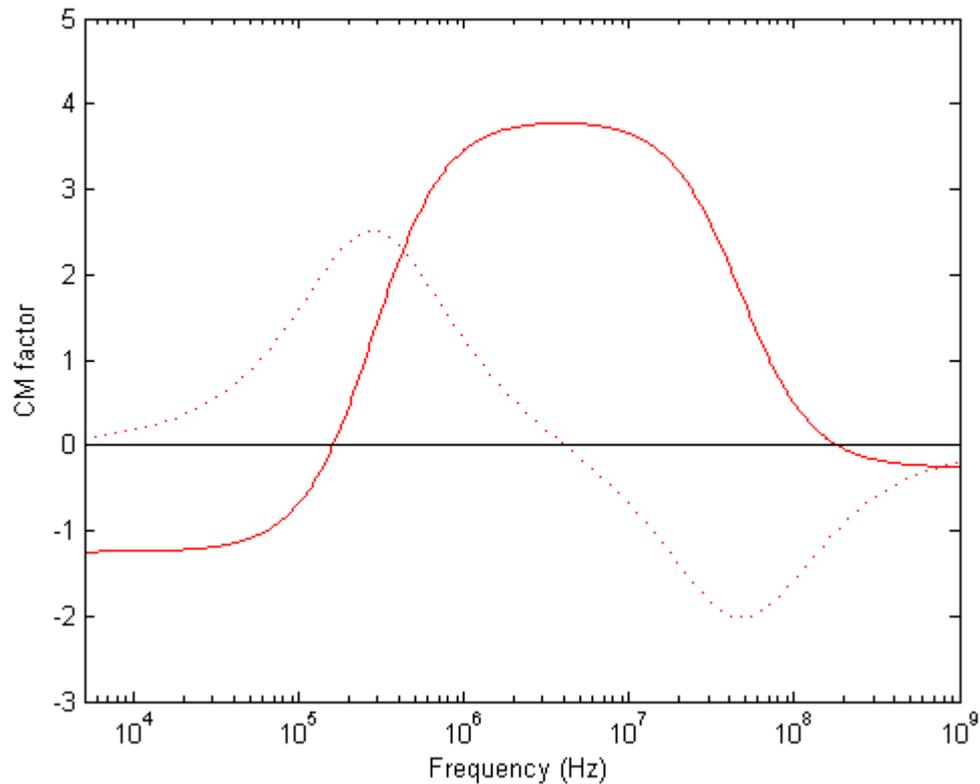
Figure 1-3: Example of the Clausius-Mossotti factor of an ellipsoidal cell model using a single shell to model the cell membrane. Solid line shows the real part and the dotted line shows the imaginary part of the CM factor. For details on this model (a red blood cell) see Chapter Four.

1.1.1 Travelling wave dielectrophoresis

Traditional DEP causes short displacements of particles toward or away from regions of high electric field. These high fields usually occur at the electrode edges and once a particle is at the edge of the electrode, or at a sufficient distance away from it, the movement caused by DEP will cease. However, an alternative mechanism for translational movement of particles over large distances can be achieved through the application of a travelling electric field [6]. This field is applied over a set of electrodes with a phase shift other than 180° between them. The most common such configuration is that of four electrodes and a phase shift of 90° from one to the next. The configuration bears similarities to that of four electrodes used for electrorotation.

Gascoyne and colleagues provided a unified theory that combines traditional DEP and TW-DEP into one set of formulae [7]. This approach will be used in this work to describe the forces acting on particles in TW-DEP devices. The applied AC

electric field exhibits a spatial phase and magnitude dependency, which can be described by:

$$E = E_{xo} \cos(\omega t + \varphi_x)\, i + E_{yo} \cos(\omega t + \varphi_y)\, j$$
$$+ E_{zo} \cos(\omega t + \varphi_z)\, k$$

[Eq. 1.1.1-1]

The dielectrophoresis (DEP) force comprises the sum of two components: F_{DEP} = F_{cDEP} + F_{twDEP}, the first component, is a result of the interaction of the in-phase component of the dipole moment with the field magnitude non-uniformity (F_{cDEP}); the second component is a result of the interaction of the out-of-phase dipole moment with the field phase non-uniformity. The dipole approximation of the DEP force can then be written as:

$$\bar{F}_{DEP} = \frac{1}{4} V \varepsilon_m Re(CM) \nabla \bar{E}^2 + \frac{1}{2} V \varepsilon_m Im(CM)(E_{xo}^2 \nabla \varphi_x$$
$$+ E_{yo}^2 \nabla \varphi_y + E_{zo}^2 \nabla \varphi_z)$$

[Eq. 1.1.1-2]

where the first and second terms correspond to F_{cDEP} and F_{twDEP} respectively and $V = \frac{4}{3}\pi abc$ is the volume of the ellipsoidal particle. The magnitude and direction of the DEP force is given by the CM factor and the electric field non-uniformities. (E_{xo}, E_{yo}, E_{zo}) and (φ_x, φ_x, φ_x) are the spatially dependant vector components of the field magnitude and phases respectively.

An important application of TW-DEP (especially in the context of this work) is the separation of two different species of cells or particles. This is usually (e.g. [8]) achieved by choosing a frequency regime where one particle is levitated above the electrode array (negative value of the real part of the CM factor) and experiences a non-zero force due to the phase gradient of the field (non-zero imaginary part of the CM factor), whilst at the same time the other cell experiences positive DEP. This causes one cell type to be moved up and out of the area where the travelling electric field is applied while the other cell type is trapped.
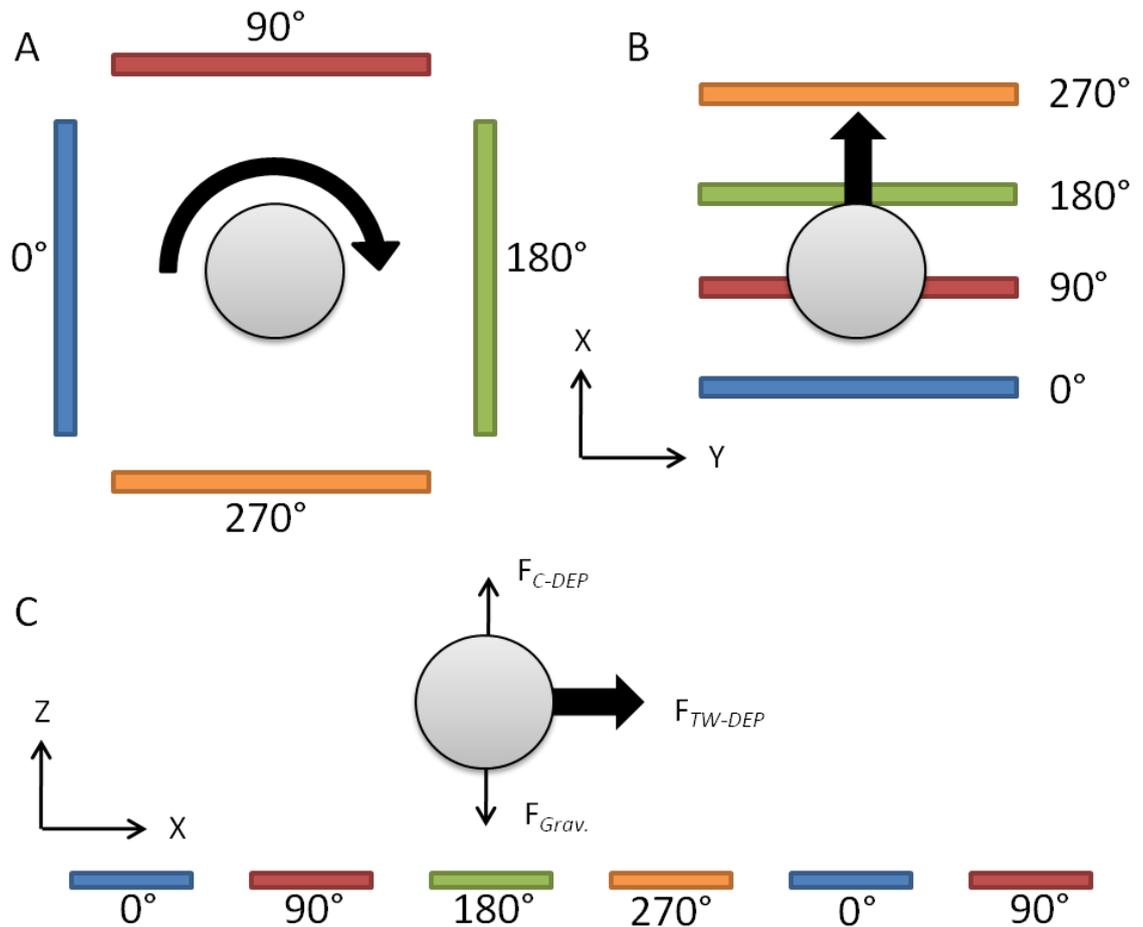
Figure 1-4: Cartoons illustrating travelling wave dielectrophoresis (TW-DEP). A) Electrorotation of a particle placed in the centre of four electrodes energised with a travelling electric field. As the field rotates around the particle, the particle will rotate as well according to the torque generated dipole moment. This torque is related to the imaginary part of the Clausius-Mossotti factor. B) TW-DEP caused by the travelling electric field of electrodes that are placed at the bottom of a chamber, while the particle is suspended above them. A) and B) represent a top-down view of the electrodes and particle. C) A side view of a particle suspended above a set of electrodes, energised to create a travelling electric field. The particle is levitated off the electrodes by conventional (negative) DEP. The TW-DEP component of the force moves the particle along the phase gradient of the field (its direction is given by the imaginary part of the CM factor).

Of special interest for this work is the special case of bidirectional TW-DEP, which refers to the simultaneous movement of two types of particles in opposing directions. This can usually not be achieved by a single travelling electric field on a single set of electrodes. Frequency regimes where both cells experience negative DEP will have F_{twDEP} pointing in the same direction for both species.

Bidirectional TW-DEP is useful, since it allows the simultaneous concentration of the agent of interest while removing unwanted cells. While such a feat is obviously possible through other means, bidirectional TW-DEP allows for a convenient way to achieve this on small devices.

1.1.2 Optoelectronic tweezers

In order to utilize DEP it is necessary to generate non-uniform electric fields in a chamber or channel where they can interact with the suspended cells. This is traditionally achieved using metal electrodes patterned on glass. These electrodes can be arranged in many different ways to generate non-uniformities of the applied field (e.g. interdigitated electrodes [9]).

A second way to generate a non-uniform electric field is to use a photoconductive layer on top of a conducting layer. The photoconductor increases in conductivity (by several orders of magnitude) when exposed to light. Consequently, the area that is exposed will act as a 'virtual electrode' and cause the formation of a field with a spatial gradient (see Figure 1-5). A common material to use as a photoconductor is amorphous silicon (a:Si).
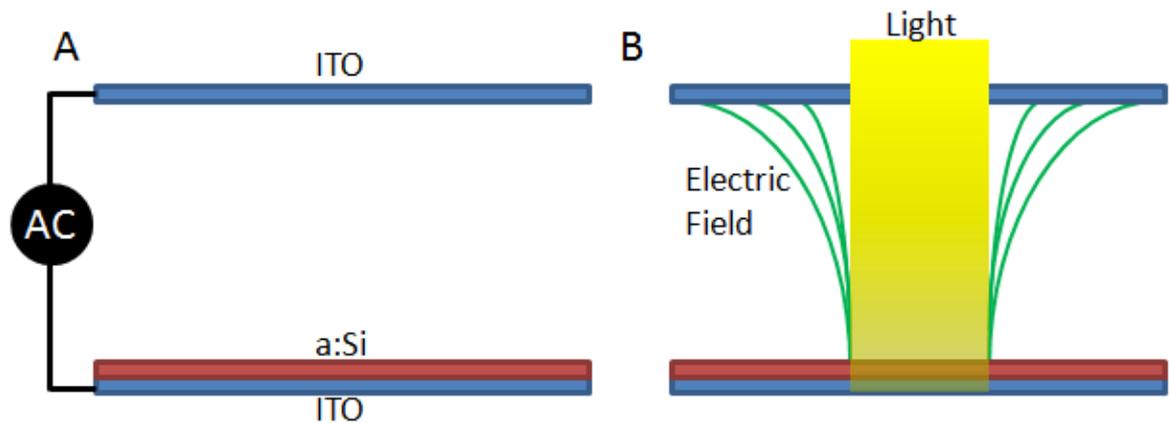
Figure 1-5: Cartoon depicting the working principle of optoelectronic tweezers (OET). A) 'Dark state' with no light being applied to the setup. The two electrodes (composed of indium tin oxide (ITO) patterned on glass) are connected to a function generator and the bottom electrode is also covered by a layer of amorphous silicon. B) 'Light state' with the layer of a:Si being illuminated. The photoconductor reduces in resistance by several orders of magnitude and creates a virtual electrode. This creates a non uniform electric field in the medium between the two electrodes (green lines).

This technique (commonly referred to as optoelectronic tweezers or OET) offers great flexibility for particle manipulations as the electrodes themselves can be rearranged on the fly [10]. The important difference to traditional electrodes is the additional layer of dielectric material. Depending on the configuration, this layer of a:Si is usually between 300 nm and 1 µm. Even in the 'light state' the amorphous silicon has a much higher resistance than metal electrodes and a significant portion of the applied potential is dropped across the a:Si layer. This

effect becomes even more pronounced with high conductivity media, preventing the generation of dielectrophoretic forces of meaningful magnitude.

1.2 Dielectrophoresis review of literature

The term dielectrophoresis was first used by Pohl [11] in 1951 and the technique has since found many applications for diagnostics, biophysics and biomedical sciences. As pointed out above, cells will either undergo negative or positive DEP. The individual response of a particle or biological cell will depend on its dielectric properties. These properties are a function of its shape, size and the effective permittivity. In the case of cells the morphology and composition of the lipid bilayer can affect this permittivity and for fields of high frequency the internal make up of the cell is of importance as well. This then allows for the separation of different cells based on their dielectric properties. Since differential forces can be generated on different cell species without the need to apply markers or to alter the cells in some other way, this a valuable tool for diagnostics. Biological cells can be concentrated, patterned or their biophysical properties can be investigated.

As R. Pethig pointed out in his review article [12], in the time span between the years 2000 and 2010 around 2000 publications have been published addressing the theory, technology or application of dielectrophoresis. Only a few examples of different applications of DEP are mentioned here: Kim *et al.* (2007) used DEP for fractionation of human breast carcinoma cells based on the cell cycle phase [13]; Ho *et al.* (2006) achieved the patterning of liver cells and endothelial cells using DEP traps in a microfluidic chip [14]; Vykoukal *et al.* (2008) demonstrated the enrichment of putative stem cells from adipose tissue using DEP field-flow-fractionation [15]; Labeed *et al.* (2003) used DEP for the evaluation of multi-drug resistance in leukemic cells [16].

Of greater interest for this work is the literature regarding travelling wave dielectrophoresis. In 1992 Hagedorn and colleagues [6] were the first to describe translational movement of particles (pollen) over large distances due to the application of a travelling electric field. The electrode array used in their experiment to create the field was a linear design, which requires complex fabrication techniques as electrodes need to be layered on top of each other. A

simpler two dimensional solution is presented by the introduction of a spiral array for TW-DEP. Wang *et al.* (1997) were the first to describe the use of a spiral for TW-DEP (in their case to enrich breast cancer cells) and analyse the force generated in such a setup [17]. Later that same year Goater *et al.* used a spiral array to concentrate parasites (*Cryptosporidium parvum* oocyst) and determine their viability through electrorotation [18]. Another important demonstration of the applicability of spiral based TW-DEP for the diagnosis of infection was the isolation of erythrocytes infected with malaria from normal red blood cells by Gascoyne et al. (2002) [8].

However none of these approaches implemented bidirectional movement of particles. Pethig and colleagues (2003) were the first to report bidirectional TW-DEP through the superposition of two electric signals over the same set of electrodes [19]. The electrode array used here however was a linear track rather than a spiral design. Other approaches include the use of two sets of electrodes (one on the bottom and one at the top of the chamber) by Huang *et al.* (2008) to generate bidirectional movement [20].

The optoelectronic tweezers (OET) technique was first demonstrated by Chiou *et al.* (2005) [10]. In this pioneering work Chiou and colleagues demonstrated the impressive flexibility of the technique for both single cellular and massive parallel (15,000 particle traps were created on a 1.3 mm X 1.0 mm area) manipulation of cells. The limitation of low conductivity media was addressed by Hsu *et al.* (2009) through the use of phototransistor based OET, to increase the photo conductivity [21].

Of special interest for this work is the use of OET as a tool for electroporation and electrically induced lysis. The relevant literature will be discussed below (see 1.4).

1.3 Electrically induced lysis review of theory

Healthy mammalian cells are surrounded by a membrane consisting of a lipid bilayer with embedded proteins [22]. There has been a longstanding interest in manipulating the cell membrane in order to introduce molecules into the intracellular medium or to lyse the cell. Poration of the membrane causes holes

to form through which materials can be inserted into the cell (e.g. transfection). Lysis describes the irreversible disruption of the cell membrane which causes the cell to die as intracellular medium diffuses out of the cell.

Electrically induced lysis is thought to be triggered because the transmembrane potential (TMP) reaches a potential threshold value and pores form that then merge or increase in size and cause the irreversible breakdown of the lipid bilayer [23-25], although the exact process is still not fully understood. Any cell has an electric potential across its cell membrane due to the unbalanced ion concentrations in the intra- and extracellular medium. In an average healthy cell this value will be some tens of mV [22]. When the cell is exposed to an external electric field however, this TMP will increase because negative and positive charges accumulate at the inner and outer interface of the membrane [26]. The induced TMP is not evenly distributed over the cell surface because this accumulation mainly takes place at areas of the membrane closest to the electrodes.

For an AC bias acting on a spherical cell in a homogeneous electric field the TMP is given by the Schwan equation [27]:

$$\Delta V = 1.5 r E \frac{cos\theta}{\sqrt{(1 + (\omega\tau)^2)}} \qquad \text{[Eq. 1.3-1]}$$

where ΔV is the induced transmembrane potential, r is the radius of the cell, E is the electric field strength, θ is the angle between the normal vector protruding from the cell membrane at the point of interest and the electric field and ω is the angular frequency of the applied bias ($\omega = 2\pi f$). The relaxation time of the membrane τ can be written as:

$$\tau = r C_{mem} \left(\frac{\rho_{int} + \rho_{ext}}{2} \right) \qquad \text{[Eq. 1.3-2]}$$

Where C_{mem} is the capacitance of the membrane and ρ_{int} and ρ_{ext} are the resistivities of the internal and external medium respectively. Equation 1.3-1 is only valid given the restrictions outlined in [27], specifically a conductivity of the surrounding medium that is significantly less than the intracellular medium.

Once the TMP reaches a certain value, pores begin to form in the bi-layer and at lower voltages this process is still reversible [25]. This is commonly referred to

as electroporation and has many uses, such as transfection, drug delivery and gene therapy [28]. If however the voltage is too high (~1 V) [29], the damage to the membrane is irreversible and the cells lyse. The intracellular medium diffuses out of the cell and it is no longer viable.

In general, the cells to be lysed are placed in a uniform electric field or at least the electric field is produced by conductors (electrodes) that are in direct contact with the medium that contains the cells. In this case, the total voltage drop across the cell (and thus the TMP) is directly correlated to the total size of the cell or rather its size with respect to the direction of the field (see Figure 1-6). If no cell is present, the voltage drop across the liquid is linear while placement of a cell causes a deformation of the electric field (and consequently a difference in the voltage distribution). Since the membrane has a very low conductivity (high impedance at low frequencies) when compared to the interior or exterior of the cell, most of the voltage variation occurs across this thin coat [30]. The membrane acts as a shielding layer and the voltage across the inside of the cell remains constant. This means that a large voltage drop will occur across the membrane. The larger the applied total voltage and the larger the size of the cell, the larger the voltage drop will be. Since larger cells experience a higher TMP, they are lysed at lower voltages than smaller cells.
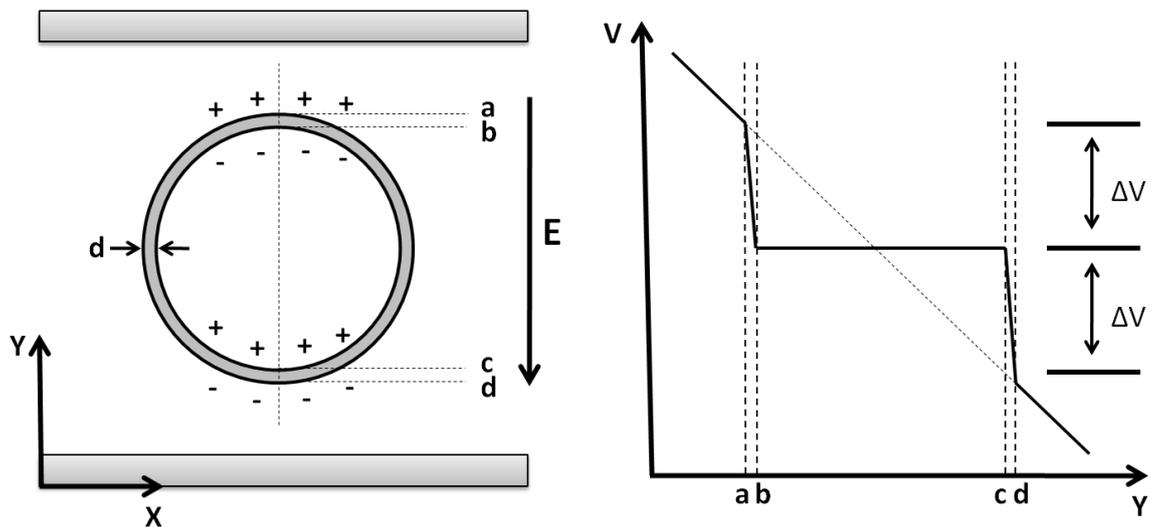
Figure 1-6: Diagram of a spherical cell between two parallel electrodes (left) and the voltage plotted against distance (right). The voltage is plotted along the dotted line on the left, through the middle of the cell. The voltage drop would be linear if no cell were present (dotted line on the right). The induced transmembrane potential is given as ΔV and it can be seen that a greater total voltage drop or a larger cell would lead to increased potentials across the membrane.

An important property of the cell membrane is its capacitance in applied electric fields. As already stated, it presents a high resistance (near perfect insulator) for fields of low frequency while for fields of higher frequency the resistance decreases. Figure 1-7 shows a COMSOL simulation of electric fields "going around" a cell at low frequencies and through the cell membrane at higher frequencies (as the internal conductivity is higher than the surrounding medium). In this case the cell is placed at an equal distance from each electrode and the applied electric field is uniform (for details see figure legend).
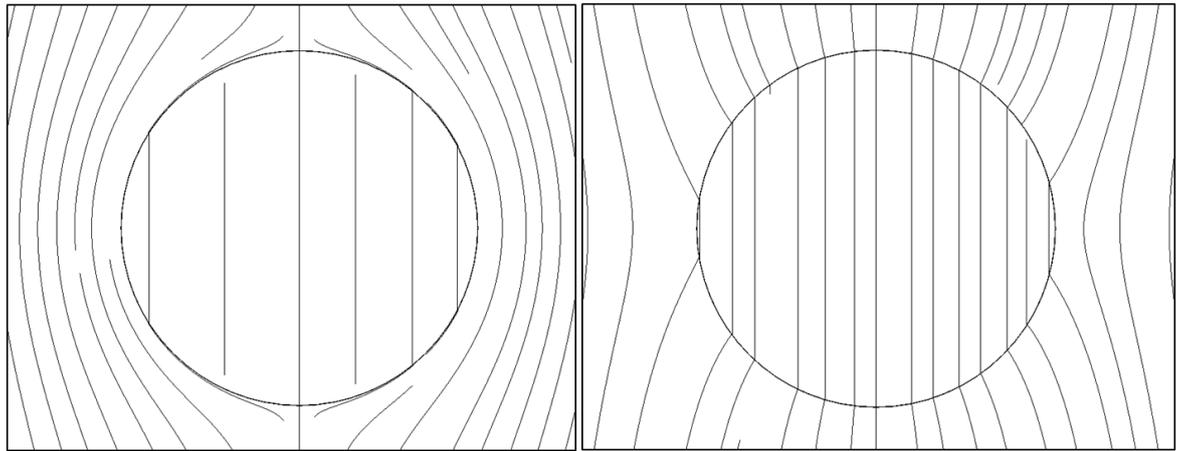
Figure 1-7: COMSOL simulation depicting the ability of the cell membrane to act as an insulator at low frequency (10 KHz) (left) and how it loses this ability at higher frequency (100 KHz) (right). Conditions used for the model included 10 nm thick membrane, 10 μm diameter of the cell, total chamber height 100 μm and medium conductivity of 100 mS/m.

1.4 Electrically induced lysis review of literature

As one would imagine a subject as widespread and well studied as cellular lysis has a very large and diverse body of literature to offer. Since this work is only concerned with electrically induced lysis only a few recent examples are given of the other physical ways that are used to break down cell membranes.

Mahalanabis et al. (2009) demonstrated the chemical lysis of bacteria from blood to extract their DNA [31]. Vandeventer et al. (2011) achieved the same goal but used mechanical disruption to lyse thick walled cells (*Bacillus* spores and *Mycobacterium* cells), that are otherwise resistant to disruption [32]. Another approach (of which an example is given below) is to utilise osmotic pressure to lyse cells.

Selective lysis describes the lysis of certain cell species while retaining the integrity of other cells. This may be used to enrich cells (remove unwanted cells

from a sample), improving the outcome of polymerase chain reactions by washing away unwanted DNA from lysed cells and to enable detection of rare cells.

Selective lysis can be achieved for bulk solutions with agents (e.g. antibodies [33]) that target certain cell types. Recently, promising results have been published by Nederberg *et al*. (2011) presenting selective lysis of microbes using nanoparticles [34]. An interesting publication about selective lysis is the 2007 paper by Parekkadan *et al*. in which the authors used osmotic pressure to selectively lyse red blood cells and thus enrich stem cells from umbilical cord blood [35].

Another approach is to lyse cells individually. This has been achieved recently though electrical lysis induced by micropipette electrodes [36], using lasers [37] or by using optoelectronic tweezers. OET was first used by Valley *et al*. (2009) for electroporation and lysis [38]. Since then other authors have demonstrated electrical lysis using the technique [39].

In 1965 Hans Coster discovered the reversible electrical breakdown of cell membranes (which he termed 'punch-through') at a certain well defined electrical potential [40]. A good summary of the phenomenon and its discovery can be found in the 2009 tribute written by Coster himself [41]. The exact explanation of what is happening at a molecular level during electroporation is still subject to debate (e.g. see [24]).

One of the first to develop a mathematical framework for the electrically induced lysis process was H. P. Schwan [27, 42, 43] who established equations to calculate the transmembrane potential for both DC pulses and AC bias. This set of equations has been expended upon by later authors, for example by J. Gimsa to include ellipsoidal particles [44]. These approaches however rely on a uniform electric field for their calculations.

When dealing with irregularly shaped cells or non-uniform electric fields, numerical modelling is usually applied to gain a better understanding of the problem. For example Pucihar *et at*. (2009) used a finite element model to calculate time-dependent changes in the induced TMP of an irregularly shaped cell [26].

Chapter 2: The Problem

2.0 Abstract

This Chapter contains an overview of sleeping sickness and the burden it presents as well as a review of the current methods of detection used in the field. The Chapter closes with a summary of the motivation for this work.

2.1 Sleeping sickness

Human African trypanosomiasis (HAT) is a deadly disease found in sub-Saharan Africa. It is caused by the single cellular parasite, *Trypanosoma brucei*, which infects a human blood stream through the bite of the Tsetse fly [45-48]. Once infected the parasite proliferates asexually in the bloodstream of the host and remains extracellular. This first stage of the disease has only mild symptoms and the infection is often not recognized. After a long incubation period (months or years) the parasite enters the central nervous system (CNS) of the host and causes a number of serious symptoms through inflammations in the CNS. This second stage of the disease is always fatal if not treated.

There have been three major epidemics of sleeping sickness in the last century [49]. The first one (around the turn of the century) was mainly restricted to central Africa and killed nearly 800,000 people. The second one emerged during the 1930s and caused the colonial powers at the time to initiate large scale screening and treatment programmes. These two epidemics also prompted the colonial powers to seek medication for sleeping sickness. Most of the drugs used today were invented during the first half of the last century [49, 50]. Suramin (the drug commonly used to treat stage 1 infection) was developed in 1916 and Melarsoprol (still used for stage 2 infection, despite causing fatal reactions in up to 10% of the patients) in 1949. These continued control measures caused the disease to be nearly extinct during the 1960s but decolonization of most African nations and the following unrest caused monitoring programs to slip [51]. As a consequence HAT re-emerged and peaked again during the 1990s with ~37,000 new reported cases in 1997 (25,000 of which were from the Republic of Congo) [52]. Through political cooperation and help from non-governmental organisations (NGOs) the control and treatment of HAT was intensified again, and the number of cases reduced drastically. In 2010 the total number of new

reported cases was 6631 of which 5595 were from the Republic of Congo [52]. These encouraging numbers have led the WHO to announce a target for elimination of the disease in 2020 [53].
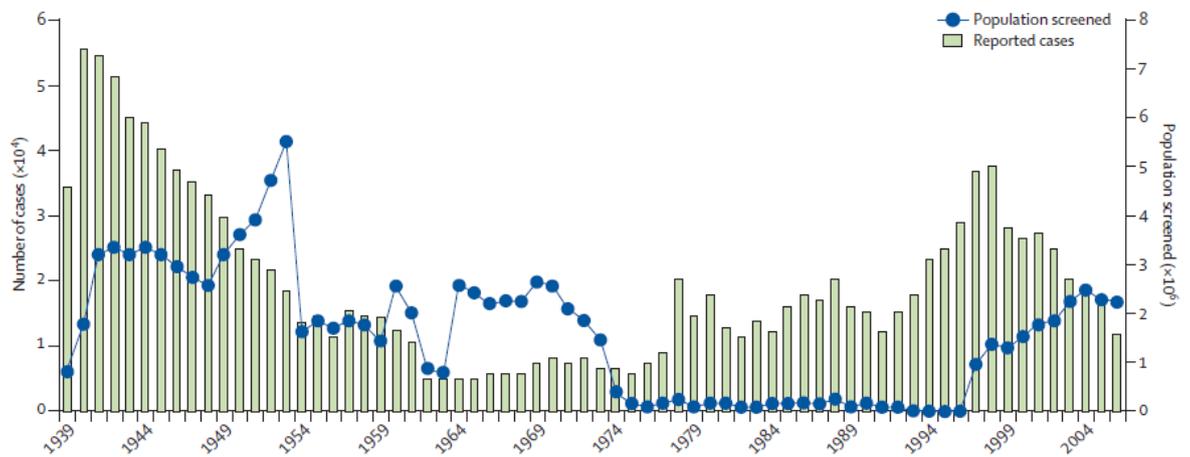
Figure 2-1: New reported cases per year and number of screened people for HAT (image modified from ref [46]). The disease was nearly eradicated during the 1960s but a break in the screening program resulted in the resurgence of the disease in the following years. In 2009 the number of reported cases dropped below 10,000 for the first time in 50 years due to the reinstatement of successful control measures.

It should be noted however that this target can only be achieved if control of the disease is kept up and not relaxed, least the disease return again. The actual number of cases is much higher than the reported new cases per year. In 1998 the WHO estimated [53] that while the number of reported cases was ~40,000 the actual number of cases was about 300,000. For 2010 the WHO estimated [53] the number of actual cases at about 30,000.

2.2 Trypanosomes

The trypanosome is a single cellular protozoan parasite. It has a typical length of 15 to 30 μm and is usually motile through the use of a flagellum. Of the species *Trypanosoma brucei* (*T. b.*), there are three subspecies [54], *T. b. brucei, T. b. rhodiense* and *T. b. gambiense,* the latter two being infectious to humans. Human blood contains a trypanosome lytic factor (TLF) which is able to destroy *Trypanosoma brucei* in the blood stream [55]. The two types of trypanosomes that are infectious to humans are able to resist this TLF. *T. b. gambiense* is responsible for over 95% of the reported cases of sleeping sickness [53]. This is due to the fact that the parasite is much better adapted to the human immune

system. While infection with *T. b. gambiense* is chronic and can last for years [56], giving the parasite ample time to spread to new hosts, infection with *T. b. rhodiense* is acute and only last weeks or months. The two subspecies are separated geographically [57], with *T. b. gambiense* only being present in western and southern parts of Africa. Another difference between the two is that *T. b. gambiense* is chiefly transmitted from person to person (via a tsetse fly). While it is possible for wild animals to act as reservoirs, this is rare [58]. On the contrary, *T. b. rhodiense* has large reservoirs in cattle and infections from animal to humans are frequent [59]. In this work the terms trypanosome and parasite will only refer to *T. b. gambiense* and West African sleeping sickness, although experiments were carried out with *T. b. brucei* (*T. cyclops* in some cases) which is considered non infectious to humans.

Trypanosomes are transmitted to humans through the bite of the blood-feeding tsetse fly (genus *Glossina*). The fly takes up trypanosomes when acquiring a blood meal from an infected host [60]. The parasite then travels from the mid-gut of the fly to the salivary glands from where it can infect a healthy human when the fly feeds again. This process takes three to five weeks, which is close to the life span of the fly. Only a very old tsetse fly that was infected at a young age can transmit the disease. This is rare and only 0.1% of a tsetse population are actually infectious [46, 60]. During its life cycle, the parasite undergoes several transformations [45]. The bloodstream form of trypanosomes is able to proliferate through binary fission and is well adapted to the human blood stream. It is however unable to survive in the gut of a tsetse fly. Therefore some of the parasites (a small part of the total population) change into a smaller 'stumpy' form which is unable to reproduce, but is pre-adapted to the environment inside the fly. Only these parasites will survive after being taken up in a blood meal. A similar process takes place in the fly where the parasite has to change forms to adapt to the environment in the salivary glands and some of the parasites change into a form that is pre-adapted to the human blood stream (but unable to proliferate in the fly) [61]. While in the human blood stream the parasite will eventually enter the central nervous system [62] and cause the severe neurological symptoms that gave the disease its name, and ultimately lead to the demise of the patient.
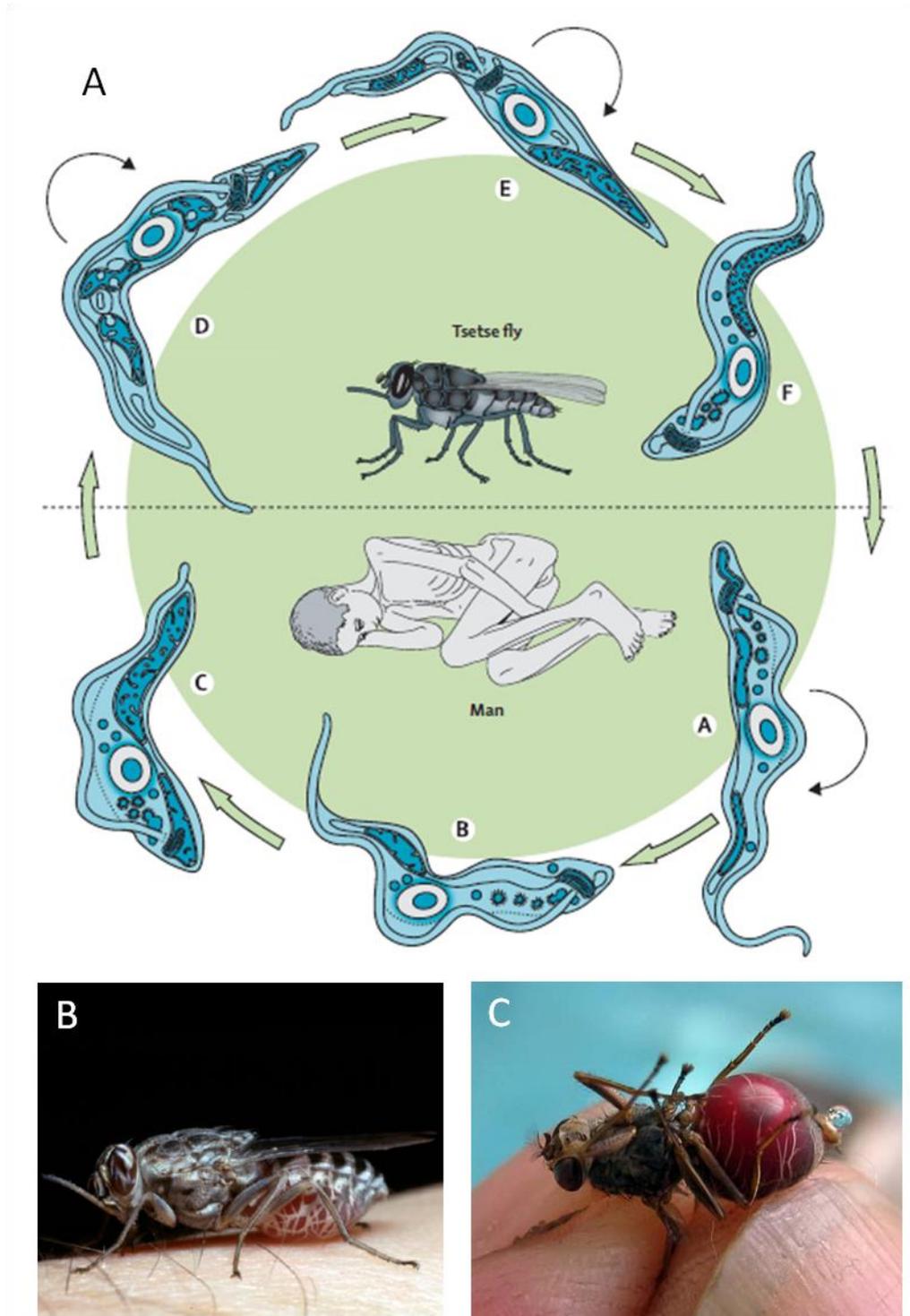
Figure 2-2: Life cycle of *T. brucei*, Tsetse fly as vector. A) Life cycle of the *T. brucei* parasite (image modified from ref [46]). The parasite features different forms in the human host and insect vector. Stages marked with a black arrow (a,d,e) are capable of reproduction through division. Sexual reproduction is thought to happen solely in the insect vector. In the human host a portion of the trypanosomes in the reproductive stage (a) change (though an intermediate stage (b)) into a form that is pre-adapted to the tsetse fly (c). After take up, during a blood meal, the parasites have to migrate from the midgut to the saliva glands (d-e). There a reproductive form (e) and a form partly adapted to the human bloodstream (f) coexist. Only the latter is able to survive injection into the human bloodstream after a bloodmeal. B) Tsetse fly (*Glossina morsitans*) during bloodmeal, a proboscis penetrates the skin and initiates feeding (image modified from ref [63]). C) Well fed Tsetse fly, weight can double due to the amount of blood taken during a meal (image modified from ref [64]).

2.3 Variant surface glycoprotein

T. brucei exists in the human bloodstream as an extracellular parasite. As such, it is constantly exposed to the body's immune response. The fact that the parasite can persist in the human body for years is a testament to its extreme level of adaptation. The key to ensuring the parasites survival in the human body is the so-called variant surface glycoprotein (VSG) [65, 66].

Glycoproteins are proteins with one or several covalently bound sugar groups. While they fulfil many functions in mammalian bodies, glycoproteins are often integrated into the cell membrane where they are involved in cell to cell interaction.

T. brucei (and in fact all trypanosomes) has developed a special defence mechanism using these glycoproteins. The surface of the parasite is covered in $\sim 10^7$ identical glycoproteins that enclose the trypanosome like a suit of armour. This dense, forest like network protects the membrane from contact with the immune system. What is more, only the part of the glycoprotein that is embedded in the membrane is conserved, the N-terminal part of the protein is variable, hence the name variable surface glycoprotein. The VSG, while homogenous for any given parasite, can vary greatly from one trypanosome to the next. Every 100 cell divisions one or both of the daughter cells will carry a completely new surface coating. The stochastic process by which this variance occurs (a combination of 200 active genes and about 1000 inactive ones) allows for near infinite variability.
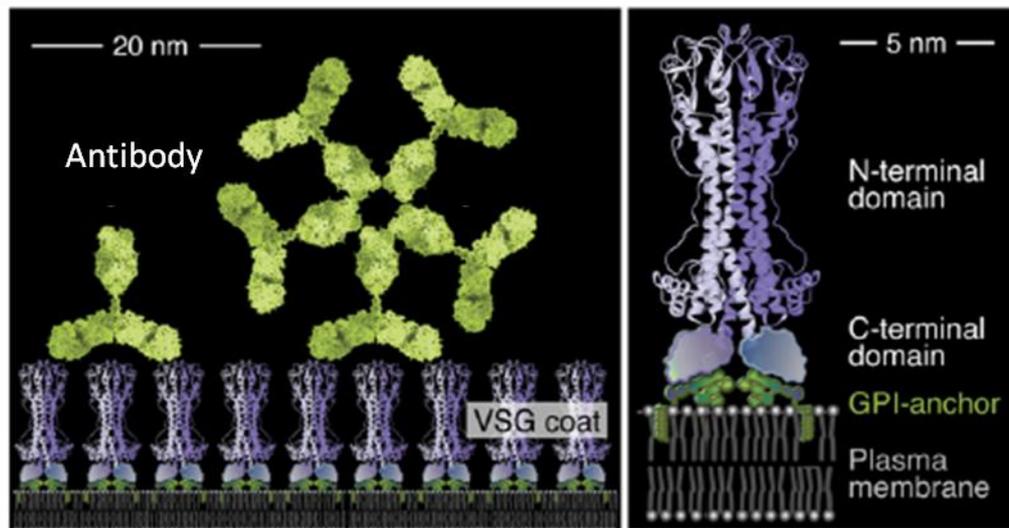
Figure 2-3: Variant surface glycoprotein coating of trypanosomes (image modified from ref [67]). The variable N-terminal end of the protein protrudes into the extracellular medium, attached to an anchor that is embedded in the membrane. The coating covers the entire surface of the trypanosome and antibodies can only bind to the variable part of the glycoprotein.

In the time it takes the immune system to produce specific antibodies for the currently prevalent VSG in a trypanosome population, one or several new sub-populations with a different VSG will have emerged. While the immune response is killing the trypanosomes with the old surface coating the numbers of the new population increase, until the process repeats itself again. This continued evasion of the immune system has several implications for the disease and the diagnostics needed to detect it [65].

Firstly the number of trypanosomes will change periodically. For *T. b. gambiense* the number of trypanosomes in a millilitre of blood varies from 10^2 to 10^4 parasites. This number is very low compared to the number of blood cells in the same volume (approximately 10^9). The low numbers allow the human body to cope well with infection and there are only few, unspecific symptoms [47]. This means that the host is often unaware of the infection during the chronic first stage of disease. Meanwhile it is at this first stage that treatment should ideally be administered.

The excellent evasive qualities of the VSG also result in the high rate of mortality of the disease. Sleeping sickness is always fatal when not treated because the parasite has unlimited time to eventually cross over the blood brain barrier. The exact mechanism of how this occurs is not fully understood, but it

takes a long time (months to years) for the parasite to achieve [62]. The VSG ensures the trypanosome has all the time it needs in the hosts bloodstream.

A more direct consequence of the presence of the VSG is the inability to use antibody based testing for diagnostic purposes [68] (although it can be used for screening). Antibodies are a powerful tool in diagnostics but can only ever be specific to one glycoprotein. Since the VSG shields all other parts of the membrane from contact it is necessary to detect the parasite by other means, and currently optical detection is the only reliable option.

2.4 Current methods of detection

Diagnostics of human African trypanosomiasis (HAT) involves three necessary steps: screening, confirmation and staging. Cheap and sensitive screening tools are important to ensure successful control programs for HAT, especially considering the continued suppression of outbreaks and eventual eradication of the disease [69]. Screening has to be followed by diagnostic confirmation of the parasite in the human blood stream, lymph nodes or cerebrospinal fluid. It is estimated that the standard diagnostic tests used at the moment miss about 20% to 30% of infected patients [51]. Staging is a vital final step to choose correct treatment and medication for the infected individual. Diagnostics are further hindered by non-attendance to screening or necessary recurring treatment. Lack of knowledge of infected individuals contributes to these issues. A 2008 study in the Republic of Congo showed for example, that 40% of patients attributed their HAT infection to supernatural sources like sorcery or transgression of rules [70].

2.4.1 Screening – clinical features

Clinical features are only a poor indicator for infection. The site of the insect bite sometimes presents an ulcer (called a chacre), but even if this symptom is present it disappears after a few weeks without the need for treatment. During the first stage of infection signs are non-specific such as fever, headaches or fatigue. The so-called Winterbottom's sign describes a painless swelling of a lymph node in the neck of the patient. It was described by Sir Thomas Masterman Winterbottom in 1803, when he noticed that slave traders used neck

swelling to identify slaves that showed sleepiness or abnormal behaviour (making them undesirable). However, Winterbottom's sign is absent in up to 50% of patients and is not specific for sleeping sickness.

Figure 2-4: Possible clinical features of sleeping sickness infection (images modified from ref [45]). A) Parasitical chacre at site of insect bite. B) Winterbottom's sign.

Once the disease moves to the second stage and the parasite enters the central nervous system (CNS) the clinical signs become more pronounced but are very variable from patient to patient. Below is a summary taken from Chappuis *et al.* [51] :

> "The clinical features can be grouped into categories such as psychiatric, motor, sensory, and sleep abnormalities. The mental disturbance may include irritability, lassitude, headache, personality change, and overt psychiatric presentations such as psychosis. Pyramidal (e.g., focal paralysis), extrapyramidal (e.g., rigidity and tremor), and cerebellar (e.g., dysarthria and ataxia) disorders are common. Delayed and increased sensation to pain (Kerandel's sign) can also be noted. Reversal of the normal sleep-wake cycle, with daytime somnolence alternating with nocturnal insomnia, is typical. Weight loss and endocrine abnormalities such as amenorrhea and impotence are also frequent complaints. If left untreated, patients ultimately die from the consequences of severe wasting, dysfunction of the immune system, deep coma, and seizures, often due to bacterial infections such as pneumonia or meningitis."

Of these clinical features, psychiatric symptoms such as apathy, aggressive or psychotic behaviour often dominate and can be confused with psychosis [71].

2.4.2 Screening - CATT

Card Agglutination Test for Trypanosomiasis (CATT) is a powerful, fast and easy-to-use screening tool. Developed in the late 70's, it is a simple agglutination test detecting antibodies against *T. b. Gambiense* [72]. As such it is a serological test that can be used with blood, serum or plasma. Freeze dried, stained trypanosomes act as the antigen [73]. Reagent and sample are usually mixed 1:1, but in order to increase specificity different dilutions can be used. The trypanosomes are usually bloodstream forms with variable antigen type LiTat 1.3, although other antigen types or combinations of variable antigen types have also been used (e.g. LiTat 1.6 for a latex based assay). Antigen production involves extraction and purification of trypanosomes from infected rats.

The reported sensitivity of whole blood CATT (undiluted) is up to 98% and the negative predictive value is very good [74]. Nonetheless false negatives can occur, as some strains of trypanosomes lack the LiTat 1.3 antigen. Although the specificity is high (about 95%), the positive predictive value is limited for a number of reasons. The number of infected individuals is usually less than 5% in populations that are screened. False positives can occur due to infections with malaria or other parasitic diseases. While the number of potentially infected individuals can be further reduced by diluting the sample (increasing the specificity) this is not sufficient to confirm infection.

The test result is checked with the naked eye and due to its nature hundreds of people can be scanned in a single day using CATT. This makes it a valuable tool for diagnostics but actual detection of the parasite in a blood or lymph node sample is still necessary.
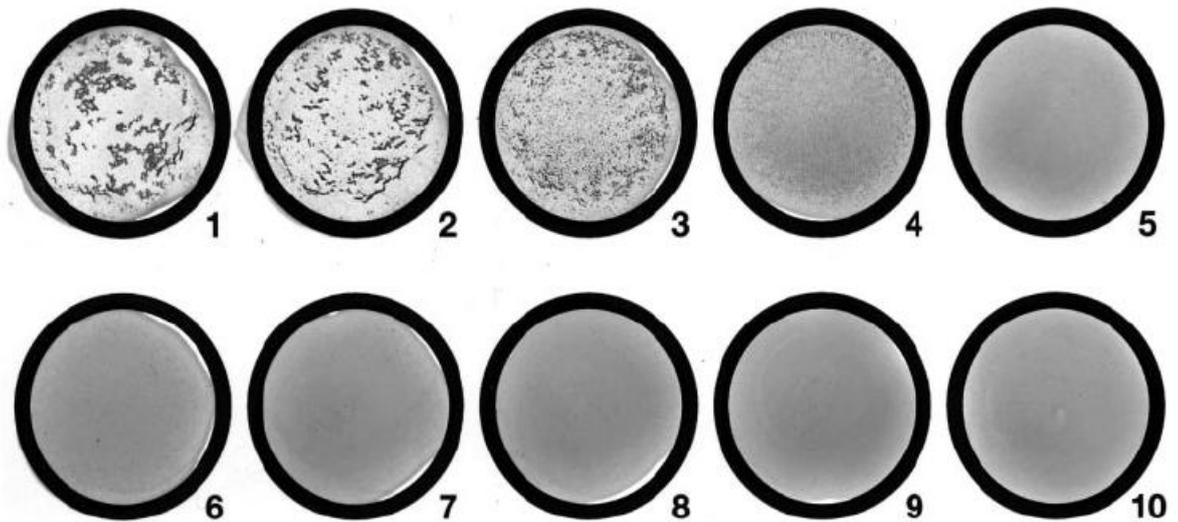
Figure 2-5: Example of a CATT (10 serum samples diluted 1:4). Results 1-4 are positive and 5-10 are negative results (image modified from ref [51]).

2.4.3 Detection

Microscopic examination and consequent confirmation of parasites being present is a necessary step in diagnosis of Human African Trypanosomiasis. Unfortunately the number of trypanosomes in a given blood sample can be very low. It varies from approximately 10,000 to 100 parasites / ml of whole blood. This variation is due to the immune response of the host (see Section 2.3). The methods of detection presented below have different limits of detection and only the mAEC method (see Section 2.4.8) can diagnose the disease at the lowest levels of parasitemia. However, the diagnostic work is usually carried out by mobile teams in the field and sensitivity is not the only deciding factor. The tools have to able to operate under the adverse conditions found in the field. Not all teams have access to electricity and the necessary reagents or tools. In addition, a cold chain cannot always be established or maintained. In general, the methods of detection can be labour intensive and might require special skills or training from the field workers. It is necessary to keep the time between sampling and examination as short as possible as the trypanosomes are killed easily (e.g. by prolonged exposure to direct sunlight).

The descriptions of current methods of detection in this chapter include detailed sketches. They help to illustrate the needed steps and equipment of each technique and how it compares to the diagnostic test that will be presented in this work.

2.4.4 Wet blood film

Preparation of a wet blood film is a simple method for detection of trypanosomes that is still being used in the field, despite its shortcomings, due to its cost and simplicity. Blood from a finger prick is applied to a glass slide (under a coverslip to create a thin film) and the sample is directly observed with a microscope. The trypanosomes themselves are hard to see and it is mainly their movement and displacement of RBCs that is observed. The technique has a poor detection limit of about 10,000 parasites / ml, corresponding to one trypanosome per 200 fields of view [51]. It is also time consuming as it takes about 20 minutes to search a slide.
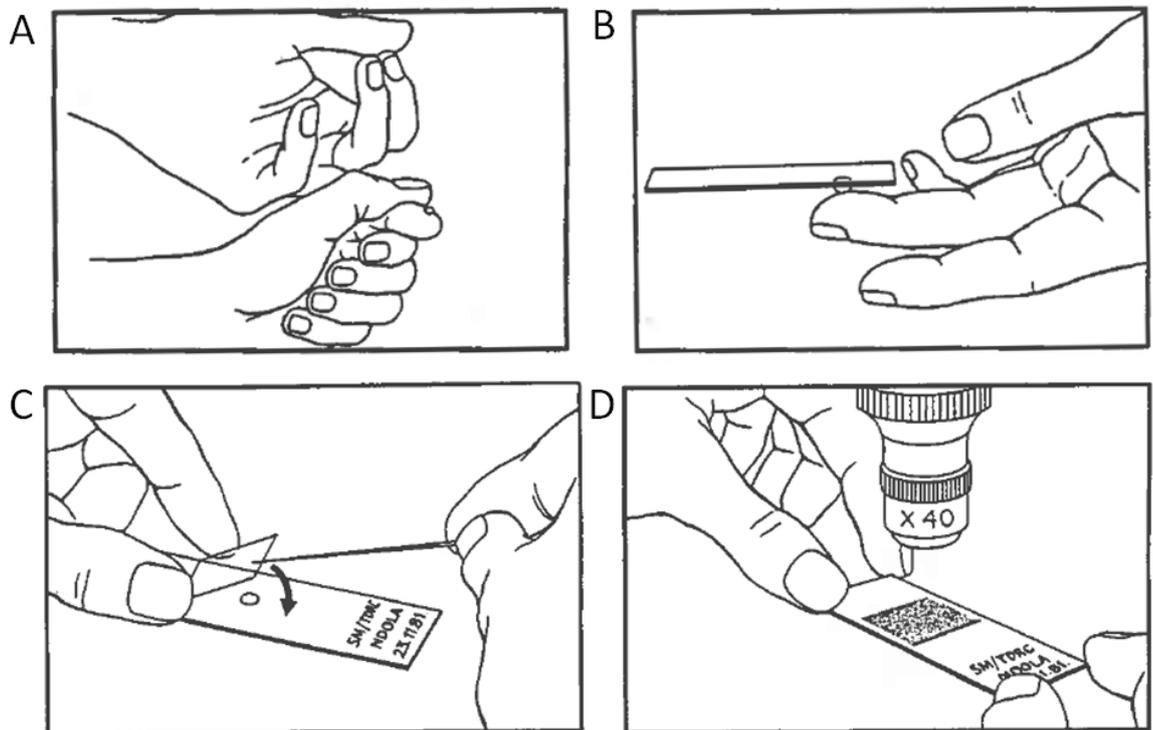
Figure 2-6: Preparation of a wet blood film (image modified from ref [75]). A) The patient's finger (or other extremity like toe or earlobe) is pricked and squeezed until a drop of blood accumulates. B) The drop is carefully placed on the glass slide without touching the finger with the slide. C) Coverslip is placed on sample to create a thin blood smear. D) Sample is immediately scanned with a microscope. This step is time consuming as many fields of view need to be checked.

2.4.5 Thick blood film

A thick blood film is similar to a wet blood film but involves extra steps and equipment with the benefit of increased sensitivity. Instead of creating a thin

blood smear, a larger sample (about 20 µl) of blood is spread on the microscope slide to create a thick film. The sample is then dried and stained using Gimsa or Field staining. The stain causes the trypanosomes (and white blood cells) to become blue and stand out more with respect to the red blood cells. However the parasites are killed in the procedure and are often deformed (making them harder to spot). The staining is a time-intensive process which takes an additional 30 minutes (although several slides can be stained at once). Because of the larger volume of blood and the stain, the limit of detection is improved to about 5000 parasites / ml of blood [51].
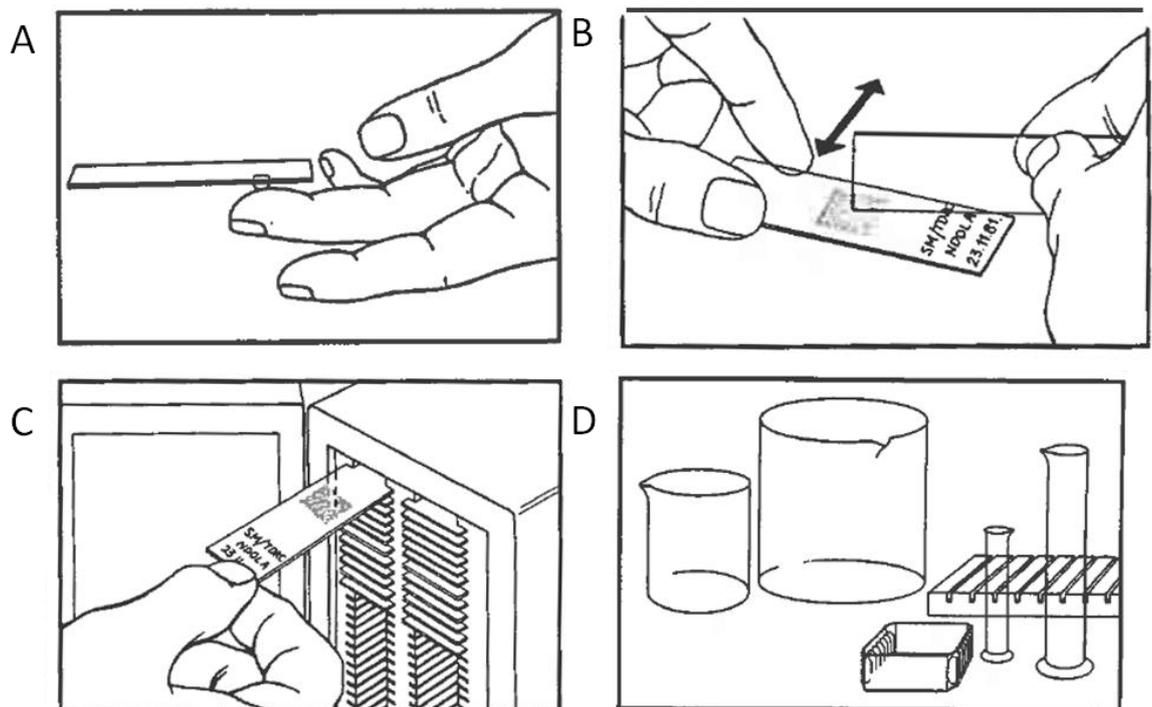
Figure 2-7: Thick blood film preparation (image modified from ref [75]). A) Sample is collected through finger pricking similar to the thin blood film technique. B) The blood is spread out using another slide creating a thick blood film. C) The sample is then dried in a dark space where it is protected from dust and insects. D) The sample then has to be stained before examination. Staining is a lengthy procedure that requires at least 30 minutes per batch of slides and additional chemicals [75]. It is therefore sometimes performed in medical facilities rather than in the field. After staining the slides need to be observed under a microscope.

2.4.6 Lymph node aspirate

It is suggested that all patients with a positive CATT undergo palpation of the cervical lymph node (CLN) [75]. If a swollen CLN is detected, it can be punctured to test for trypanosomes. Testing is similar to wet blood film preparation. The lymph node aspirate contains a much lower number of RBCs making detection of

trypanosomes easier. The technique has a sensitivity of 40% to 80% depending on a number of factors like the parasite strain or the stage of the disease (detection in lymph fluid is more difficult at later stages of the disease) [51]. Swollen lymph nodes may also result from other diseases. Before the establishment of more sophisticated methods lymph node aspiration and blood film examination were the only methods available to field workers. Palpation and puncture of CLNs were used as a screening tool for large populations before the CATT came into widespread use. It can be possible to find trypanosomes in the lymph fluid and not the blood of a patient or vice versa. As such the technique is still being used today as a complementary method to more sensitive techniques focusing on blood samples. The medical worker has to have a higher level of training than is necessary for simple finger pricking. The needle has to be inserted into the centre of the CLN but not too far in order to prevent penetration of the jugular veins and arteries.
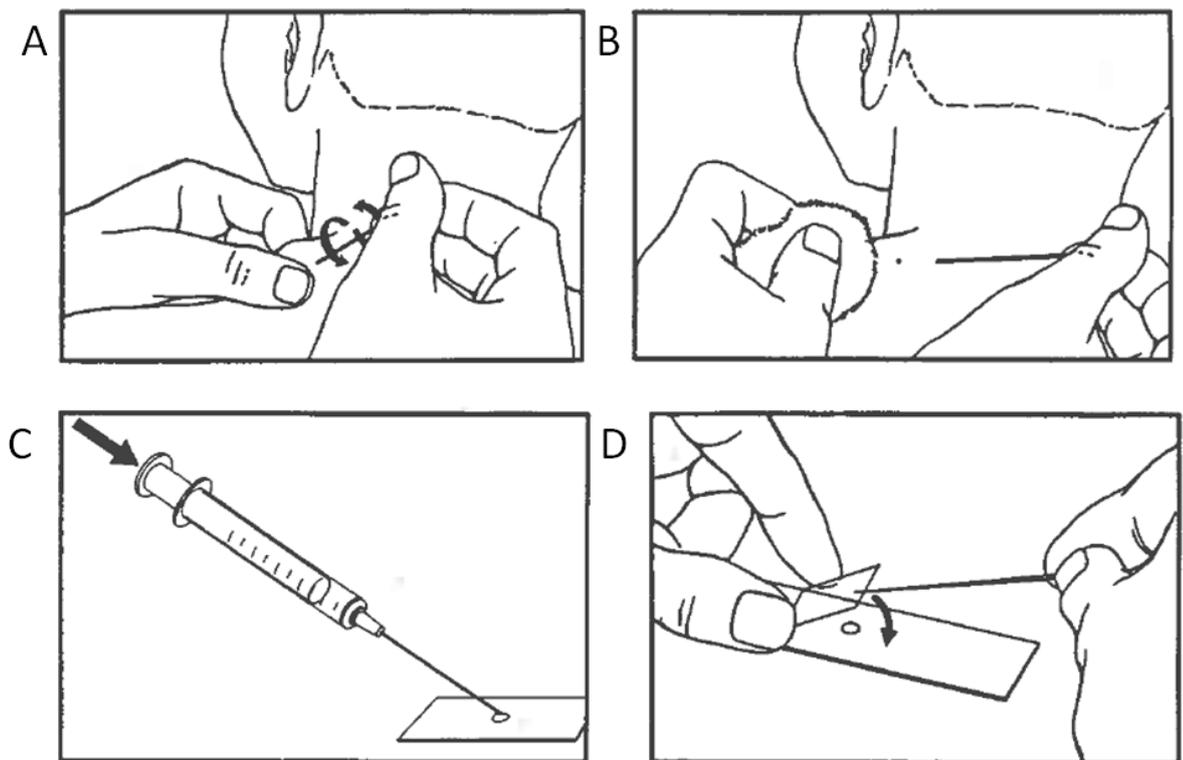
Figure 2-8: Preparation of lymph node aspirate (image modified from ref [75]). A) The cervical lymph node has to be held firmly with one hand to make it stand out. Then a syringe needle is inserted into the swollen lymph node. The needle is revolved in both directions for about one minute while glandular fluid oozes into the needle. B) The needle is withdrawn in one rapid movement and a swap with disinfectant is applied to the puncture immediately. C,D) The aspirated fluid is dispensed on a microscope slide and a thin film is prepared. This thin film is observed under a microscope.

2.4.7 Techniques aided by centrifugation

There are two principal techniques that rely on centrifugation to greatly increase sensitivity above the methods presented above. The first one is the microhematocrit centrifugation technique (mHCT), also known as the Woo test, and the second one is the quantitative buffy coat (QBC) [51]. In order to perform the mHCT a number of capillaries are filled with donor blood and then (after one end has been sealed) centrifuged for several minutes at high speeds in special hematocrit centrifuges. Through the centrifugation process the trypanosomes are concentrated at the same layer as the white blood cells. The capillaries are then placed in a holder and examined under a microscope. Because of this pre-concentration step the limit of detection is much improved. The actual limit depends on the sample volume (and thus the number of capillaries) but for six to eight capillaries it is about 500 trypanosomes / ml [51]. While the technique is time consuming and microfilia in the blood might impede detection it is widely used for field diagnostics. The mobile teams employing mHCT need to have access to a high speed centrifuge and, consequently, electricity.
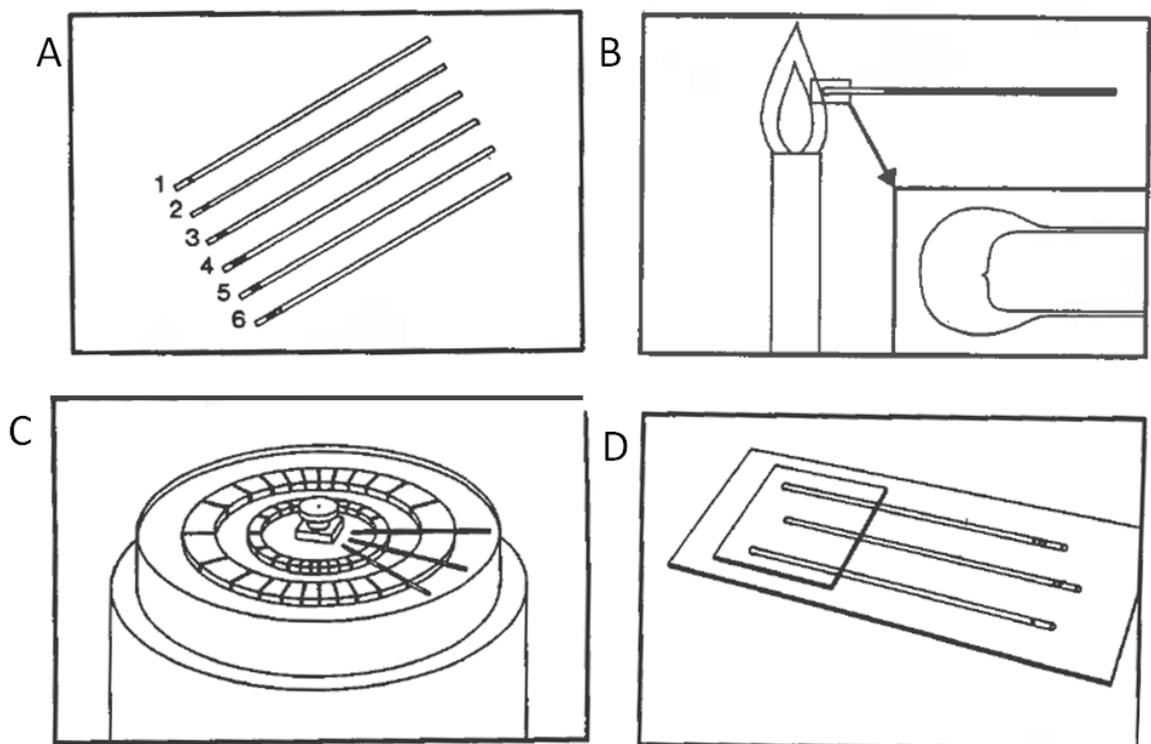
Figure 2-9: Microhematocrit centrifugation technique (image modified from ref [75]). A) Six to eight samples are collected per patient, the blood is drawn into capillaries (the capillary should be about three quarters full). B) The capillaries are sealed at the dry end. C) Using a special hematocrit centrifuge the samples are spun at high speeds for six to eight minutes. D) Samples are placed on a holder and examined under a microscope. Through centrifugation, the trypanosomes are concentrated at the same level as the white blood cells.

Another method utilizing concentration through centrifugation is the quantitative buffy coat (QBC). This technique has the added benefit of staining the trypanosome using acridine orange, a fluorescent dye. For an example of trypanosomes stained with acridine orange please see Section 3.2.2. The capillary tubes used for centrifugation already contain ethylenediaminetetraacetic acid (EDTA) and acridine orange when the blood is drawn into them. After centrifugation the samples are viewed under a microscope but a UV light source and filters appropriate for the dye are needed as well as a darkroom. While the QBC offers comparative sensitivity to the mini-anion-exchange centrifugation technique (mAECT) described below, the complexity and fragility of the needed equipment prohibit rapid transport to different sites during field work.

2.4.8 Mini-anion-exchange centrifugation technique

The mAECT utilizes an important property of the trypanosome, its surface charge. While red blood cells have a negative surface charge, the trypanosomes surface carries no significant charge [76]. This can be used to separate out trypanosomes from RBCs, by passing a mixture though a positively charged matrix. While the RBCs are bound in the matrix, the trypanosomes are carried through and collected at the end of a column for observation. This technique was established [77, 78] in the late 70s and has excellent sensitivity while being mobile enough to carry around for field operations [79].

Just prior to testing, the columns need to be prepared with a mixture of phosphate buffered saline (PBS) and glucose, also prepared at that time. Then the blood sample is loaded into the column and centrifuged. Large volumes of intravenous blood can be loaded into the column (about 300 µl), which increases diagnostic efficiency. The centrifugation does not need to be high speed and a hand operated centrifuge is sufficient. After the centrifugation the column is fixed under a microscope with a special holder to allow examination of the sample. The reported limit of detection for mAECT is 100 trypanosomes / ml of whole blood. Although the preparation is time consuming, the mAECT is currently the gold standard for trypanosome detection [51].
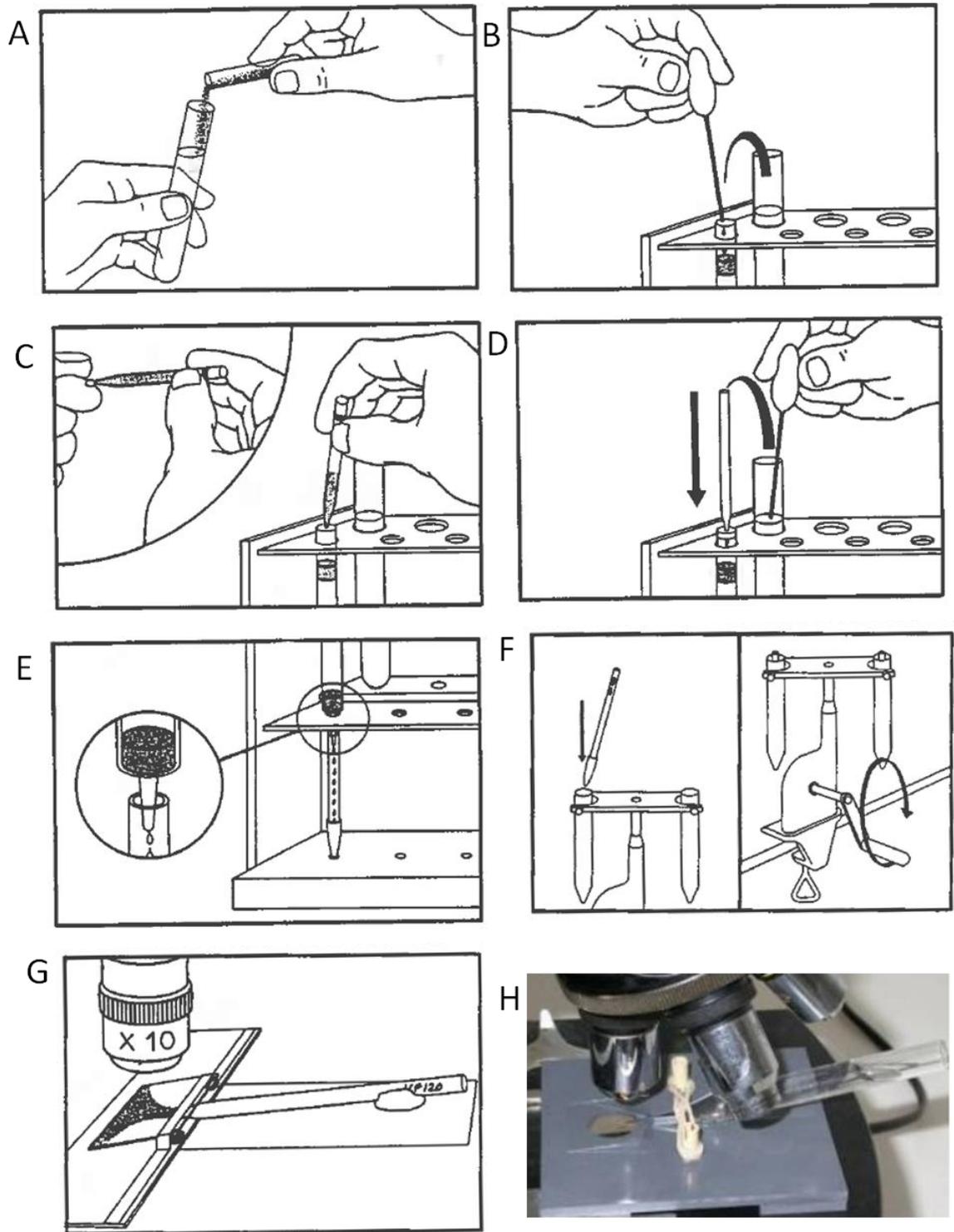
Figure 2-10: Preparation of a mini-anion-exchange column (images A-G modified from ref [75], Image H modified from ref [80]). A) A pre-weighed amount of glucose is mixed with a predetermined amount of PBS. **B)** The column is loaded with this mixture to prepare it for the sample. **C)** Patients blood is loaded into the column. Up to 300 µl of intravenous blood can be loaded to improve sensitivity. **D,E)** The rest of the buffer is gradually loaded into the column and the outflow is collected at the bottom. This process may be aided by gentle centrifugation to speed it up. **F)** The collected outflow is centrifuged to concentrate the trypanosomes. This can be done manually at 1500 RPM for 5 minutes. **G,H)** The sample is fixed under a sample holder to allow inspection with a microscope.

2.4.9 Other methods of detection

There are a number of other proposed methods of detection that are not widely used in the field for various reasons. In vitro cell culture and animal inoculation are possible, but the technique takes weeks before results are observed [51]. Antigen detection (as opposed to antibody detection) is an interesting approach as it would allow the user to differentiate between active and cued infections. Field studies however have shown strong doubts about its specificity [81]. Separation of trypanosomes from blood was also demonstrated using a lateral displacement flow chip [82]. This approach remains to be verified with *T. brucei* though. PCR is another technique being considered for diagnostic application [68]. While traditional PCR requires complicated machinery and is not suited well for field work, isothermal PCR has been recently proposed as a potentially viable option for trypanosome detection [83].

2.5 Summary of aims and objectives

The motivation for this work is laid out in detail in Section 2.4. The current methods of detection available for sleeping sickness are old and all have flaws one way or another. The fundamental question of this work was:"Can we do any better?"

An improved method of detection for sleeping sickness would be of great benefit in controlling and eventually eradicating the disease. While the ongoing control programs have shown great success in reducing the number of new cases reported each year, Figure 2-1 confirms that even after a decade of dedicated control the disease can re-emerge quickly, when left unattended. The actual diagnostic techniques used the field today have changed little from what was being employed in the mid and late 70's.

The goal of this work was to explore the possibility of using dielectrophoresis to enrich trypanosomes from a sample of infected blood. A proof of principle electrode array was to be created that could remove the unwanted red blood cells and ideally concentrate the trypanosomes into a single central spot where they would be easy to identify.

During the work an interesting phenomenon regarding electrically induced lysis of red blood cells was observed. The aim of the thesis was then extended to include the assessment of the novel technique and if it can be used to enrich rare cells from mixed populations and to study the origin of the unusual observations made in the experiments.

Chapter 3: Materials and Methods

3.0 Abstract

In this Chapter the methodology used in this work will be discussed and described. This includes the biological samples and their preparation, the instrumentation and the experimental procedures.

3.1 Materials

Whole mouse blood was collected via cardiac puncture for experimental purposes (see below). Screened human blood was also acquired from the blood transfusion service. Blood samples were stored at 4° C with anticoagulant and used within 2 days of acquisition.

T. cyclops and *T. brucei* were cultured (see below) and spiked into human or mouse blood for experimentation. In vivo samples of mouse blood infected with T. brucei (see below) were also used for experimentation.

Dielectrophoresis buffer medium was prepared with 3 mM HEPES, pH adjusted to 7.4, 9 % sucrose and 0.3 % glucose for an osmolality of 290 mOsm/kg , measured with an osmometer (The Advanced Micro Osmometer, model 3300, Vitech Scientific Ltd). After adjusting the pH value the base conductivity of the medium was approximately 15 mS/m, measured with a conductivity meter (4071 Yenway). This value was then adjusted to the desired values by adding phosphate buffered saline (PBS).

Different sets of electrodes patterned on glass (see below) and special chambers for optoelectronic tweezers (see below) were used during the experiments. These chips were connected to either a standard function generator (TTi, TG5011 LX1) or, in the case of travelling wave dielectrophoresis, a four channel function generator (TTi, Arbitrary Waveform Generator, TGA12104).

3.2 Methods

3.2.1 Cell culture

Trypanosomes of the subtype *T. cyclops* and *T. brucei* were cultured *in-vitro* for experimentation.

T. cyclops were cultured in Cunningham's medium (See appendix) supplemented with 20% foetal bovine serum (FBS, Gibco) and maintained at 27°C. The parasites were passaged once a week and were grown to a density of 2×10^6 /ml. Human blood spiked with *T. Cyclops* was used for experimentation.

Bloodstream forms of T. *brucei* (Strain 427) were cultured in Hirumi's Modified Iscove's medium (HMI-9, see appendix) supplemented with 10% FBS. The cells were maintained at 37 °C, 5% CO2 and passaged three times a week. The trypanosomes were grown to a density of 2×10^6 /ml. Mouse blood from non infected animals or human blood spiked with cultured *T. brucei* was used for experimentation.

3.2.2 Sample preparation

To prevent lysis of the parasite through the trypanosoma lytic factor (TLF) and in order to control the conductivity of the medium, the trypanosomes were washed in the DEP buffer solution. Cells were washed three times through centrifugation (2500 rpm for 5 minutes) and, after the supernatant was removed, re-suspended each time in the medium of desired conductivity. Samples were then loaded quickly onto the corresponding chips for experimentation.

After initial experiments with *T. cyclops* it was necessary to work with *T. brucei* as it is clinically more relevant. While *T. cyclops* is used in limited amount in research and for demonstration purposes, nearly all published data regarding research of trypanosomes connected with sleeping sickness is performed using *T. brucei*.

While performing this washing step with *T. brucei*, an interesting phenomenon was observed. The trypanosomes and the red blood cells seemed to 'stick' together. This agglutination caused the trypanosomes to be completely covered in red blood cells (see Fig 3-1). The parasites were still motile and the red blood cells appeared to be tightly packed on the surface of the trypanosomes. In

samples of pure trypanosomes the parasites agglutinated to each other, forming large conglomerates of cells.

This agglutination was highly undesirable for experimentation, as the larger cell-conglomerates showed differing, unpredictable dielectric behaviour depending on size. Therefore a washing procedure was developed that would ensure the correct conductivity medium but would prevent cell-agglutination.

Washing the trypanosomes in PBS or cell culture medium did not result in agglutination. Since the main constituent of our buffer was sucrose, attempts were made to replace it with a different sugar. However the agglutination process was still observed in buffer made up with mannitol, lactose, maltose or fructose. Another attempt was made by decreasing the pH value from 7.4 to 7.0 and 6.0. This did not prevent agglutination either and at lower pH values the cells were being destroyed.

Finally the sample of trypanosomes was treated with trypsin and this process prevented the phenomenon from occurring. When incubating the infected (or spiked) blood with trypsin for 5 minutes at room temperature prior to adding the sugar solution, no agglutination was observed. The trypsin was inhibited after the incubation using cell culture solution. Obviously the sample has to be washed thoroughly, in order to restore the desired conductivity, after adding cell culture medium (which has a conductivity in excess of 1000 mS/m).

It was possible to reverse cell agglutination after the fact by incubating in trypsin, although the process was slow (~45 min). Most experiments were carried out with *T. brucei* and mouse blood. Hence, there was no danger of the parasites being lysed through the TLF. Both blood from infected mice and blood from healthy animals, spiked with trypanosomes from in vitro culture, were used for experimentation. For later experiments *T. brucei* were mixed with human blood and thus care had to be taken to apply the same washing procedure as for *T. cyclops*. All experiments to quantify TW-DEP were done with cells that were washed 3 times by centrifugation.
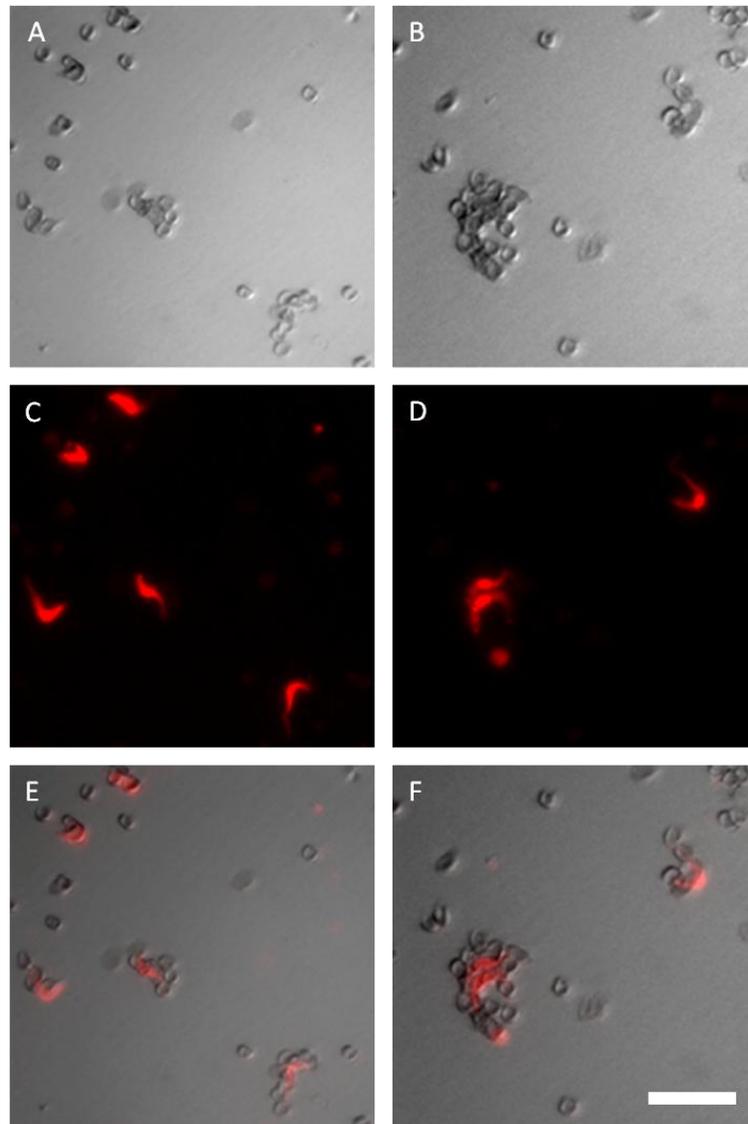
Figure 3-1: Agglutination of red blood cells and trypanosomes. A, B) Differential interference contrast (DIC) image of agglutinated RBCs and trypanosomes. Parasites were still motile but their movement was restricted because of the attached blood cells. C, D) Fluorescent image of the same field of view. Trypanosomes were stained with acridine orange and are clearly visible. E, F) Overlay of the DIC and fluorescent images. The parasites were located at the centre of the larger clumps of blood cells. Scale bar is 50 μm.

In the field, however, centrifugation can be difficult to perform and thus experiments were also conducted to demonstrate that enrichment can be achieved with a diluted (to reduce the conductivity) sample of blood (see Section 5.2.2). Since trypsin normally comes suspended in a solution with a high salt content, salt free trypsin powder (Promega) was therefore used and added to the prepared buffer medium. Experiments with this buffer medium showed that it was unnecessary to inhibit the trypsin and that the cells were still motile after extended periods of time (1 hour). In order to rule out any effect the trypsin might have on motility or viability of the cells however, it was inhibited

for experiments performed on the TW-DEP device with a diluted sample. To do this, powdered salt free trypsin inhibitor (Sigma-Aldrich) was added to DEP buffer and the sample was first diluted 1 in 20 with trypsin buffer for 5 minutes and then diluted 2 fold again with trypsin inhibitor buffer for a total dilution of 1 in 40. With a conductivity of about 15 mS/m for the buffer the end conductivity of the diluted sample was between 40 and 50 mS/m.

3.2.3 Animal work

Female adult 'imprint control region' (ICR) mice were inoculated with *T. brucei* (wild type 427 strain) from a bloodstraw, ~ 20 µl of $1x10^8$ cells/ml, using intraperitoneal injection. Parasitaemia was monitored daily via tail venepuncture and microscopic observation of blood smears. Mice were culled via a schedule 1 protocol at the desired parasitaemia level (~$1x10^8$ cells/ml or ~$1x10^5$ cells/ml). All animal work was carried out by Dr. Pui E. Wong and samples were kindly provided for experimentation.

3.2.4 Fabrication

The experiments to determine the crossover frequencies and to perform travelling wave Dielectrophoresis were carried out with metal electrodes patterned on glass slides. These electrodes were fabricated using standard metal evaporation procedures which will be briefly presented here. Since the electrodes could be reused many times (after cleaning them thoroughly with 70% ethanol) only a relatively small number of devices needed to be made for this work.

Glass substrates were cleaned in acetone, methanol and water each for 5 minutes then the water was removed by blow drying and a dehydration bake at 180°C for 15-30 minutes. Positive photo-resist S1818 (Shipley) was spun on the glass slide at 4000 rpm for 30 seconds, creating a 10 µm thick layer of resist. This was followed by a soft bake (95°C for 5 minutes on a hotplate) and exposure to UV light (4.2 seconds, Suss Microtec MA6 mask aligner). The exposure was patterned through a chrome mask. Since S1818 is a positive resist, the areas that were exposed to the UV light will be removed during

development. The sample was then developed in a 1 in 1 mixture of Micro DEV (Shipley) and water for 95 seconds (the sample is then washed under running water and blown dry). No post exposure bake or hard bake were necessary. At this point the glass surface was exposed in the areas where the metal electrodes are going to be placed. This was achieved through evaporation of a 10 nm chromium seed layer and then a 200 nm layer of gold (Plassys Electron Beam Evaporator). The metal on top of the resist (not in direct contact to the glass) was removed in a lift-off procedure, by submerging the sample in acetone at 50°C (in a hot water bath).

The chromium masks were created by technicians of the James Watt Nanofabrication Centre through etching. The author merely provided files, created with the AutoCAD software (Autodesk), with the designs to the technicians and collected the finished mask. These files were kindly provided by Dr. Anoop Menachery. The spiral design was created using the MATLAB software and then imported and finalised in AutoCAD.
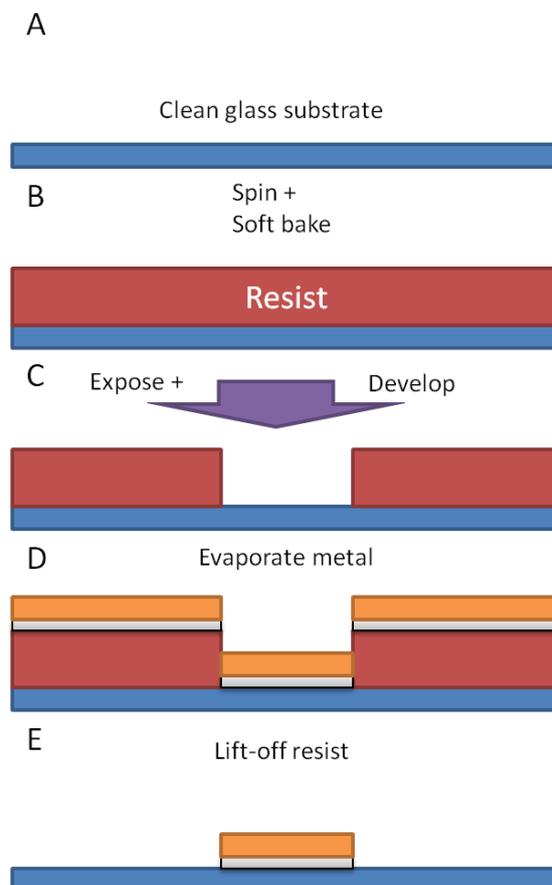
Figure 3-2: Cartoon (not to scale) of the fabrication process (details see text). A) Clean glass substrate. B) Application of photo-resist and soft bake. C) Exposure through a chrome mask and development to remove resist. D) Evaporation of a 10 nm layer of chromium and a 200 nm layer of gold. E) Removal of resist (and unwanted metal) through exposure to acetone.

3.2.5 Instrumentation for DEP

In order to create a non-uniform field and determine the crossover frequency, a set of quadrupole electrodes was employed (see Figure 3-3). The electrodes were patterned on glass (200 nm of gold evaporated onto a 10 nm seeding layer of chromium) using standard photolithography techniques (see above). The inter-electrode distance (tip to tip in the central area) was 400 μm. The design has been used previously for studies on dielectrophoretic forces [84], or electrorotation [85].

The chamber to hold the sample is created by cutting a well into a strip of insulating tape. The chamber is closed off at the top with a small cover slip. Wires are attached to the electrodes and attached to a standard function generator (Thurlby Thandar Instruents, TG5011 LX1).
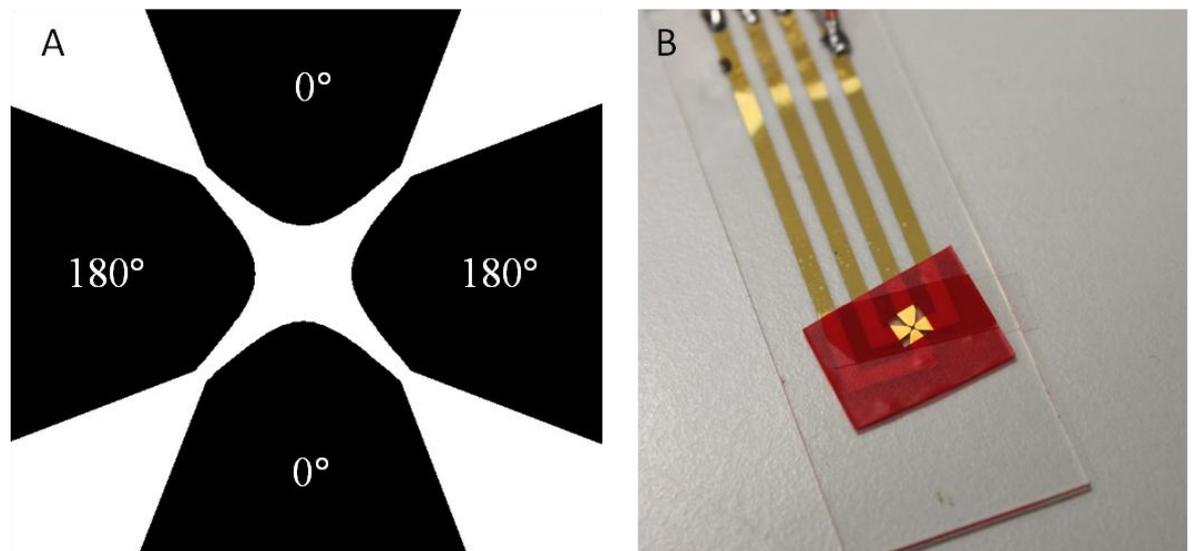
Figure 3-3: Quadrupole electrodes used for characterisation of cross-over frequencies. A) Schematic of the quadrupole electrode array, with an interelectrode separation of 400 μm (from tip to tip). The electrodes are energised with an opposing two phase electric field. B) Photograph of the chip used for characterization of the crossover frequency.

TW-DEP experiments were carried out on two different sets of electrodes. Both were 4 arm spiral electrode arrays. The first design was only used initially, in experiments concerning the particle density (see Chapter 5). This chip had a spiral with arms that do not extend all the way into the centre. The electrodes were patterned platinum on glass (electrode width and spacing of 30 μm each) and the chip itself was not made by the author of this work. It was instead kindly provided by Dr. Anoop Menachery for the initial experiments.

All other experiments involving TW-DEP were performed on a different spiral electrode array with spiral arms that extend into the centre of the array (see Figure 3-4). The electrodes were patterned on glass using the same standard photolithography techniques employed to make the quadrupole electrodes for crossover measurements (200 nm of gold on a 10 nm layer of chromium). The electrodes themselves had a width of 30 microns and an inter-electrode spacing of 30 microns as well. The total width of the array was approximately 2.9 mm. A square chamber of approximately 6 mm length and 150 µm height was created around the array from insulating tape. Wires were soldered to contact pads connected with each arm and connected to a four channel function generator (TTi, Arbitrary Waveform Generator, TGA12104) that was able to provide the necessary quadrature-phase electric signal. The sample was loaded (and the chamber cleaned) the same way as for the quadropole electrodes.
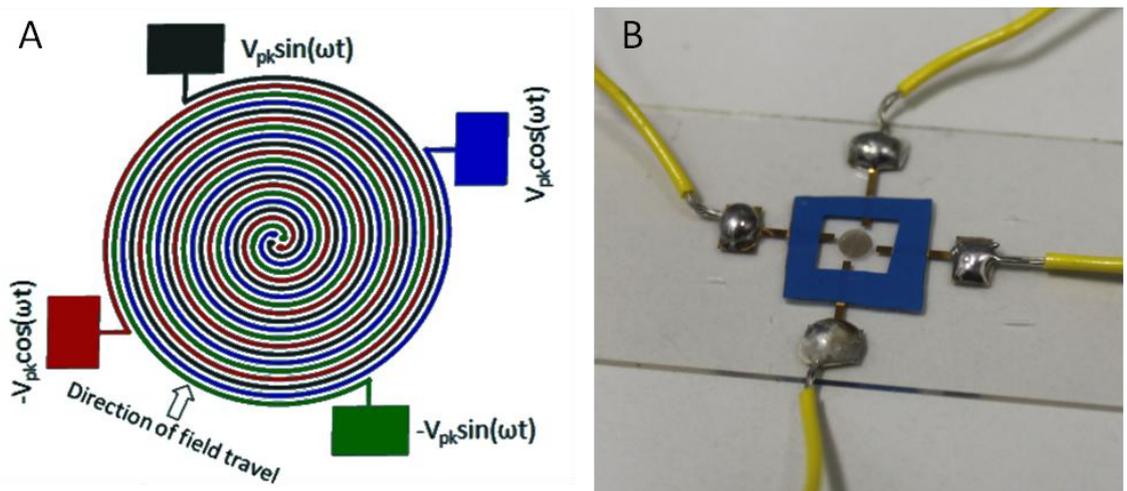
Figure 3-4: Schematic diagram and photograph of the electrode array used for experimentation. A) Electrodes of the 4 arm spiral electrode array had a width and spacing of 30 µm each. The array was energised with a 90° phase shift from one arm to the next, creating a travelling electric field. B) Photograph of the gold electrodes on a glass slide. The total width of the array was approximately 2.9 mm. The sample was enclosed in a square chamber and sealed with a glass cover slip during experimentation.

Initial experiments for DEP and some of the control experiments regarding selective lysis were performed using interdigitated electrodes. The electrodes were simple parallel rectangular strips of 100 µm or 30 µm width and interelectrode spacing.

3.2.6 Measurement for DEP

Each experiment involving DEP followed the same basic procedure. After washing the cells in the buffer medium of the desired conductivity, the sample was pipette into the chamber until it was fully filled (~5 µl). The electrode array was then placed on an inverted microscope and a video was captured during the experiment. After each experiment the chamber was thoroughly cleaned using 70% ethanol and after four to five experiments a new chamber was created, to prevent the build up of residue in the corners of the well.

Blood is a heterogeneous mixture of cells with a high density of erythrocytes. In a healthy human, the red blood cells (hematocrit) make up approximately 50 % volume, with about 10^9 erythrocytes / ml. Other blood cells (leukocytes and thrombocytes) make up a comparatively negligible part of whole blood. During experiments with non uniform electric fields complex particle interactions can arise, for example chaining of cells [1, 2]. In order to assess the effect the particle density would have on TW-DEP experiments several dilutions of mouse blood were prepared.

The experiments were conducted in 30 mS/m buffer solution at 90 kHz with a 4 V_{pk-pk} voltage. It should be noted that these initial experiments were not intended for enrichment of trypanosomes. The conditions best suited for enrichment (also used for the simulations) were established at a later date. The blood was re-suspended in the buffer at the original (whole blood) concentration of cells as well as 1 in 5, 1 in 10 and 1 in 20 dilutions. For whole blood concentrations it was observed that the red blood cells cleared from the spiral, albeit slowly. The sample also showed complex patterns that emerged during the process (see Figure 3-5). These varied from experiment to experiment but resembled eddies and other streaming phenomena (bright areas in Figure 3-5 indicate the absence of cells).
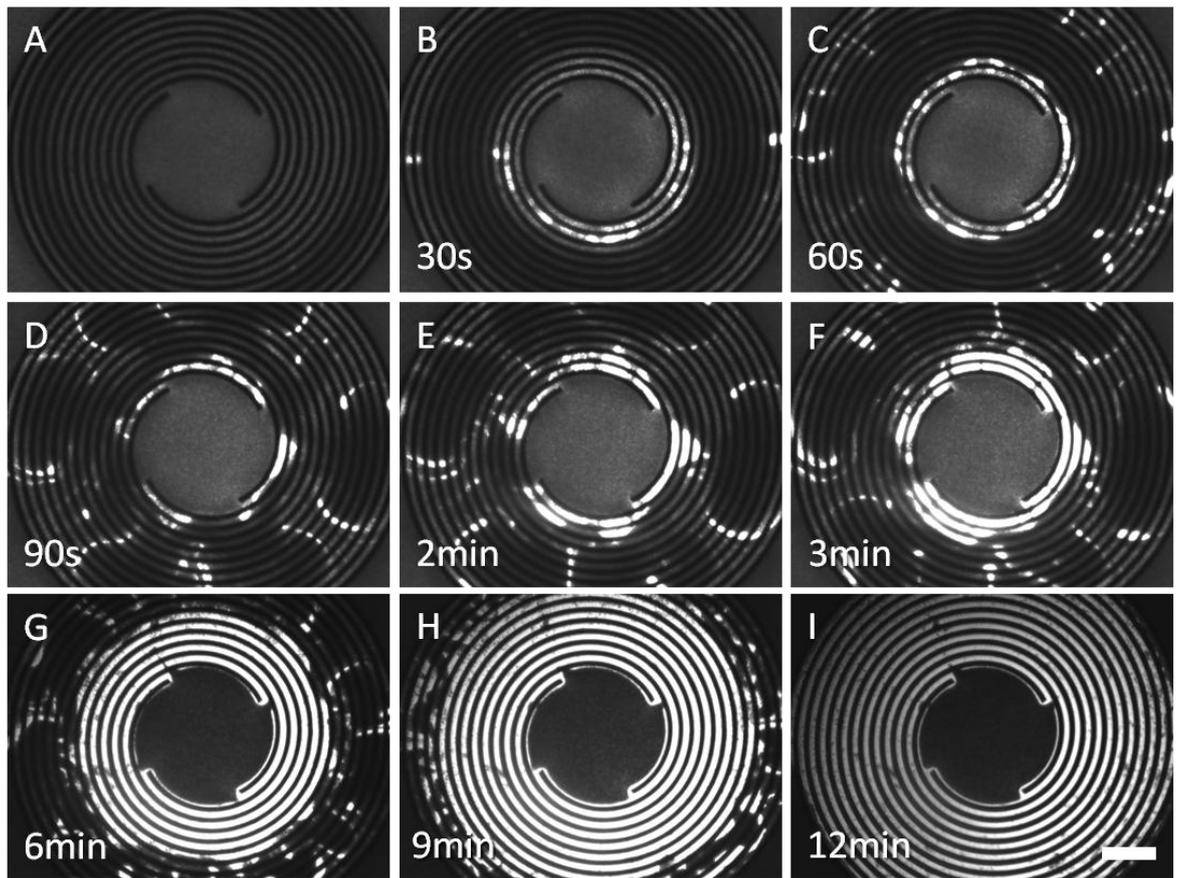
Figure 3-5: High density blood sample being moved with TW-DEP. Electrode width and inter-electrode spacing are 30 µm each. Mouse RBCs were washed with 30 mS/m buffer and re-suspended at whole blood concentration. A 90 kHz quadrature-phase signal with 4 V$_{pk-pk}$ was applied to the array. A) Initial distribution at the onset of the experiment. B-I) show the translational movement of the RBCs due to the TW-DEP force acting on them. D-F) show complex particle-particle interaction according during the anti-field motion of the cells. Even after 12 minutes (I) the outer spiral was not cleared of erythrocytes. Scale bar is 300 µm.

As the particle density was reduced by diluting the blood, the removal of the red blood cells from the spiral, due to TW-DEP, was more and more uniform. The speed by which the spiral array was cleared of RBCs also increased. By comparison the whole blood concentration took more than 12 minutes to clear (see Figure 3-5) while for the 1 in 20 dilution the spiral was cleared in about 5 minutes (see Figure 3-6). For all experiments that were performed to demonstrate or quantify the enrichment process, the dilution was set at 1 in 20. For experiments demonstrating preparation through dilution (see Section 5.2.2) the samples were diluted even further.
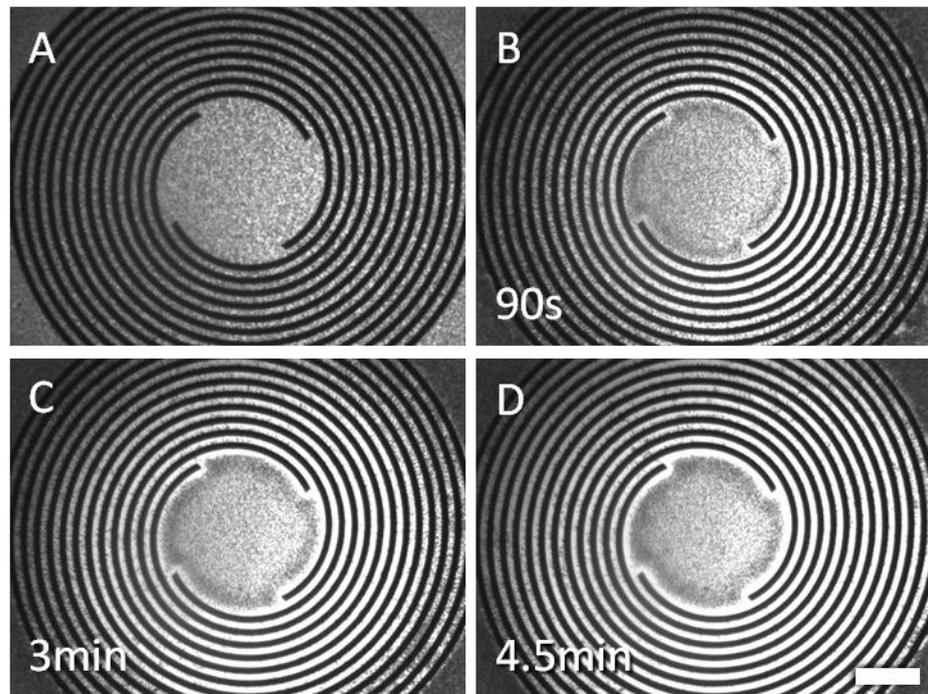
Figure 3-6: Low density blood sample (1 in 20 dilution) undergoing anti-field motion due to TW-DEP. A) Initial distribution of cells at the onset of the experiment. B-D) show the removal of RBCs from the electrode array. The movement is uniform and after approximately 5 minutes the array has been cleared of red blood cells. Scale bar is 300 μm.

To quantify the concentration process, the velocity and enrichment numbers were determined for varying frequencies and voltages. The velocity was the average velocity of a trypanosome travelling inward towards the centre of the spiral, and was determined from the videos, by comparing the total distance the trypanosome covers with the amount of time it took to travel from the edge of the field of view into the central area of the array. In experiments with low parasitemia, the velocities of all parasites were determined and in cases of high parasitemia up to 40 parasites per experiment were evaluated. At least 7 experiments for each value of voltage and frequency were averaged to generate the data presented here.

The enrichment number is simply the number of trypanosomes that are counted in the central field of view during the experiment (coming in from the outer areas of the spiral). The duration of the experiment was set as ten minutes and parasites that entered the field of view after this time were not taken into account. This number is directly related to the concentration of parasites in the sample (e.g. high number of parasite above the spiral at the start of the experiment will give a high enrichment number). Since the concentration of

parasites varies every time a sample is drawn from a mouse (from 10^5 to 10^8 parasites / ml), the enrichment number was normalized in order to compare results from different experiments. Obviously all parasites that came into the field of view were taken into account (unlike the evaluation of the velocity). The averaged data was also composed of at least 7 experiments per point (the same experiments as for the velocity).

Further experiments were conducted to demonstrate enrichment of trypanosomes from mouse blood, using the dilution procedure outlined in Section 3.2.2, as well as experiments to demonstrate enrichment of trypanosomes from human blood using standard washing procedures described above.

Finally the sensitivity of the device was determined. The sensitivity of the system as defined here is the number of parasites detected in the centre of the spiral after the experiment, compared to the number of parasites that were contained in the sampling volume (see below) at the onset of the experiment. In contrast, the limit of detection is the minimum number of parasites that have to be present in a sample for the test to give a positive result.

The sampling volume is the volume of liquid above the electrode array. Given a total diameter of 2.9 mm of the spiral array and a height of 150 μm, the sampling volume is approximately 1 μl of liquid (a cylinder with a radius of 1.45 mm and a height of 0.15 mm). Assuming a sensitivity of 100 % (that is every single parasite on top of the spiral is concentrated into the centre) this already gives a limit of detection of 1×10^3 parasites / ml of whole blood. However in order to reduce the conductivity of the medium to the required value, the sample is diluted further.

The initial concentration of parasites was determined with a Neubauer counting chamber from whole (infected) mouse blood.

3.2.7 Instrumentation for optoelectronic tweezers

Since the light used to form the virtual electrodes during an OET experiment does not need to be provided by a laser, a regular data-projector is sufficient to generate the light patterns. This has the added advantage of allowing easy and flexible creation of complex patterns through regularly available PC software (e.g. PowerPoint). The light from the projector has to be projected onto the sample while simultaneously allowing for inspection of the sample with a microscope. The two setups that were used in this work are shown in Figures 3-7 and 3-8.

In the both setups two filters were used (see Figure 3-7 B) to create a pattern with strong illumination over the target and still be able to view the sample. A long pass filter in front of the projector caused the projected light to be red. It was then combined with the background illumination from a lamp and projected onto the sample through an objective. After being reflected off the sample the light hit the camera, but a second filter (short pass) removed the strong illumination of the projector. In this way, the intensity of the projector can be high without impeding the observation of the sample.
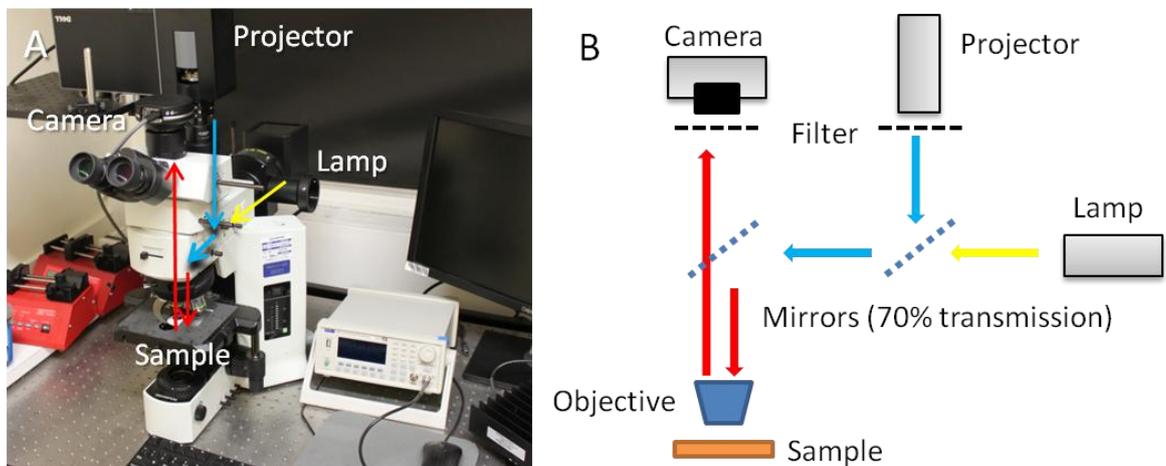
Figure 3-7: Optoelectronic tweezers setup. A) Photograph of the setup using an upright microscope (Olympus). B) Cartoon of the light-paths inside the setup. The patterned image from the projector is combined with background illumination from a lamp and projected onto the sample. The reflected image from the sample is then recorded with a camera. In order to be able to view the sample, including the shaped light from the projector, two filters were used. The two filters were a long pass filter in front of the projector and a short pass filter in front of the camera. This causes most of the light form the projector to be filtered out before it reaches the camera, as it would otherwise be too bright to observe the cells inside the illuminated region.

Initially a self made setup was used with a simple optical path (see Figure 3-8 A). While this was upgraded to an upright brightfield microscope (Olympus Bx51 TRT-5) with a better camera (Olympus U-TV0.5XC-3), there were limitations regarding the possible magnification that could be used in this second setup however. Since the sample sat at the bottom of a 100 μm high chamber and the top of the chamber was a thick microscope slide (rather than a thin coverslip), the working distance of the objective has to be high enough to accommodate this fact. While objectives that meet this requirement can be integrated into a microscope easily for lower magnification (10x and below), higher magnification lenses were too large to fit the Olympus setup (see Figure 3-8 B).
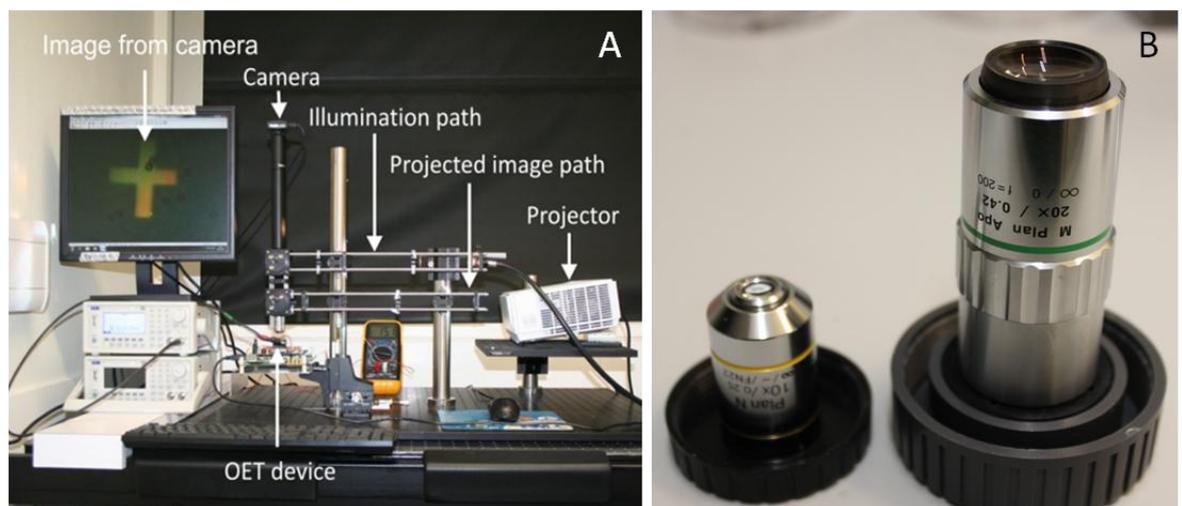
Figure 3-8: Alternative OET setup. A) Photograph of the alternative setup used for higher magnification work. This setup allowed for the use of a higher magnification lens that still offers the needed working distance to use the optoelectronic chip. B) Photograph of the long-working distance objective (Mitutoyo M Plan Apo 20X) compared to a traditional 10X objective (also M plan). The objective has a 20mm working distance and a numerical aperture of 0.42.

The chamber used to hold the sample during the experiments is pictured in Figure 3-9. The bottom of the chamber, on which the cells will come to rest during the experiment, consisted of a glass slide covered with a 10 nm layer of indium tin oxide (ITO) and on top of that a 1 μm thick layer of amorphous silicon (a:Si). The glass slides were bought pre-coated with ITO (Diamond coatings, UK) and the layer of amorphous silicon was deposited using Plasma Enhanced Chemical Vapour Deposition from a silane gas. The coated slides themselves were provided by Dr. Steven Neale and Prof. Mervyn Rose (University of Dundee). The a:Si was scratched off in order to reveal the ITO beneath and wires were attached to the conductive layer using silver paint (Electrodag, Agar

Scientific Ltd) and a film of epoxy glue was applied to protect the contact. Care has to be taken in removing the silicon film and the resistance of the contact has to be tested (in some cases the contact presented a large resistance).

In order to create a chamber to hold the liquid sample, two spacers were placed on the bottom chip. These simply consisted of double sided adhesive tape (Scotch) and that was cut into strips and placed directly on the silicon. The height of the chamber was approximately 100 µm (determined using a Veeco Dektak 6M height profiler). The top of the chamber is formed by another glass slide coated solely with ITO. The two pieces of glass are positioned to leave an opening for the sample to enter the chamber (see Figure 3-9 C).
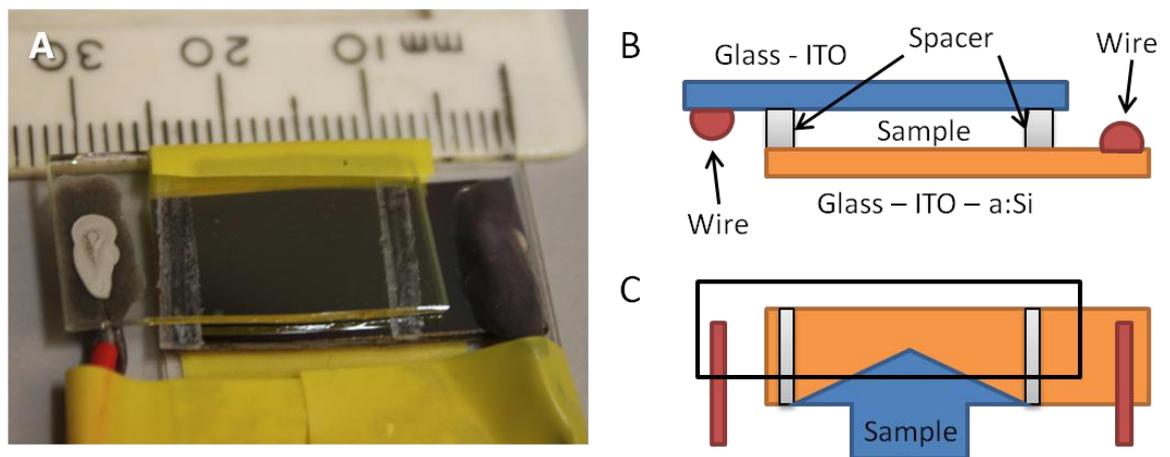
Figure 3-9: Chamber used for experimentation. A) Photograph of the chamber being used for experiments with the optoelectronic tweezers. The wire is attached to the top and bottom slide with silver paint and the contact is protected with epoxy glue. Strips of double sided tape are used to create a chamber of 100 µm height. Additional tape is applied to provide stability for the chamber during handling and experimentation. B) Cartoon of the cross sectional view of the chamber. C) Cartoon of the top down view of the chamber. The sample is loaded into the chamber by placing it on the narrow strip where the bottom substrate is exposed. The sample is then drawn into the chamber through capillary forces.

3.2.8 Measurement for OET

For experiments with the optoelectronic tweezers configuration the sample is placed at the opening of the chamber and drawn in by capillary forces. The OET chip was then placed on an inverted microscope and the experiment was recorded with a video camera. During experimentation both the light pattern and the AC bias were applied. The video footage was evaluated by either counting out the lysed cells manually or using the LabView Vision Assistant software (National Instruments). A macro was written for Vision Assistant to automate the counting process.

The software first converts a frame of the video into a binary image and calculates the total area of the visible cells. This area was then divided by the average area of a red blood cell and this then gave the number of red blood cells currently visible in the frame. The number of RBCs before and after the lysis experiments was then used to determine the percentage of lysed cells. This process was verified by comparing hand counts and automatic counts of the same frame and there was found to be only a small difference (less than 5%) in the number of cells. This small discrepancy could easily be due to human error rather than inconsistency in the algorithm.

An important step in ensuring that the algorithm was accurate is to set the correct initial threshold filter when converting the video frame to a binary image. Figure 3-10 demonstrates how an inaccurately set filter will cause red blood cells to be removed accidentally from the image (or artefacts might be created from dark spots that are not cells). This setting of the threshold has to be done for every video individually to ensure accurate counting.

For very low numbers of cells, the software showed difficulty in identifying cells. Often, darker areas of background were mistaken as cells. In order to avoid this, frames with low numbers of cells were counted manually instead.

Another limitation of this algorithm is that it can only identify a single cell type at a time. A mixture of cells cannot be processed automatically but has to be counted manually instead.
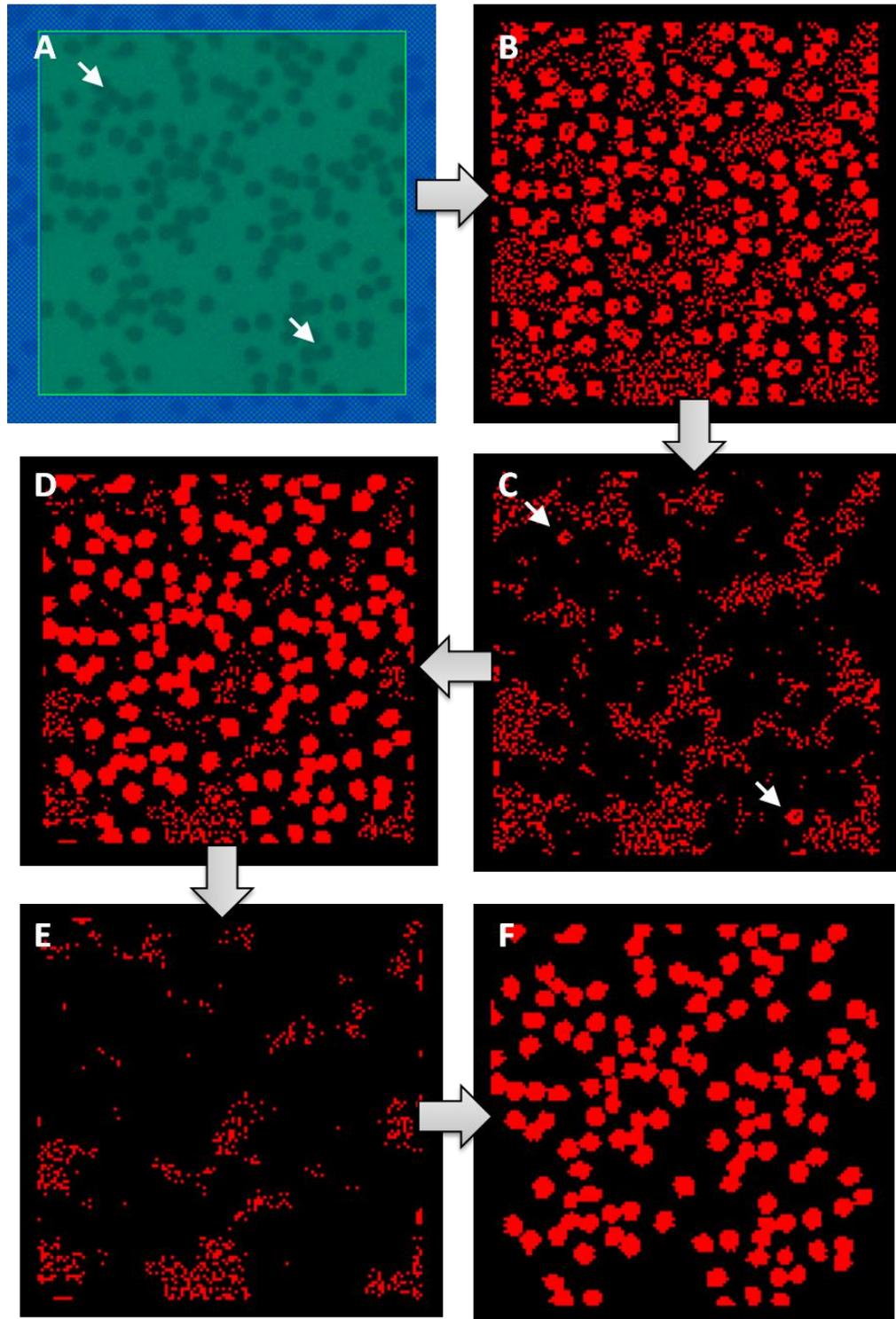
Figure 3-10: Example of the automated cell counting algorithm used to determine the number of red blood cells. A) Frame from the experiment with the region of interest (ROI) highlighted. This ROI has to be set by hand prior to the application of the counting macro. B) The software converts the full colour image to a binary image using a certain threshold. C) In order to allow automated counting of cells, the software needs to remove all small objects from the image. In order to determine if the software will not create errors by removing valid cells from the frame, the objects that are to be removed can be displayed. In this example, the threshold was set incorrectly as two RBCs would be removed from the image (marked with white arrows in C and A). In D) and E), the threshold was then corrected until only background is removed from the image. F) Final image after the correct threshold has been applied. The software then calculates the total area taken up by the cells and this was then divided by the area of an average RBC.

Chapter 4: Dielectrophoresis modelling

4.0 Abstract

In this Chapter, two different models will be applied to gauge the dielectrophoretic response of red blood cells and trypanosomes. The first is a model, developed by J. Gimsa [86], for ellipsoidal cells to estimate the Clausius-Mossotti factor (CM factor) of the two cell types. Then a COMSOL simulation is employed to give a visual representation of the total forces acting on the cells during a travelling wave experiment.

4.1 Summary of Methods

In order to better understand the frequency dependent polarisability response of trypanosomes and RBCs, a single shelled RC model of an ellipsoidal dielectric is implemented using a MATLAB (The Mathworks Inc.) environment. Similar dielectric models have been used to estimate the polarization forces acting on biological cells (e.g. [87]). Since the shape of a red blood cell or a trypanosome is not approximated well by a sphere (see Figure 4-2), a more complex model has to be applied than the one presented in Chapter 1. The method used here to compute the effective polarisability of ellipsoids has been described by J. Gimsa [86].

To obtain a better understanding of the influence of the travelling electric field, simulations were performed using *COMSOL Multiphysics, a finite element analysis* simulation software. A 2D geometry model of the spiral electrode array, later used for experimentation, was created where each electrode was defined as a thin strip of metal with 30 μm spacing between adjacent electrodes (the model represents a cross section through the array and the space above it). For Travelling Wave Dielectrophoresis (TW-DEP), four signals with phase shifts of 90° are applied to the electrode array in sequence, to generate a traveling electric field with a spatially dependent phase (See Figure 3-3). The magnitude and phase of the applied electric potential can be represented as a complex quantity. It can be written as $V=V_r+jV_i$, where V_r is the real part of the electric potential and V_i is the imaginary part of the electric potential. The values for the real and imaginary part of the electric potential at each electrode is assigned a peak amplitude of 1 V, to correspond to the experimental conditions

employed. After imposing certain boundary condition restrictions [88], as shown in Figure 4-1, the potential distribution was determined by solving Laplace's equation for the real and imaginary parts of the potential phasor. The electric field E is calculated using E= -∇V, and this is used to estimate the DEP force components.
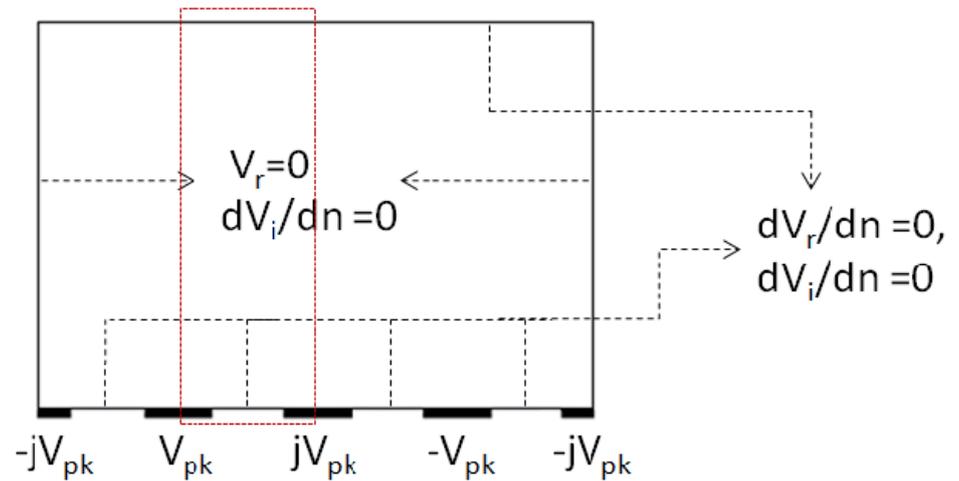
Figure 4-1: A schematic drawing of the 4-phase travelling wave electrode array showing the boundary conditions for solving Laplace's equation. The schematic represents a side view, 2D, cross section of the electrode array. The red box indicates the position of Figures 4-5 and 4-6. (image modified from [89])

4.2 Relevant Theory for Model

The model employed to determine the CM factor comprises of finite RC elements, represented by a complex conductivity σ^*, possessing equal cross-sectional area A and the length of each element, l, was given by the dimensions of the cytoplasm, membrane and the external medium.
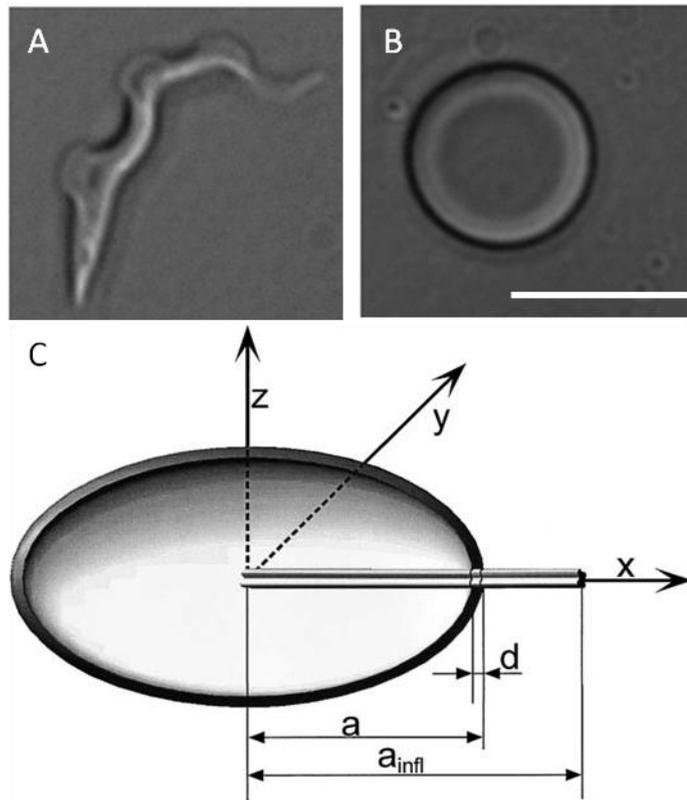
Figure 4-2: A, B) Micrograph showing the shape of *T. brucei* and a human red blood cell (scale bar is 8 µm). C) Cartoon showing the parameters used for the model, described by J. Gimsa (image modified from [86]). Here d is the thickness of the cellular membrane, a the outer diameter of the cell along the major axis of the ellipsoid and a_infl is the influential radius of the cell along the a-axis.

The length of the external medium element was set to a value which includes the effect of the dipole field on the suspended medium. The model consisted of three impedance elements $Z_{i,a}^*$, $Z_{m,a}^*$ and $Z_{e,a}^*$, describing the interior of the cell, the cell membrane and the external medium respectively. An oblate ellipsoid model (a=b>c) is used for the RBCs and a prolate ellipsoidal model (a>b=c) is used for trypanosomes. The Clausius-Mossotti factor CM_a of a cell oriented along its major axis is given by

$$CM_{a=}\frac{a_{infl}}{a_{infl}-a}\left(1-\frac{Z_{i,a}^*+Z_{m,a}^*}{Z_{i,a}^*+Z_{m,a}^*+Z_{e,a}^*}\frac{a_{infl}}{a}\right) \qquad \text{[Eq. 4.2-1]}$$

with

$$Z^*=\frac{1}{\sigma^*}\frac{l}{A} \qquad \text{[Eq. 4.2-2]}$$

$$\sigma^*=\sigma+j\omega\varepsilon_o\varepsilon_r \qquad \text{[Eq. 4.2-3]}$$

where a_{infl} is the influential radius (along the major axis). In our model it was calculated using depolarising factors (see [86] for further details). The outer diameter of the cell along the major axis is given by a and ε_o and ε_r are the absolute and relative permittivity respectively.

4.3 Results

Using values for mouse red blood cells from the literature [90] and applying the same values, except for the particle dimensions, for trypanosomes shows the difference in the CM factor solely due to the geometry of the cells. An example of a calculation using a medium conductivity of 30 mS/m is presented below.
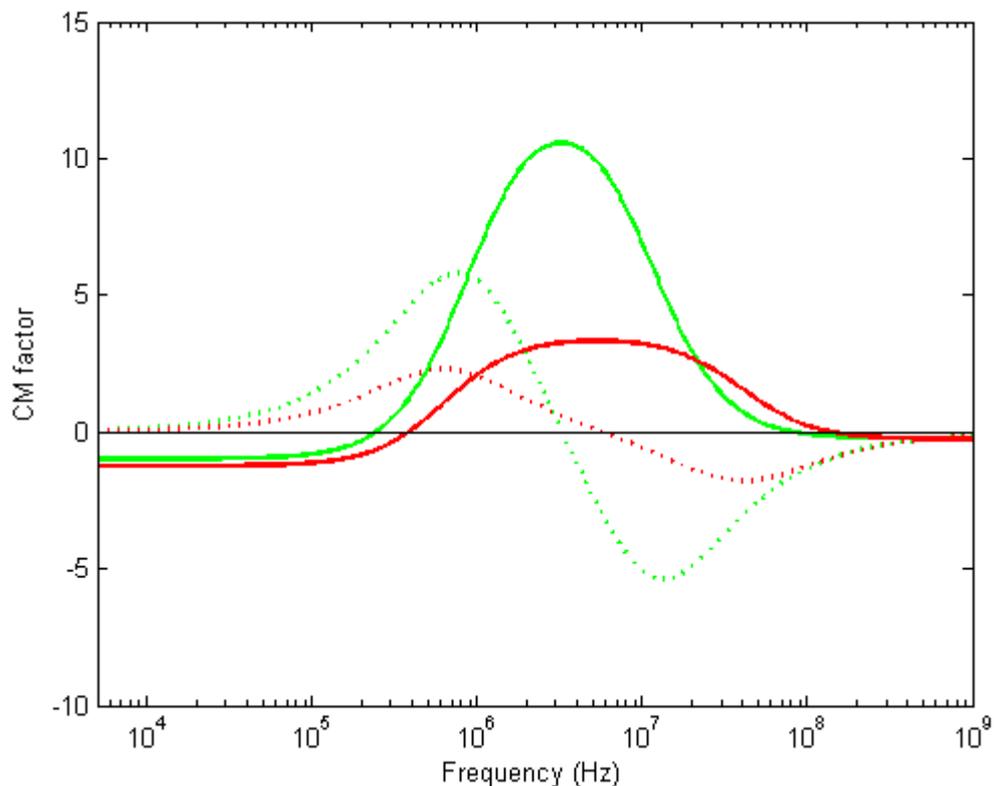
Figure 4-3: Calculated CM factor for red blood cells (red) and trypanosomes (green) using values for the dielectric properties from the literature[90]. The only differences between the two calculations are the dimensions of the cells applied in the ellipsoidal model. The solid lines show the real and the dotted lines show the imaginary part of the CM factor.

As can be seen from Figure 4-3, the crossover frequency (zero-point of the real part of the CM factor) of the trypanosomes is lower than that of the red blood cells. This is in accordance to the experimental data (see Chapter Five). The

actual values for the crossover frequencies (~250 kHz for trypanosomes and ~380 kHz for RBCs) however are much higher than in the experiments (for a medium conductivity of 30 mS/m). In order to better reflect our experimental results in the modelling, the permittivity of both the RBC and trypanosome cell membrane and their intracellular conductivity was changed in an iterative procedure until the crossover frequencies matched the experiment. The dielectric parameters used in the model are detailed in Table 4-1. The value for the CM factor derived from this model was used later to estimate the force acting on the particles (see 3.4).

Parameter	RBC value	Trypanosome value
Semi-major axis length (m)	3.3e-6	9e-6
Semi-minor axis length (m)	1.25e-6	1.2e-6
Membrane thickness (m)	8e-9	8e-9
Relative permittivities		
- Internal permittivity	60	60
-Membrane permittivity	12.64	19.87
-Medium permittivity	79	79
Conductivities (S/m)		
-Internal conductivity	0.8	0.8
-Membrane conductivity	1e-6	1e-6
-Medium conductivity	30e-6	30e-6

Table 4-1: Dielectric parameter values used for RBCs and trypanosomes in the single shelled ellipsoidal RC model employed in this work.

Figure 4-4 shows the simulated frequency dependant polarisability response of trypanosomes and RBCs obtained from the model, using these parameters. At low frequencies, as a result of capacitive membrane insulation, the effective polarisability of both cell types is less than that of the surrounding medium. Above the critical cross over frequency, the effective polarisability of the cell exceeds that of the medium, and the CM factor is positive. For viable

trypanosomes and RBCs with intact insulating membranes, the main contributions to the difference in frequency at which each cell type transitions from negative to positive are due to differences in cell size and shape. For trypanosomes, the value of the positive peaks for the real and imaginary part of the CM factor is much higher than that of RBCs. This is due to the difference in the shape of the two cells. The CM factor is also larger than what would be expected using Equation 1.1-5 (which limits the minimum and maximum values to -0.5 and 1.0 respectively) because it was defined differently in this model (see Equation 4.2-1).
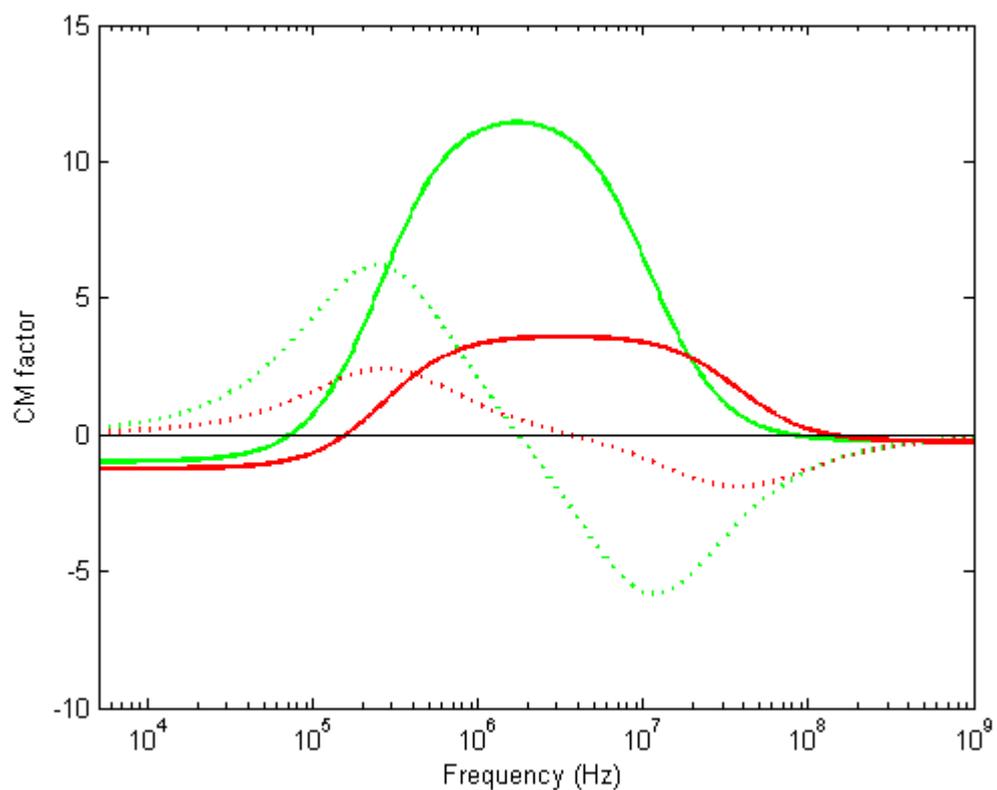
Figure 4-4: MATLAB simulation of the real and imaginary parts of the CM Factor for trypanosomes (green) and mouse RBCs (red) when the semi-major axis is oriented parallel to the electric field. The solid lines show the real and the dotted lines show the imaginary part of the CM factor.

The obtained values for the Cm factor were used to generate COMSOL models to represent the individual components of the force acting on the cell as well as the combined total DEP force during TW-DEP.

In Figure 4-5 A, the ∇E^2 vector direction for positive DEP conditions (Re(CM)>0) is vertically downwards onto the electrode edges. For negative DEP conditions (Re(CM)<0), not shown here, the vector arrows will be directed upwards resulting in the levitation of cells above the electrode plane. The factor ∇E^2 is minimal in the middle of the gap between the electrodes and reaches a maximum at the edge of the electrodes. The DEP force extends above the electrode, but with decreasing strength, i.e. at 20 μm above the electrode surface, the factor ∇E^2, has decreased by two orders of magnitude.

Figure 4-5 B shows the direction and magnitude of $E_{xo}^2 \nabla \varphi_x + E_{yo}^2 \nabla \varphi_y + E_{zo}^2 \nabla \varphi_z$ vectors above a four-phase electrode array. It can be observed that for heights greater than 10 µm, the vectors are oriented in the opposite direction of the travelling electric field, but for heights < 10 µm, the vectors are largely oriented in the same direction as the travelling field.
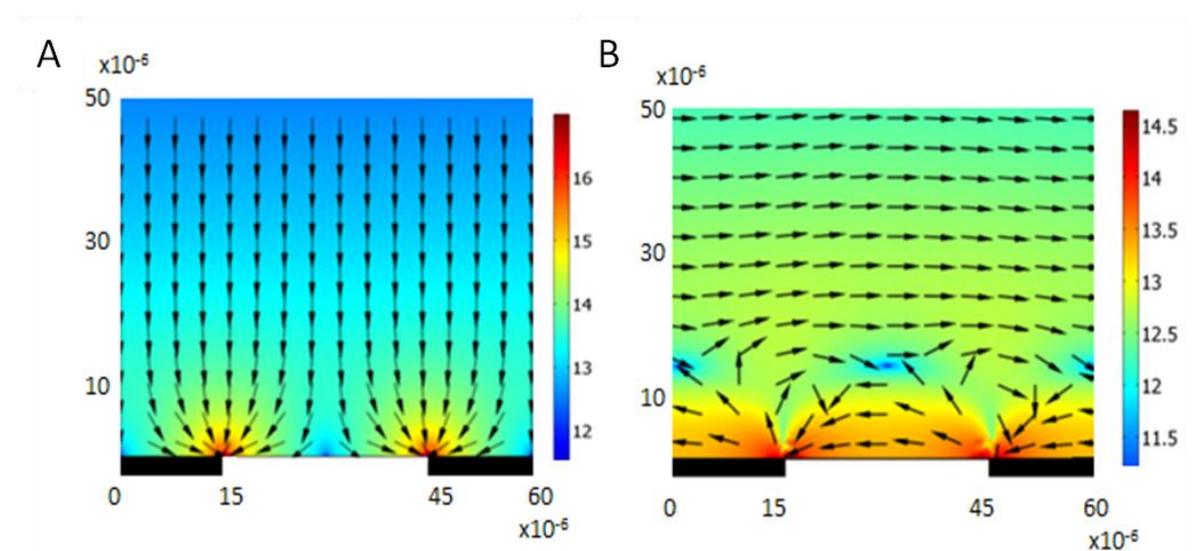
Figure 4-5: COMSOL simulation of the spatial variation of the DEP force components. Both plots show a vertical section along the electrode plane (electrodes represented by black rectangles at the bottom). The arrows represent the vector direction of the force components and the surface plot represents the magnitude of the force components (V²/m³, log₁₀ scale). The x and y scale are in metres. A) shows the spatial variation of ∇E for positive DEP, whilst B) shows the spatial variation of E²∇φ. (image modified from [89])

A spatial profile of the magnitude and direction of the DEP force was necessary to understand the differences in manipulation of trypanosomes and RBCs. This was obtained by solving Equation 1.1.1-2 with CM factor values corresponding to a frequency of a 140 kHz (taken from Figure 4-4). While Figure 4-5 shows the direction of the individual force components (F_{cDEP} and F_{twDEP} respectively), the

simulated total translational forces ($F_{DEP} = F_{cDEP} + F_{twDEP}$) acting on the two cell types are shown in Figure 4-6. The vector direction indicates that the trypanosomes experience a combination of positive DEP trapping forces and a co-field translational movement at the electrode plane. The magnitude of the force was maximum at the edge of the electrodes and was found to decrease rapidly with increase in height. For RBCs, a combination of Re(CM)<0 and Im(CM)>0, results in levitation to a height >20 μm followed by anti-field TW-DEP translational motion.
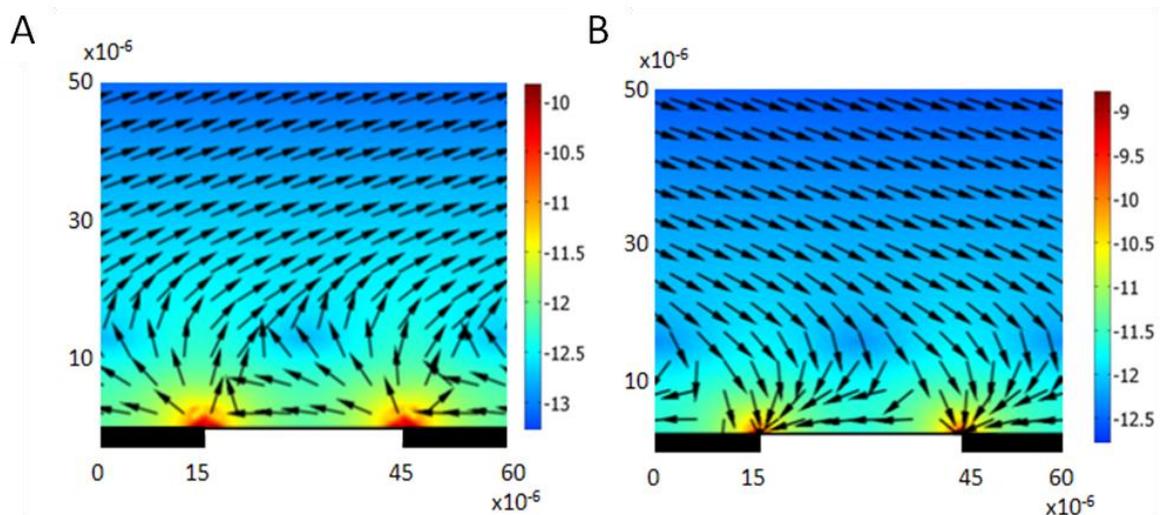
Figure 4-6: A vertical section along the electrode plane showing the spatial variation of the total DEP force. The arrows represent the vector direction of the force and the surface plot represents the magnitude of the force (log$_{10}$ scale). X and Y axis are in meter. A) Spatial variation of the DEP force acting on mouse RBCs at 140 kHz. B) Spatial variation of the DEP force acting on the trypanosomes at 140 kHz. (image modified from [89])

In summary, results from the COMSOL model indicate that DEP was capable of separating out red blood cells and trypanosomes due to different crossover frequencies (zero point of the real part of the CM factor). A frequency regime exists where the parasites undergo positive DEP while the RBCs undergo negative DEP.

Furthermore TW-DEP allowed for the enrichment of trypanosomes. The profile of the total force acting on the cells describes how the erythrocytes are moved up and out of the region containing the electrodes, while the trypanosomes are attracted to the edges of electrodes (at the bottom of the chamber containing the sample).

4.4 Discussion

It is important to put the presented modelling in this work into perspective. In general, a good model requires sufficient knowledge of the involved parameters. In this case the model of the Clausius-Mossoti factor relies on the knowledge of the relevant values of the cells, such as conductivity and permittivity of the cellular membrane and the intracellular medium. While literature exists about values for erythrocytes [90-92], no such sources could be found for trypanosomes. Several factors combine that make the determination of these values for a trypanosome a challenging proposition. Firstly, the intrinsic motility of the parasite interferes with determination of the crossover frequency as well as electro-rotation experiments. Secondly, the shape of the cell changes constantly as the trypanosome is stretching and twisting. The geometry itself is far-removed from the spherical shape, as used in most models, and in a given population the shape will differ from trypanosome to trypanosome. Even the ellipsoidal model by J. Gimsa [86] used here to estimate the CM factor is a relatively poor approximation of the slender dagger/corkscrew-like shape of the trypanosome. It is however a better approach than a spherical model.

Since the values for the trypanosome are not known, they were estimated on the basis of red blood cells (and within what seemed physiologically reasonable). This estimation was done to best reflect the experimental values that were determined for the crossover frequency of mouse erythrocytes and the capture frequency of trypanosomes. This capture frequency was used as a substitute crossover frequency in the model. Although the values used for the RBCs differ from the ones found by Asami *et al.*, the author feels their use is justified here. Asami and colleagues determined their values for erythrocytes that were swelled into a spherical shape using osmotic pressure (in order to fit their data to models using this spherical shape). It is possible that this process had an impact on the values, and in this work the cells were used in their original (biconcave) state. The most important observation, that the crossover frequency of the trypanosomes was lower than that of the red blood cells, could be confirmed even for identical values of conductivity and permittivity (see Figure 4-3).

The COMSOL simulation on the other hand seeks to explain the bidirectional character of the observed enrichment. The most important part is the reversal of the total force at very low altitudes above the electrode plane. This reversal

was already reported in earlier work [17] and, combined with the ability of the trypanosomes to detach themselves from the electrode edges, explains the observed movement of the parasites. The model, despite necessary shortcomings in addressing the values of the trypanosome, describes the observations well.

Chapter 5: Dielectrophoresis experimental

5.0 Abstract

In this chapter the experimental results of dielectrophoresis experiments will be presented and discussed. First a number of preparative experiments are shown to determine dielectric properties and overcome problems in sample preparation. Then travelling wave dielectrophoresis on a spiral electrode array is used as a tool to enrich trypanosomes from a sample of blood and various parameters are examined to determine optimal enrichment conditions.

5.1 Summary of Methods

In order to determine the feasibility of using dielectrophoresis as a tool to manipulate trypanosomes, a set of initial experiments was carried out. For these experiments *T. cyclops*, a different genus of trypanosomes, was used. These parasites are non-infectious to mammals found in the UK and can be used in biosafety level 1 facilities. While the two parasites are not closely related, they are very similar in shape and would be a good tool to infer the dielectric response of *T. brucei*.

The experimental values for the crossover frequencies were determined using the set of quadropole electrodes described in Section 3.2.5. Rather than observing individual cells, the majority (~90 %) of a sample was taken as an indicator of the sign of the DEP force. This means that the frequency values that correspond to a clear positive or negative response (see Figure 5-1) set the upper and lower error bars for the values found in Figure 5-3. This allowed for more repeatable results and greatly increased the number of cells being taken into account. Since the cells tended to settle after a short time, a new sample was loaded into the chamber for each frequency (and the chamber thoroughly cleaned, using 70 % ethanol, between each experiment).
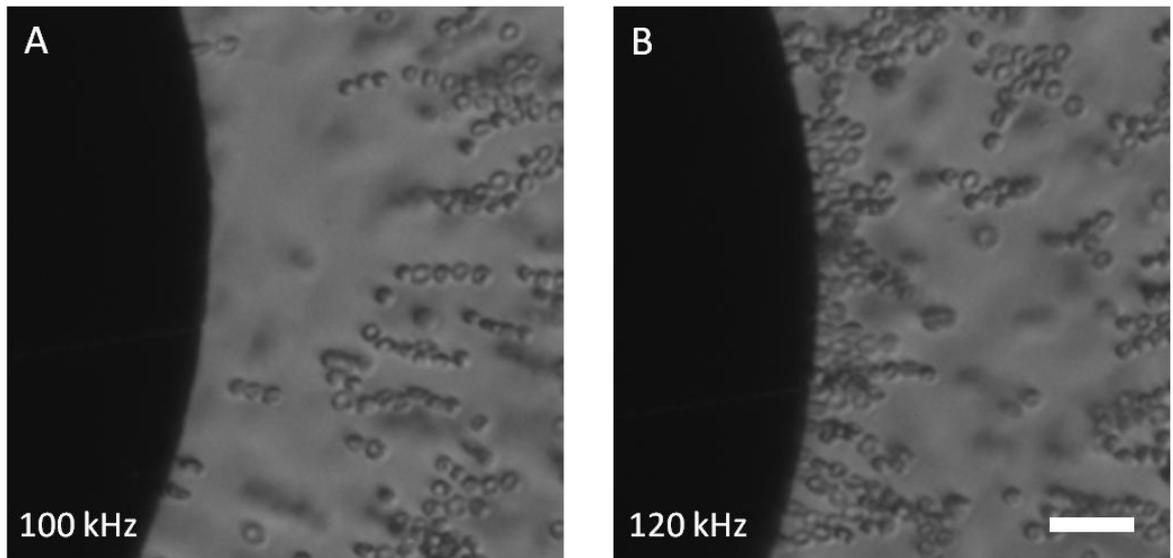
Figure 5-1: Quadrupole electrodes used for characterisation of cross-over frequencies. A) Mouse red blood cells undergoing negative DEP. At a frequency of 100 kHz the cells are predominantly experiencing a force repelling them from the edge of the electrode (edges are mostly clear). B) RBCs experiencing positive DEP at 120 kHz. The cells are predominantly attracted to the edges of the electrodes. Experiments were done at a medium conductivity of 16 mS/m (scale bar is 50 µm).

The two different trypes of spiral electrode arrays were used in this work. The first one was used only to asses experiments regarding particle density and all further experiments were done on the spiral electrode array shown in Figure 3-3. Here the electrode arms continue all the way into the centre of the array in order to allow complete removal of RBCs from the area as well as concentration of parasites into a small area at the centre of the array. The sample was washed three times in buffer solution (of desired conductivity) prior to applying it onto the chip.

The samples were viewed during experimentation with an upright microscope and the experiments recorded with a video camera for further evaluation.

5.2 Results

Initially cultured parasites (*T. cyclops*) were washed in DEP buffer medium (30 mS/m conductivity) and placed on a two dimensional array of interdigitated electrodes. The cells were exposed to a 20 kHz AC bias and it was observed that the erythrocytes underwent negative DEP while the trypanosomes underwent positive DEP (see Figure 5-2). The parasites were attracted to the edges of the

electrodes and remained trapped there. The RBCs are concentrated in regions of low electric field, between the electrodes.
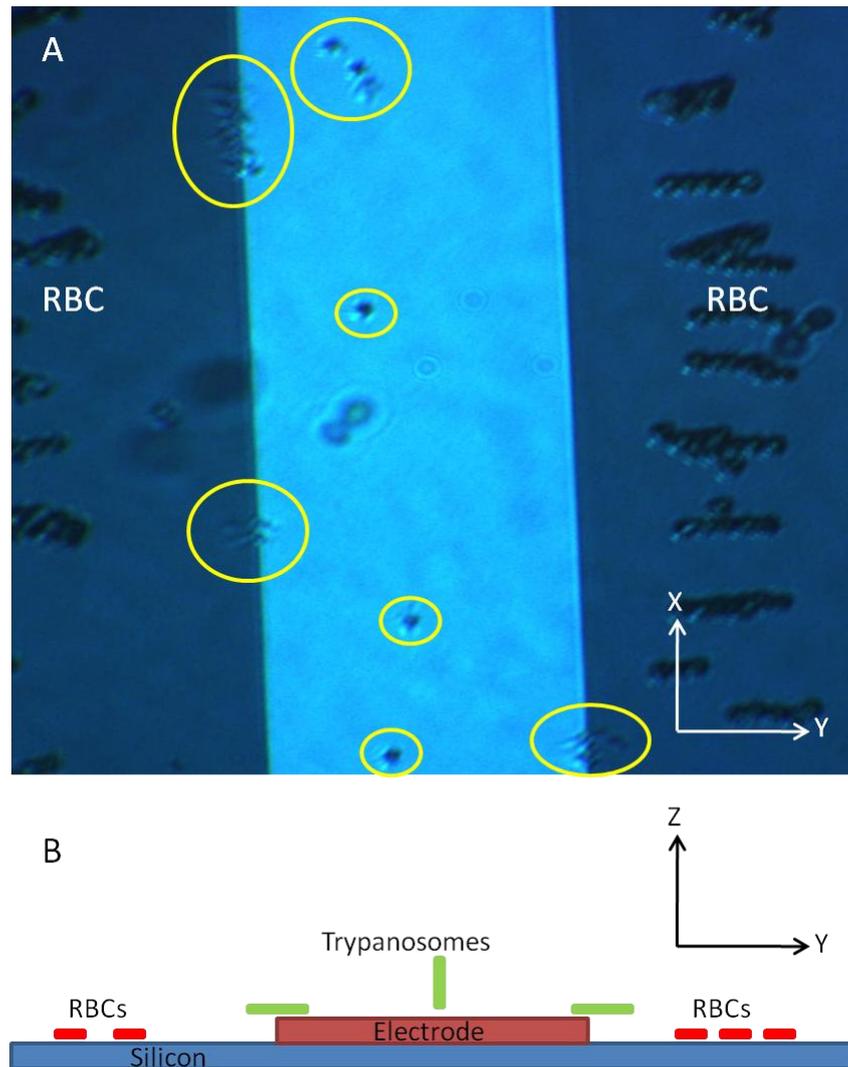
Figure 5-2: Initial Experiments with trypanosomes and red blood cells. A) Top down view of an experiment with *T. cyclops*. The trypanosomes experience positive DEP (marked with yellow circles) while the RBCs experience negative DEP and are aligned between the electrodes along the field lines. B) Side view schematic of the experiment. Interdigitated 100 µm electrodes (with 100 µm spacing) are patterned on silicon.

Next, the crossover frequency was determined. As was discussed in Chapter 1, the crossover frequency marks the frequency where the Clausius-Mossotti factor transits from one sign (positive or negative) to another. It is an intrinsic trait of cells and particles directly related to their dielectric behaviour. This value is of paramount importance for the experimental separation of different cells. The cells DEP response is observed after suspending them in a medium of known conductivity and exposing them to a non-uniform electric field of a certain frequency.

Results of the experimental characterisation of the three cells (human erythrocytes, mouse erythrocytes and trypanosomes) in working solutions of different conductivities varying from 16 mS/m to 60 mS/m are shown below (Figure 5-3). For trypanosomes, the frequencies ranged from 20 kHz to 150 kHz. For mouse RBCs crossover frequencies ranged from 100 kHz to 380 kHz, whereas for human RBCs, values were found to vary from 60 kHz to 260 kHz. For a solution conductivity of 30 mS/m, the optimal enrichment frequency was determined to be ~140 kHz for trypanosomes among mouse RBCs. The larger crossover frequencies for mouse RBCs can be attributed to a smaller mean diameter of 6 μm compared to 8 μm for human RBCs.
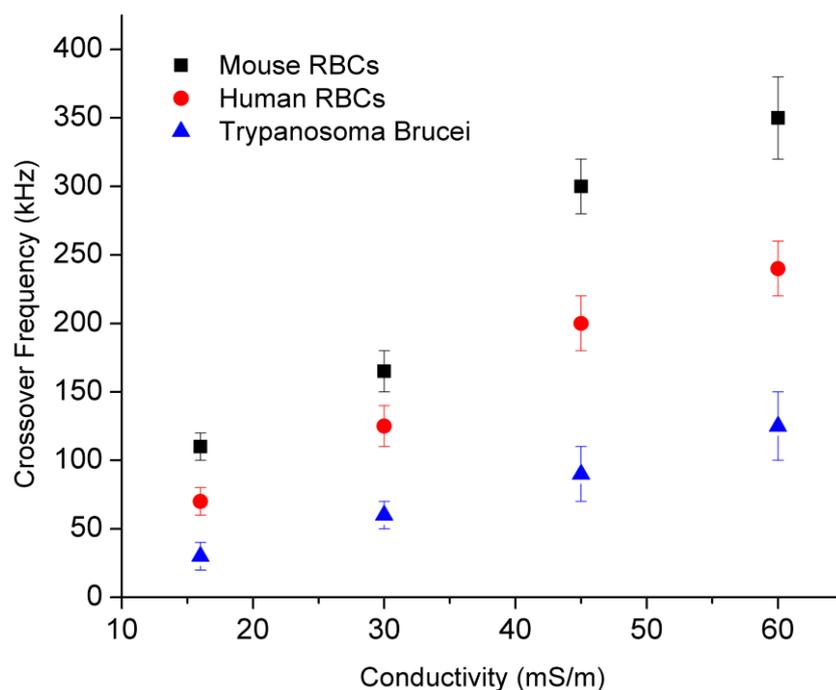
Figure 5-3: Correlation between solution conductivity (16, 30, 45 and 60 mS/m) and capture frequency of mouse RBCs, human RBCs and trypanosomes. The values mark the frequency at which the DEP force changes sign. For frequencies below the indicated value cells experience negative DEP and for frequencies above, the cells experience positive DEP.

Overall, the error of the observed crossover frequency increased with higher medium conductivity as the cells showed a more varied response. Although this was mitigated by prompt use of blood, the amount of time suspended in the buffer medium had a visible effect on the crossover frequency.

It should be noted that the frequency for trypanosomes is not the actual crossover frequency but rather a 'trapping frequency' where the DEP force is strong enough to hold the parasites at the edges of the electrodes. The actual

crossover frequency is impossible (or very difficult) to observe for motile cells as their own movement covers up any weakly positive or negative DEP force acting on the cells. More importantly, for the purpose of the further experimentation only the trapping frequency is of interest since the cells need to be trapped at the electrodes (positive DEP) in order to separate them from the RBCs. The real crossover frequencies for trypanosomes will be less than the values presented here.

5.2.1 Enrichment of trypanosomes using travelling wave dielectrophoresis

In order to confirm the complete expulsion of red blood cells from the spiral area, both human and mouse red blood cells were tested for conductivities of 30 mS/m for a number of frequencies (80 kHz to 180 kHz). As is to be expected from Figure 5-3, the red blood cells experience negative DEP for frequencies below 160 kHz and are levitated above the electrode surface. The RBCs then move outward from the spiral and collect at the outer edge, beyond the last electrode ring (see Figure 5-4, A-D). As the frequency increases more and more RBCs settle on the bottom of the electrodes instead of being moved out of the spiral (see Figure 5-4 E-G).

Removal of red blood cells took about 5 minutes at a 1 in 20 dilution for a voltage of 2 V_{pk-pk}. The trypanosomes underwent positive DEP and were trapped at the edges of the electrodes. However the inward movement and consequently the enrichment of trypanosomes, was observed without the need to superimpose a second signal or the use of a time course experiment. The trypanosomes began travelling into the centre of the electrode array while the red blood cells simultaneously travelled to the outside of the spiral, thus achieving bidirectional TW-DEP (see Figures 5-5 and 5-6).
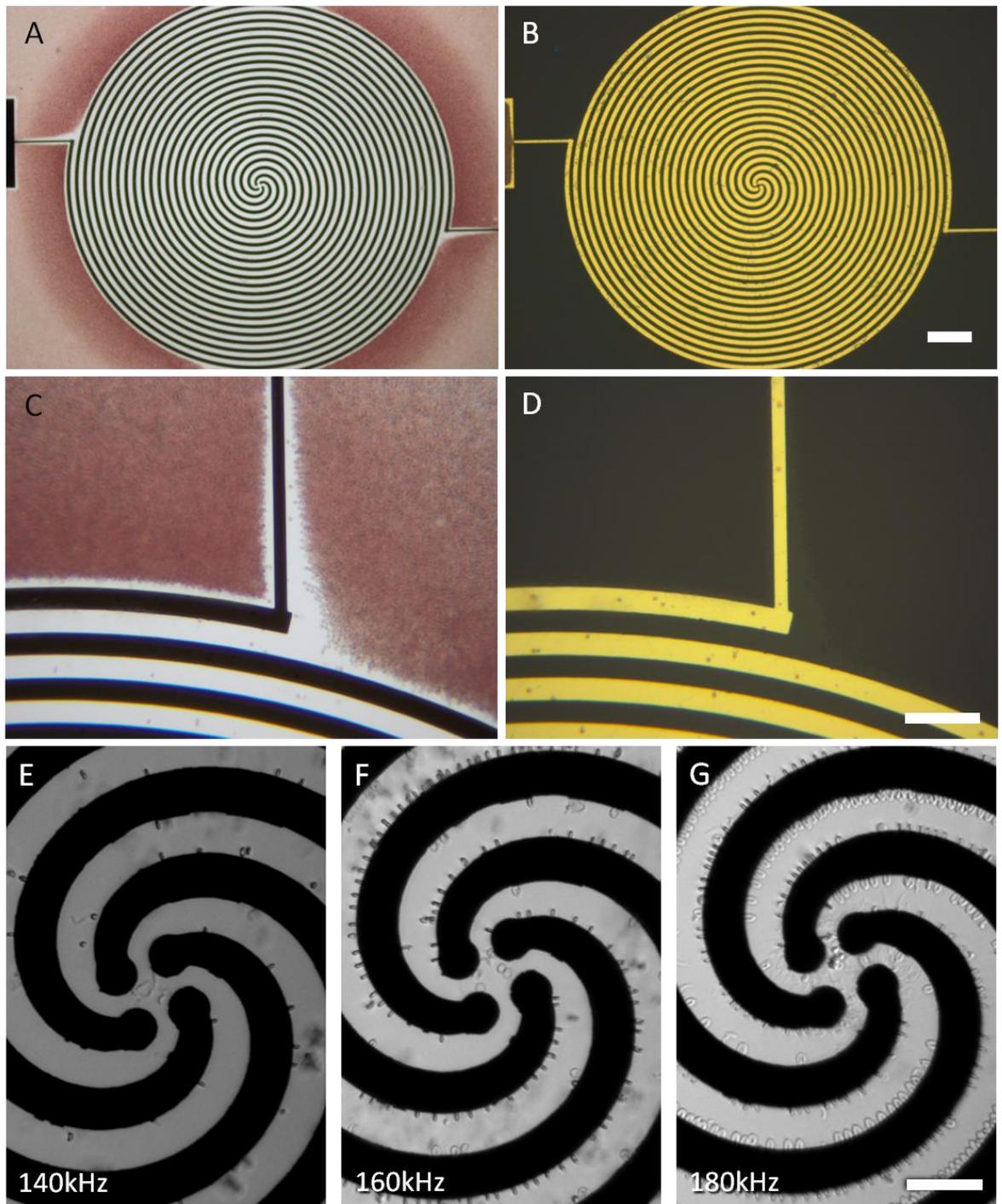
Figure 5-4: Removal of red blood cells from the spiral electrode array. Experiment was performed with a medium conductivity of 30 mS/m, a voltage of 2 V$_{pk-pk}$ and a frequency of 100 kHz. A-D) RGB colour micrographs of red blood cells after their removal from the array. A) and B) scale bar is 300 µm and C) and D) scale bar is 100 µm. A) and C) show fields of view with illumination from the bottom. Electrodes appear black and the red blood cells were clearly visible (being repelled by the electrodes). B) and D) show the same fields of view, but with illumination from the top. The electrodes (appearing in gold due to the reflected light) themselves were also cleared of red blood cells. E-G) show the effect of increased frequency as the crossover frequency of the red blood cells was approached. More and more erythrocytes undergo positive DEP and are attracted to the electrode edges. E-G) Scale bar is 50 µm.
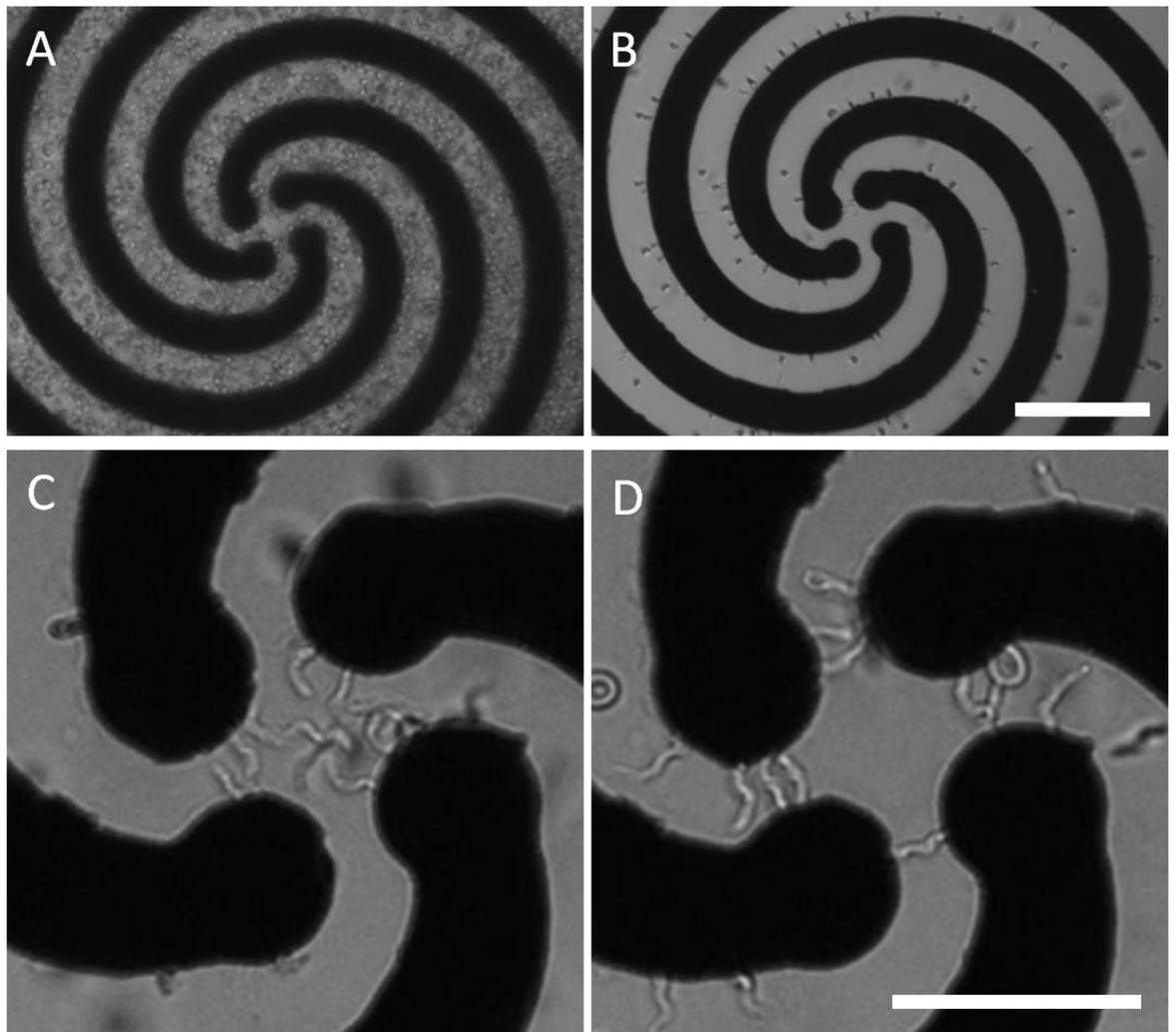
Figure 5-5: Enrichment of trypanosomes using bidirectional TW-DEP. A) and B) show the removal of red blood cells from the electrode array (scale bar is 100 µm). C) Close up of the centre of the spiral where a number of trypanosomes have been concentrated after about 10 minutes. Trypanosomes undergo circular motion in the centre of the array. D) The trypanosomes are trapped between the electrodes once the field is switched to two-phase. C) and D) scale bar is 50 µm.

Once inside the central area of the electrodes, the trypanosomes began to undergo circular translational motion. Once the field was changed from quadrature-phase to opposing two-phase, the cells exhibited normal positive DEP and were trapped between the electrodes (see Figure 5-5, D).

This inward movement of the parasites was only observed at the height (focal plane) of the electrodes. The trypanosomes were retained at the edges of the electrodes until detaching themselves and moving rapidly to the next electrode edge. While removal of the RBCs took approximately ~5 min another ~5 min were necessary to collect most trypanosomes. For a field with 140 kHz and 2 V_{pk-pk} the trypanosomes were trapped for an average of 6 to 13 seconds at the

electrode edges while it took them only 3.5 seconds to cross the gap between adjacent electrodes (average values from 10 parasites, see Figure 5-6).

The time spent at the edge of an electrode varied greatly and seemed to be dependent on the orientation of the trypanosome. The trypanosome is highly asymmetrical in shape and has one 'blunt' end and one 'pointy' end. The flagellum wraps around the cell and extends outward from the 'pointy' end (also see Figure 4-2). The parasite moves in the direction of the flagellum (it is pulled by the corkscrew like motion of the cell) in a complex pattern [93].

In the experiments the trypanosomes were observed to be either facing with their flagellum toward the electrode edges or away from it, but always at a near perpendicular angle with regard to the edge. Parasites that were facing away from the electrode edge spent less time trapped, while those that were facing the trapping region took longer to escape. Often the trypanosome would reverse its facing before escaping the entrapment region. The time spent moving between electrodes was much shorter and the trypanosome usually moved straight toward the next electrode edge.
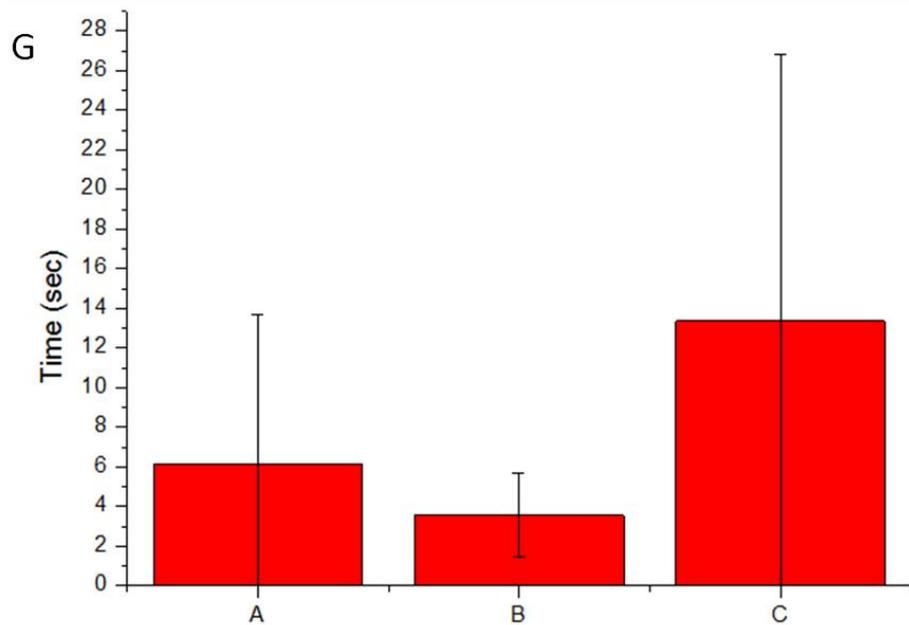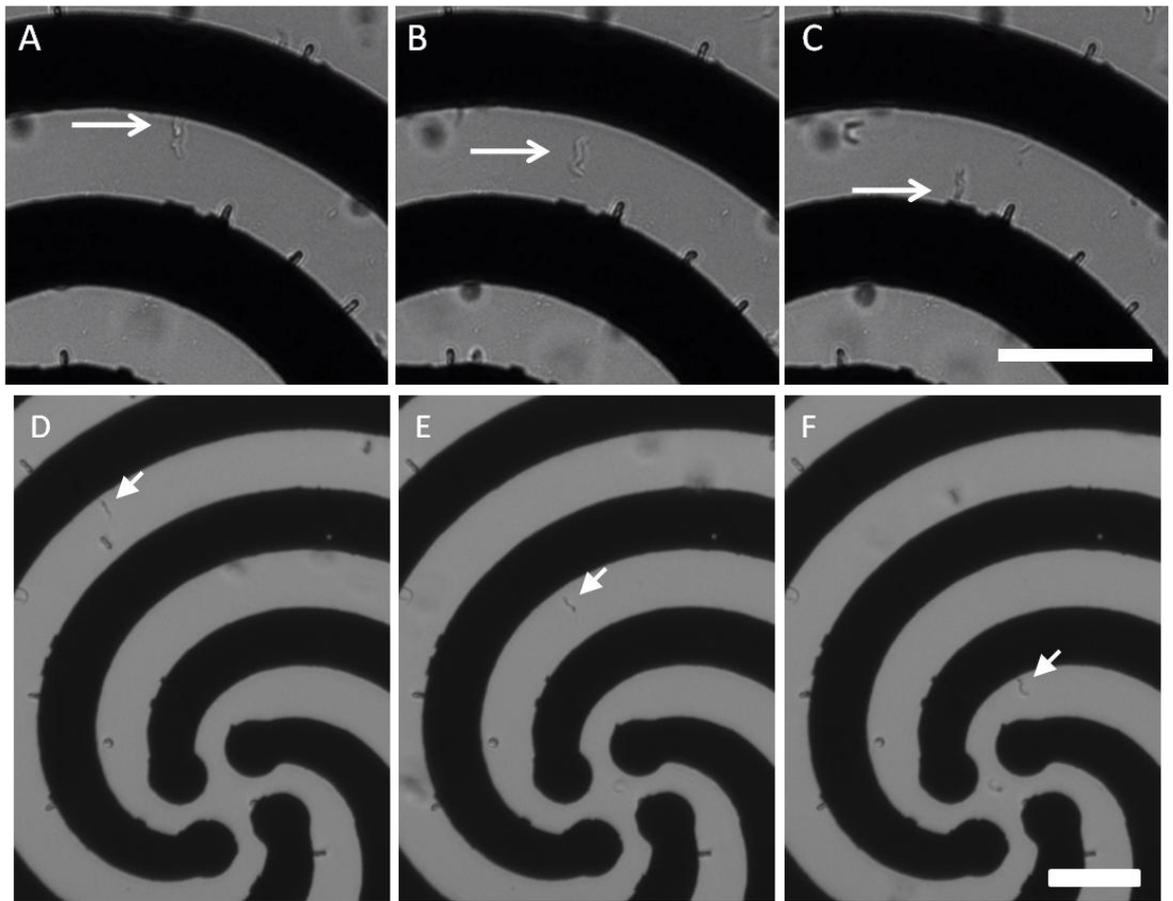
Figure 5-6: Inward movement of a trypanosome due to TW-DEP. The trypanosome (marked with the white arrow) was momentarily trapped at the edges of the electrodes and then detached itself and quickly transversed the space to the next electrode. A) Trypanosome trapped at the inner edge of an electrode. B) Trypanosome between electrodes. C) Trypanosome trapped at outer edge of an electrode. Scale bar is 50 μm. D-F) show an overview of a trypanosome travelling into the centre of the spiral. Scale is 50 μm. G) Average time of a trypanosome trapped at the corresponding positions (A, B, C) for 140 kHz, $2V_{pk-pk}$. Averaged from 10 parasites, error is standard deviation.

White blood cells also underwent positive DEP (due to their large size) but, unlike trypanosomes, were not observed to move into the central region of the spiral. The WBCs differ in shape and size from the trypanosomes but more importantly show no intrinsic motility. While the trypanosomes are seen using their flagellum to detach themselves from the edges of the electrodes, the leukocytes remain stationary during the experiment (see Figure 5-7).
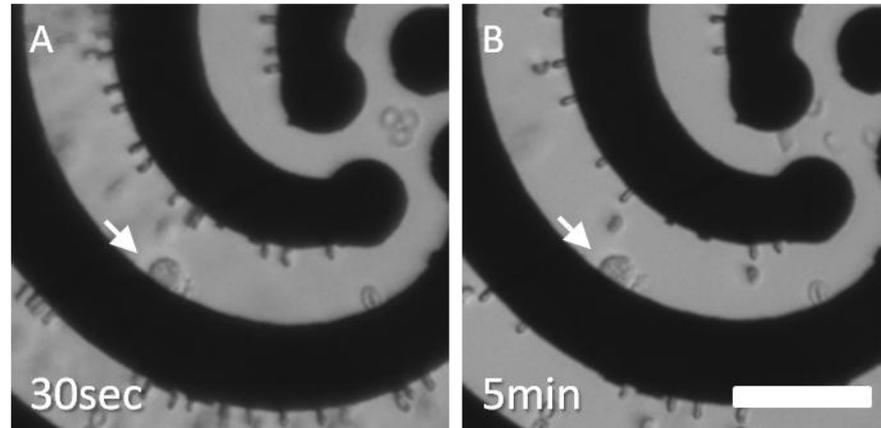
Figure 5-7: A white blood cell (white arrow) undergoing positive DEP. The cell is trapped at the edges of the electrode and does not move into the centre of the electrode. The red blood cells initially in the centre of the array (A) are expelled over time and trypanosomes enter the central area (B). Scale bar is 50 μ.

In order to quantify the enrichment process a number of videos were recorded and evaluated for different voltages and frequencies. Both the velocity of the trypanosomes and the enrichment number were recorded for voltages of 2, 3 and 4 V_{pk-pk}, as well as for frequencies between 100 kHz and 160 kHz.

Increasing the voltage from 2 to 4 V_{pk-pk} increased the average velocity from 3 μm/sec to 11 μm/sec, with the observed increase seeming to be linear with regards to voltage (see Figure 5-8).

Increased voltages lead to increased enrichment numbers. The enrichment numbers at 4 V_{pk-pk} were approximately twice as high as those for 2 V_{pk-pk}. It was observed however that for voltages above 2 V_{pk-pk} the trypanosomes were lysed as they entered the central area of the spiral between the tips of the electrode arms. No adverse effect of the voltage on the parasites was observed as they travelled from one electrode arm to the next, however the total voltage drop across the central region (with the electrodes at opposite corners having opposed phases) is much increased. Since lysis made detection of the parasites

impossible, a potential of 2 volts was used for further experiments to study the effect of frequency.
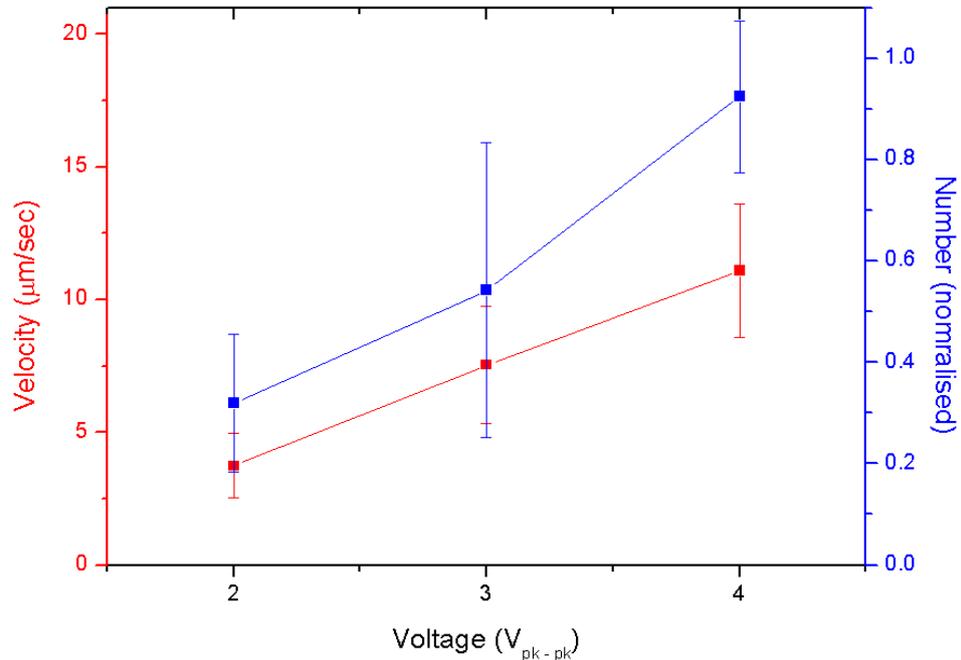
Figure 5-8: Voltage dependency of the velocity and the enrichment numbers during TW-DEP enrichment. Experiments were carried out with a fixed frequency of 140 kHz and a medium conductivity of 30 mS/m. Each data point is averaged from >7 experiments, error is standard deviation.

For frequencies of 80 kHz, or below, the positive DEP force on the trypanosomes was not strong enough to trap them at the electrode edges and no trypanosomes were observed at the electrodes of the array. An increase in enrichment numbers is observed for frequencies ranging from 100 kHz to 140 KHz, but at a frequency of 160 KHz, the enrichment numbers begin to fall (see Figure 5-9). This is due to the fact that for frequencies above 160 kHz the number of red blood cells that remain trapped at the electrode edges increases drastically, impeding the inward movement of the trypanosomes (see Figure 5-4, E-G).

Furthermore a gradual increase in velocity with increase in frequency was observed. Considering these results the optimal enrichment conditions are given for an electric field of 140 kHz and 2 V_{pk-pk}.
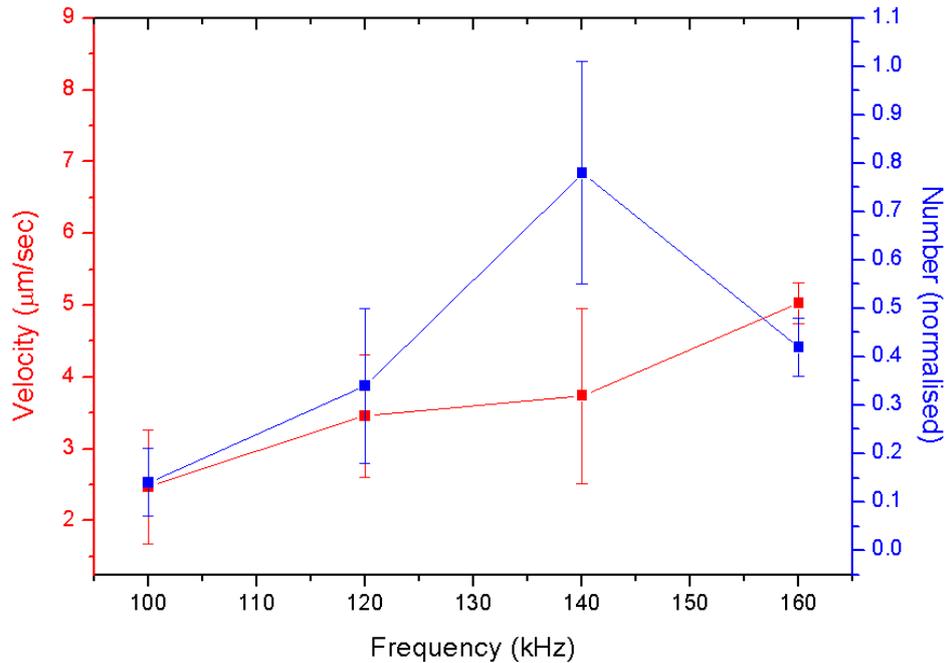
Figure 5-9: Frequency dependence of enrichment number and velocity for a set voltage at 2 V$_{pk-pk}$ and a medium conductivity of 30 mS/m. >7 experiments were evaluated for each data point, error is standard deviation.

5.2.2 Enrichment after dilution

While washing the sample in DEP buffer gives very good control over the conductivity, it requires the use of centrifuges. These can be difficult to operate in the field however. Since the technique is supposed to present an improvement over the current methods of detection it was highly desirable to demonstrate that the enrichment process would also work without the need for centrifugation. This was done using a two step dilution process of 20 fold dilution in trypsin-buffer and a further 2 fold dilution in inhibitor-buffer. Under these conditions enrichment was easy to demonstrate (at 140 kHz and 2 V$_{pk-pk}$) and experiments were carried out to determine the sensitivity of the device (see below).

5.2.3 Enrichment from human blood

While mouse blood is a good model, since the samples come directly from infected animals 'in vivo', the applicability of human blood needs to be verified.

Human blood contains the trypanosome lytic factor (TLF) as part of the plasma. This prevents the direct mixture of whole blood and cultured *T. brucei*, as the TLF would lyse the parasites. The human erythrocytes need to be washed and re-suspended in suitable DEP buffer medium to be used. The enrichment was demonstrated for a medium conductivity of 30 mS/m and frequencies of 100 and 120 kHz.

5.2.4 Sensitivity

The sensitivity was determined using the sampling volume as defined in Section 3.2.6. Under real experimental conditions the sensitivity is never 100 % as some parasites are pushed out of the spiral by RBCs undergoing TW-DEP, or simply fail to reach the centre of the spiral.

Experimental values were determined for different dilutions of parasites (see Section 3.2.6). An initial concentration of $5*10^5$ trypanosomes / ml was determined, which after a 1 in 20 dilution equates to approximately 25 parasites / µl. After washing the sample in 30 mS/m buffer and using optimal enrichment conditions (140 kHz and 2 V_{pk-pk}) an average of 5.75 (± 1.9) parasites were detected (n=7), giving a sensitivity of about 23 %. Experiments at 4 V_{pk-pk} gave increased numbers of parasites which improved this value to approximately 56 %. Given the current design of the electrode however, this value is of little use since the parasites were lysed upon entering the centre of the array (making detection impossible). Determining the initial concentration was difficult for such high concentrations of parasites from whole blood and more importantly it is unknown how many parasites are lost during the washing procedure (3 washing steps). In order to exclude these sources of error and to verify the sensitivity, a second set of experiments was conducted. The conductivity of a sample was adjusted through dilution and the concentration of parasites was then determined (again with a Neubauer chamber) to be approximately 7.5 parasites / µl (from an unknown starting concentration before dilution). For these experiments an average of 3.3 (± 1.2) parasites were detected (n=7), equating to a sensitivity of approximately 44 %. It should be noted however that with such a low average number of parasites being present in the sampling volume, even small variations in the number of parasites initially present have a large impact on the exact percentage of the determined sensitivity.

Applying these values to the limit of detection, one can assume that 3 parasites need to be present in the sampling volume to concentrate at least one into the centre of the array. This gives a value for the limit of detection of 1.2×10^5 parasites / ml. It should be noted here that while the limit of detection presented here is worse than the gold standard of $\sim 10^2$ parasites / ml (see 2.3.8) it can be improved through up-scaling (see discussion).

5.3 Discussion

TW-DEP proved to be a potent tool in manipulating samples of blood infected with *T. brucei*. It was possible to enrich trypanosomes into a small area at the centre of a spiral electrode array and simultaneously expel the red blood cells (bidirectional TW-DEP).

5.3.1 Bidirectional movement of cells

Interestingly, the bidirectional movement of cells could be created using only a single set of electrodes energised with only a single electrical signal. The inward motion of the parasites can be explained by the force profile in the TW-DEP setup (Figure 5-10). After the electrodes were energised the trypanosomes travel downward towards the bottom of the chamber (due to positive DEP) at an angle. Once at the bottom of the chip, the force switches direction and the parasites switch from anti- to co-field movement. This movement was directed toward the edges of the electrodes where the trypanosomes become trapped. Unlike other cells (like WBCs) however, the trypanosome is a motile organism and can detach itself from the electrode edges. The forces generated by the flagellum can be significant. Rodriguez *et al*. estimated that the forces the flagellum can generate are in the range of 300 pN (the average velocity of the flagellar tip is 500 µm/sec) [93]. After detaching itself from the electrode the trypanosome experiences the co-field force from the field again and travels towards the next electrode edge.

This also explains why white blood cells (or any non-motile cells for that matter) are not observed to travel into the centre of the array. They are unable to detach themselves from the electrode edges and remain trapped in their initial

position. The bidirectional movement is a direct consequence of the intrinsic mobility of one of the cells of interest.
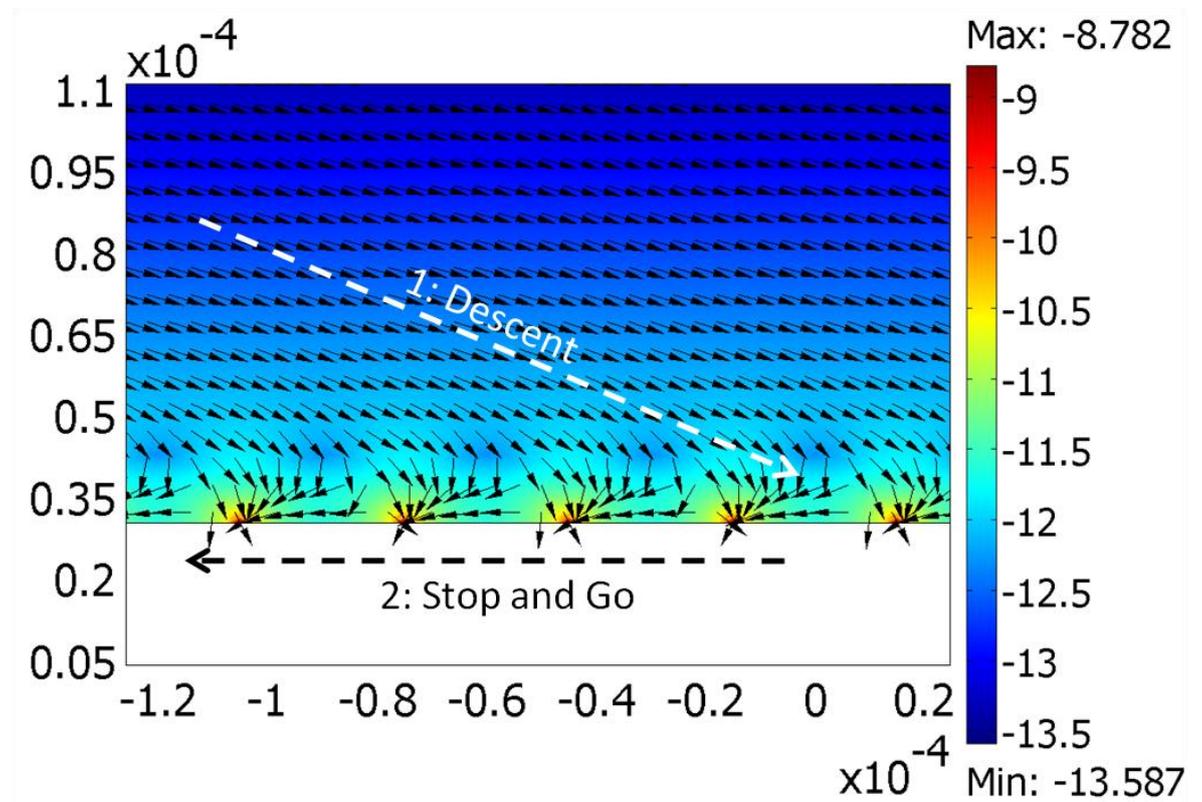
Figure 5-10: Profile of the total force acting on the trypanosomes during a TW-DEP experiment. This is the same simulation as in Figure 3-10, B. The movement of the trypanosomes follows two steps. First, the trypanosomes descend to the bottom of the chamber at an angle due to the positive DEP force. Then they travel from one electrode edge to the next since they can detach themselves due to their intrinsic motility (Stop and Go). The arrows represent the vector direction of the force and the surface plot represents the magnitude of the force (log$_{10}$ scale). X and Y axis are in metres.

5.3.2 *Characterisation of the TW-DEP experiments*

As can be seen from Figure 5-8, the increase in trypanosome velocity with increased voltage seems linear. Based on Equation 1.1.1-2 one might expect that the velocity with which the trypanosomes travel inward exhibits square voltage dependency (F_{twDEP} is proportional to E^2). The linear increase might be due to the increase of all components (in z direction as well as x and y) of the force.

The enrichment number increased with increased voltage, which was to be expected with an increase in velocity as more parasites enter the central region in the same amount of time. The downward (positive) DEP force also increased

with voltage leading to a more efficient trapping (and in turn, enrichment) of parasites.

A comparison of Figure 4-3 and Figure 4-4 (in Chapter 4) indicates that, in the frequency regime used for experimentation, the real and imaginary parts of the CM factor increase for the trypanosomes with increased frequency. Consequently an increase in enrichment numbers was observed for frequencies ranging from 100 kHz to 140 KHz. As pointed out in the Section above, at a frequency of 160 KHz the enrichment numbers begin to fall (due to the RBCs becoming trapped at the electrodes). Furthermore, a gradual increase in velocity with increase in frequency was observed. This can also be attributed to the increased CM factor, which helps to keep the trypanosomes closer to the electrode plane and provides stronger translational forces into the centre of the spiral.

5.3.3 Sensitivity and limit of detection

From the calculations in Section 5.2.5 it is obvious that the main limiting factor for the limit of detection is not the sensitivity of the device, but rather the dilution of the sample and the small sampling volume. Both can be addressed by increasing the sampling volume through up-scaling of the presented technique. Increasing the diameter of the spiral to about 1 cm (without changing the height of the chamber) will increase the sampling volume to approximately 12 µl. Care has to be taken to ensure that the electrodes are of sufficient thickness, otherwise the amount of voltage lost along the arms of the spiral is too great and the device no longer functions properly in the central region of the array. Provided the sensitivity of the device is not decreased (and the author sees no reason why this would be the case), this will lower the limit of detection to ~1 x 10^4 trypanosomes/ml. Further up-scaling (e.g. multiple spirals in parallel) can be imagined to reduce the limit of detection to the desired value (with 10^2 to 10^4 parasites / ml in the human host, see Chapter Two).

It should be noted, however, that these low levels of parasitemia have not been confirmed experimentally for detection using the technique. In general, the main limiting factor is the fact that the conductivity of the solution has to be low enough to generate the required forces for the technique. If the current technique can be optimized to include some pre-concentration step or be

combined with fluid flow to increase the sampling volume without increasing the size of the electrode array, the limit of detection could be improved.

Chapter 6: Electrically induced lysis modelling

6.0 Abstract

In this Chapter the electric field acting on a cell during an optoelectronic tweezers experiment will be modelled using COMSOL. The model will be used to draw conclusions about the induced transmembrane potential and the special influence the layer of amorphous silicon has on the cell.

6.1 Summary of methods

The analytical model used in this work was created using the COMSOL multi-physics, finite element analysis, software. Below is a schematic (not to scale) displaying the boundary conditions used in the model (Figure 6-1).
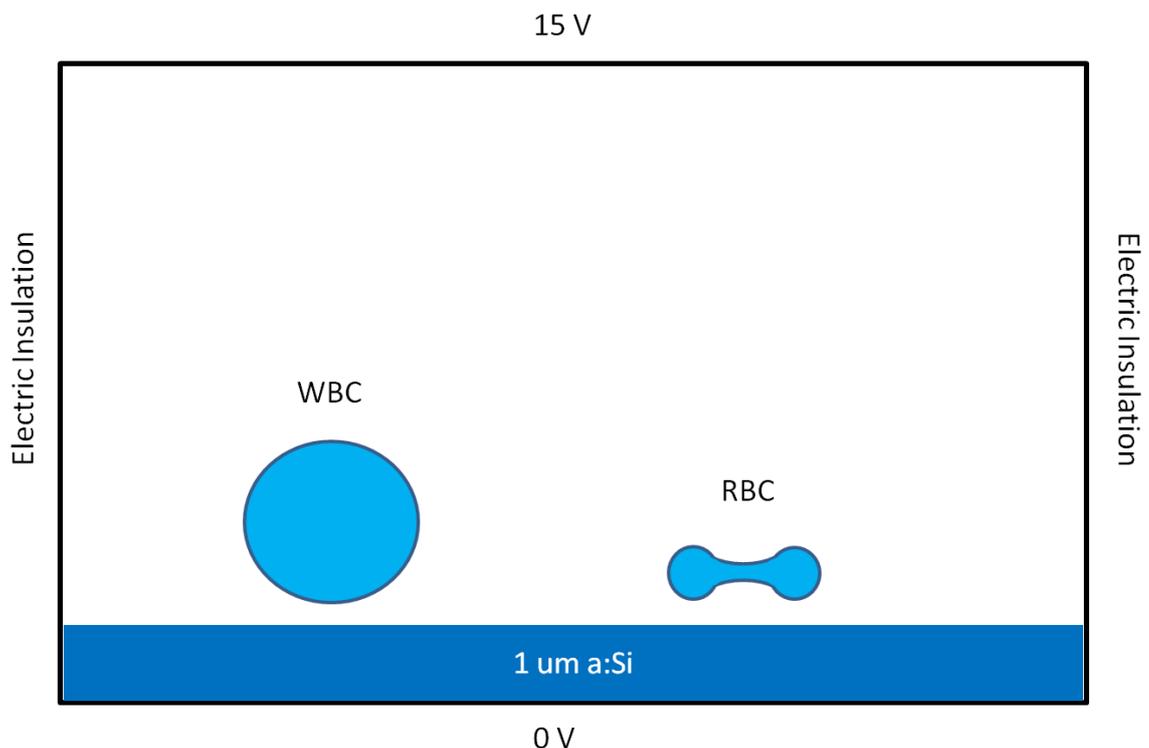
Figure 6-1: Cartoon (not to scale) of the boundary conditions and general layout used for the simulations. The cellular membranes are modelled as individual sub-domains. Boundary conditions are set to 'continuity' on all but the outer boundaries of the model (values indicated above).

The parameters for the geometry and the electric properties of the subdomains were chosen to represent the experimental conditions. The chamber height was 100 μm and the model used a 2D geometry representing a cross-section through

the electrodes, chamber and cells, including the cell membrane as a distinct subdomain with a thickness of 7 nm. All values used can be found in the Table below (Table 6-1), where ρ and σ are electric conductivity and relative permittivity respectively (-Mem. donates values for the membrane layer).

Values for the cellular membrane and the intracellular medium were taken from Chapter 4. Values for the amorphous silicon layer were (unless noted otherwise) taken from the literature[94].

	Shape	Height	Width	ρ*	ρ*-Mem.	σ	σ –Mem.
Chamber	Rectangular	100 μm	200 μm	25,100, 1400	-	79	-
a:Si layer	Rectangular	1 μm	200 μm	5.7e-3, 0.44†	-	14	-
RBC	Biconcave‡	3 μm	8 μm	800	1e-3	60	12.5
WBC	Spherical	10 μm	10 μm	800	1e-3	60	12.5

Table 6-1: Table for the parameters used for the COMSOL simulation. *All values in mS/m. † Dark state and Light state conductivity respectively, see text. ‡ Flattened biconcave for high conductivity, see text.

The conductivity of the amorphous silicon has two values, one for the illuminated state, another for the dark state – these values were generated by measuring the intensity of the light at the focal point (1.97 W/cm^2 and 1.99*10^{-2} W/cm^2 respectively) on the optoelectronic chip using an optical power meter (Thorlabs, PM100A) and comparing it to the literature[94]. In the simulation, the conductivity inside the a:Si layer changes from dark to light and back again, following a saturated Gaussian, in order to simulate the change in conductivity due to a light spot – thus causing the electric field inside the chamber to be non-uniform. The biconcave geometry of the red blood cell was created as a composite object of circles, ellipses and a rectangle. Figure 6-2 shows a simulation and the corresponding mesh for a medium conductivity of 25 mS/m and a frequency of 10 kHz (15 V$_{pk-pk}$).
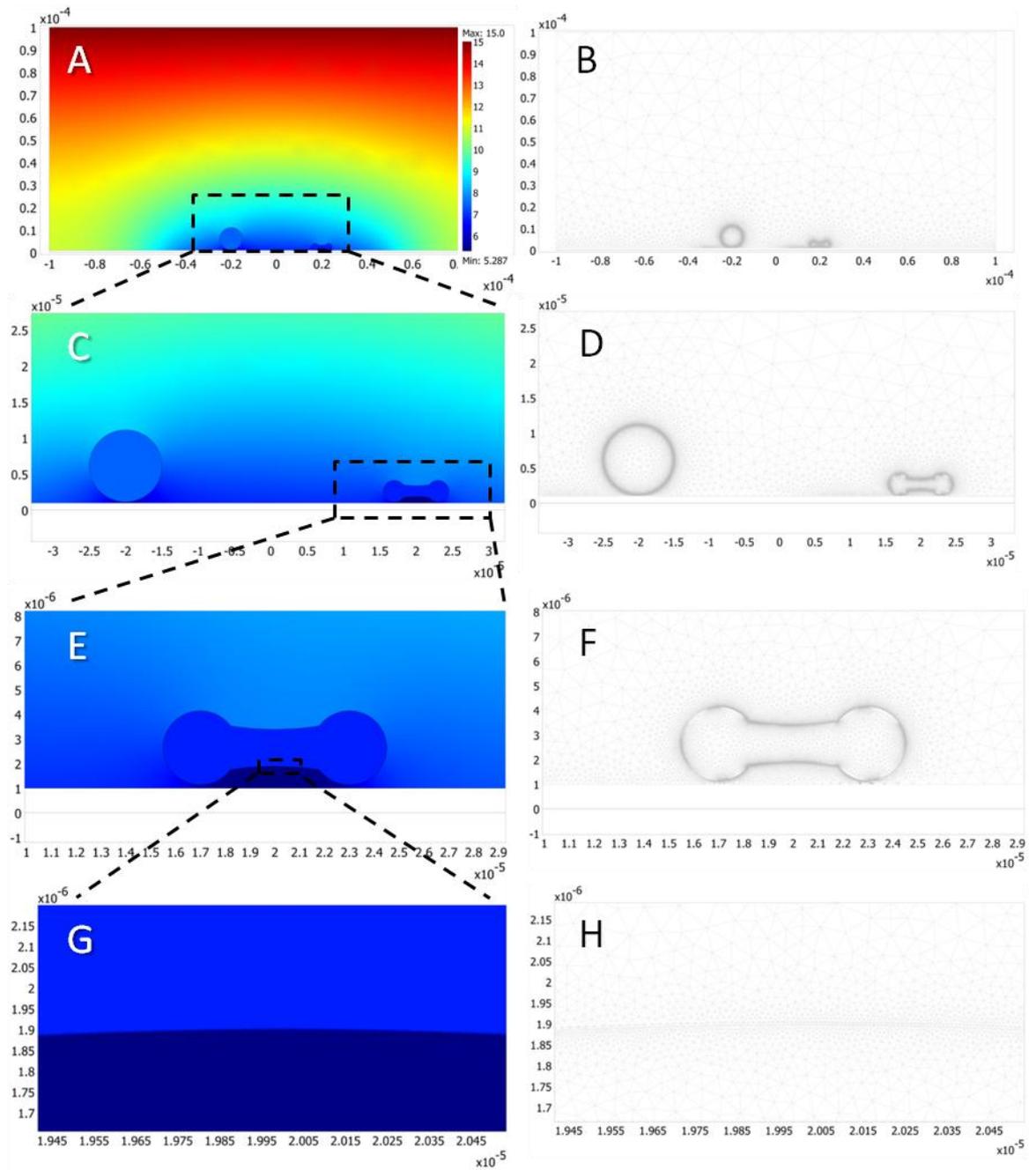
Figure 6-2: Overview of the model and the corresponding mesh. The total width of the chamber was 200 µm and the height 100 µm. The cell membrane was modelled as a 7 nm thick layer of high resistance. Colour scale in V, x and y axis in metres.

The above model depicts the chamber and cells while the voltage inside the amorphous silicon is not shown (for clarity). Due to this the minimum voltage is ~5.2 V as the rest is dropped across the silicon layer. For an example of the simulation without any suppressed sub-domains, see Figure 6-5 A.

6.2 Results

The 1 μm thick layer of amorphous silicon will act as a resistance of variable ohmic strength, based on illumination. Even in the 'light state' the conductivity of the a:Si is still in the order of 10^4 mS/m however [10]. This caused a considerable amount of voltage to be dropped across the silicon layer rather than the voltage being dropped across the liquid. This had a direct effect on the generation of dielectric forces as well as electrically induced lysis. A cell suspended in the liquid between the top and bottom electrodes only experiences the electric potential dropped across the suspension layer. Thus a reduced amount of voltage dropped across the liquid will cause a decrease in the induced TMP.

Figure 6-3 shows values for the amount of voltage dropped across the amorphous silicon layer extracted from the simulation. The value was taken from the point of the silicon layer that is at the centre of the simulated light spot. As can be seen, the voltage drop does not show a significant frequency dependency in the regime considered here. The voltage does, however, depend greatly on the medium conductivity. The total potential applied across the chamber was 15 V in all three cases. The voltage dropped across the liquid is the amount shown in Figure 6-3 subtracted from 15 V. So for a conductivity of 25 mS/m about 8 V are dropped across the medium, while for a conductivity of 1400 mS/m that number is reduced to less than 0.5 V.
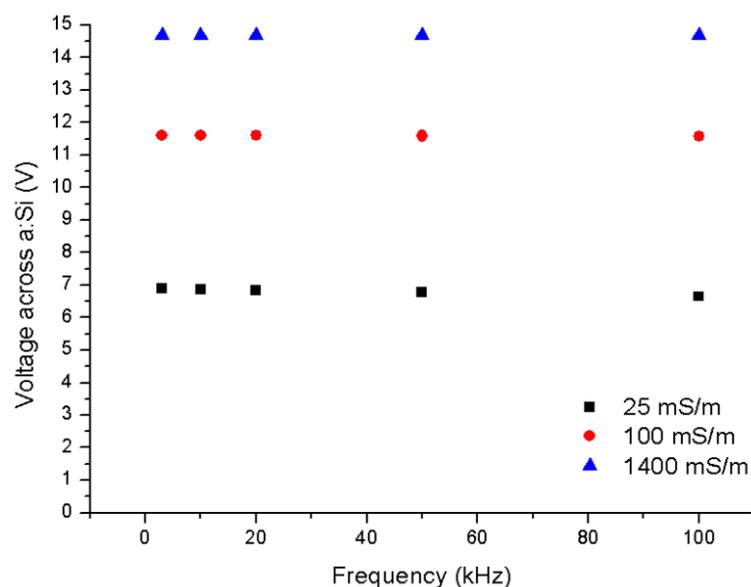
Figure 6-3: Comparison of the voltage drop across the amorphous silicon layer (1 μm thickness) for different frequencies and medium conductivities in an optoelectronic tweezers setup. Values measured at the centre of the modelled light spot.

6.2.1 'Electrical shadow'

The most important observation from the COMSOL modelling was that of non-uniformities in the distribution of the electric potential inside the layer of a:Si directly beneath the resting cells. Since the conductivity of the a:Si layer has an intrinsic non-uniformity (due to the saturated Gaussian to model the light spot, see above) in the model, this will cause a non-uniformity in the voltage distribution. This non-uniformity, however, is of a large scale and covers the entirety of the silicon layer. A much smaller non-uniformity can be observed directly beneath cells resting on the a:Si.
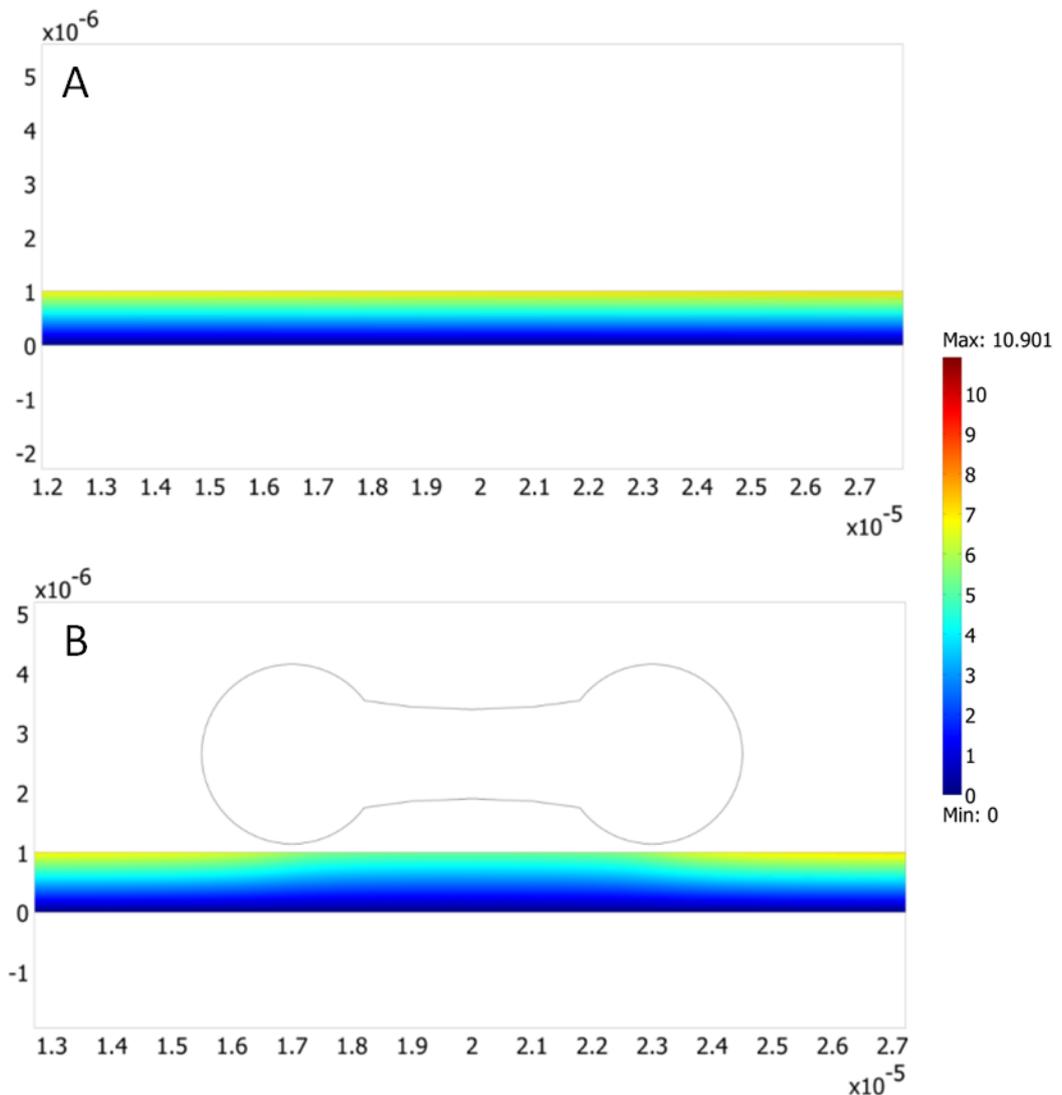
Figure 6-4: Model of the voltage inside the amorphous silicon, both with (top) and without (bottom) a RBC being present (25 mS/m 10 kHz 15 Vpk-pk). A) No inhomogeneity in the voltage distribution can be observed without a cell being present. B) Presence of a cell causes the non-uniform distribution underneath the RBC, causing a local decrease in the voltage dropped across the a:Si layer. This non-uniformity changes with the distance of the cell from the surface and the shape of the cell (see below) and is reminiscent of an "electrical shadow". X and Y axis in metres, colour scale in V.

While Figure 6-4 gave a good visual presentation of the non-uniformity, the effect was better understood when all areas of the simulation are included in the colorimetric presentation (all sub domains except the a:Si layer are suppressed in Figure 6-4).

As can be seen from Figure 6-5 and 6-6, the area directly underneath the RBC has a reduced potential with regard to the liquid above and beside the cell. Effectively the cell creates a pocket of reduced potential. This result was only observed for low frequencies (see Figure 6-5) while it seems to disappear for higher frequencies (100 kHz), owing to the loss of the cell membrane's ability to act as an insulator at these frequencies.

This observed effect will be tentatively referred to as an 'electrical shadow' in this work. This term does not refer to an actual shadow (this is worth emphasising, since light is a central part of the experimental setup), but rather the electric shielding of the dielectric silicon layer through the cellular membrane (and consequently the cell itself).

The biconcave shape of the erythrocyte, although the cell is resting on the surface, might seem questionable but the author feels it is a justified geometry for the presented simulations. The RBC naturally assumes the biconcave shape (given physiological osmolarity) because it represents its state of lowest potential energy [95]. Red blood cells will return to this shape when deformed and this process is well documented (e.g. [96]). Gingell and colleagues used interference reflection microscopy to study the adhesion of erythrocytes to glass and other substrates [97, 98], and clearly showed that for suspending media of low conductivities, the resting RBCs keep their biconcave shape and form 'pockets' of liquid under the cell. Their work is also of importance, as will be discussed later on, when estimating the distance of the cell from the surface whilst resting. The same publications show that for media of high conductivity (like phosphate buffered saline with a conductivity of ~1400 mS/m) the cells seem to be in contact with the substrate and the pocket, formed by the biconcave shape, disappears. When modelling the cells under these high conductivities, this change was taken into account through a changed geometry of the RBCs (see Figure 6-10).
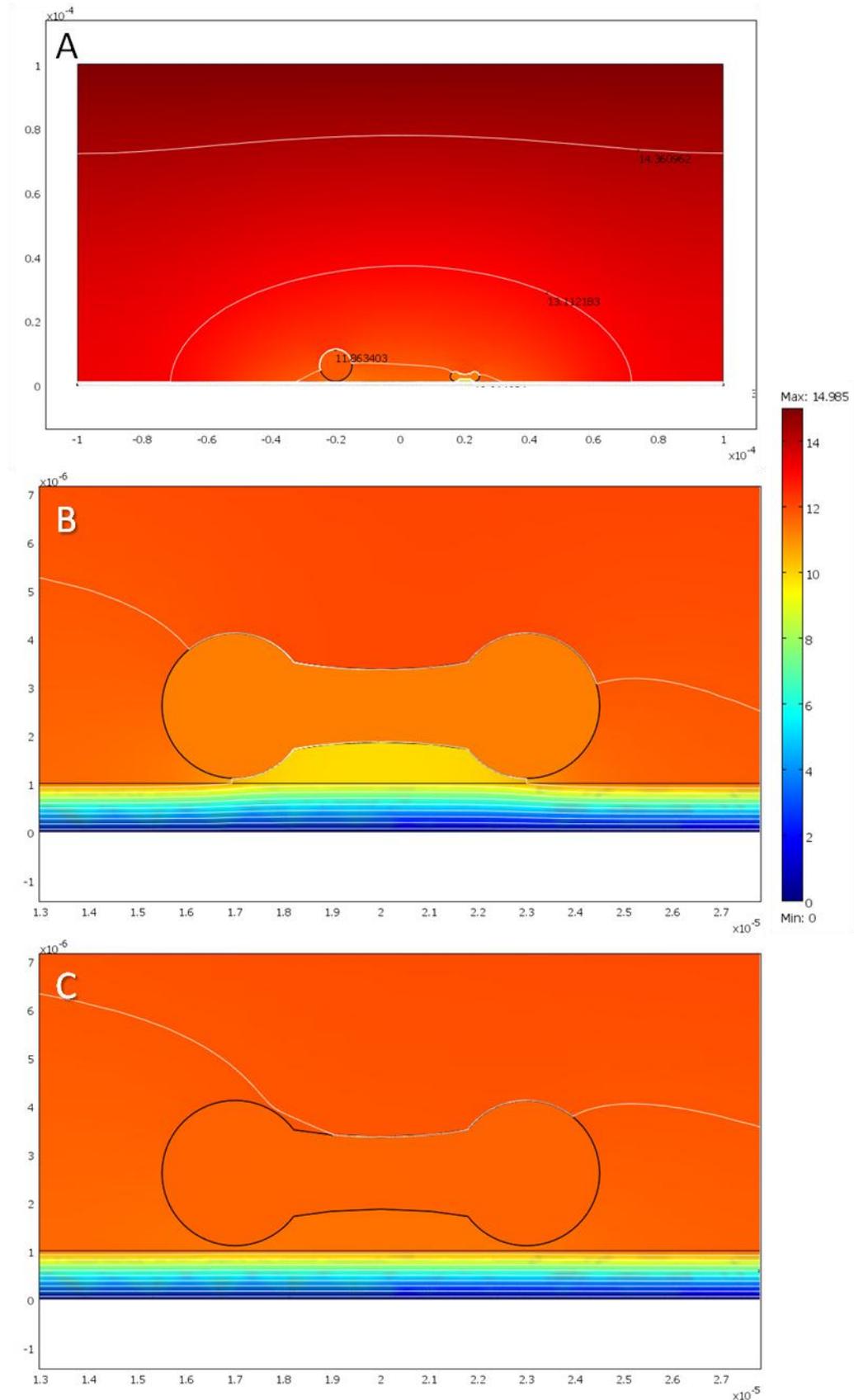
Figure 6-5: COMSOL model of the voltage distribution in an OET experiment (100 mS/m, 15 Vpk-pk). A) Overview of the whole model. White lines represent equipotential lines (1.2 V difference from one line to the next). B) Close up of a RBC at a frequency of 3 kHz. The equipotential lines can be seen going into membrane and the overall electrical shadow is visible. C) shows the same cell, but at frequency of 100 kHz instead. No electrical shadow was visible in this case. Colour scale in V, x and y axis in metres
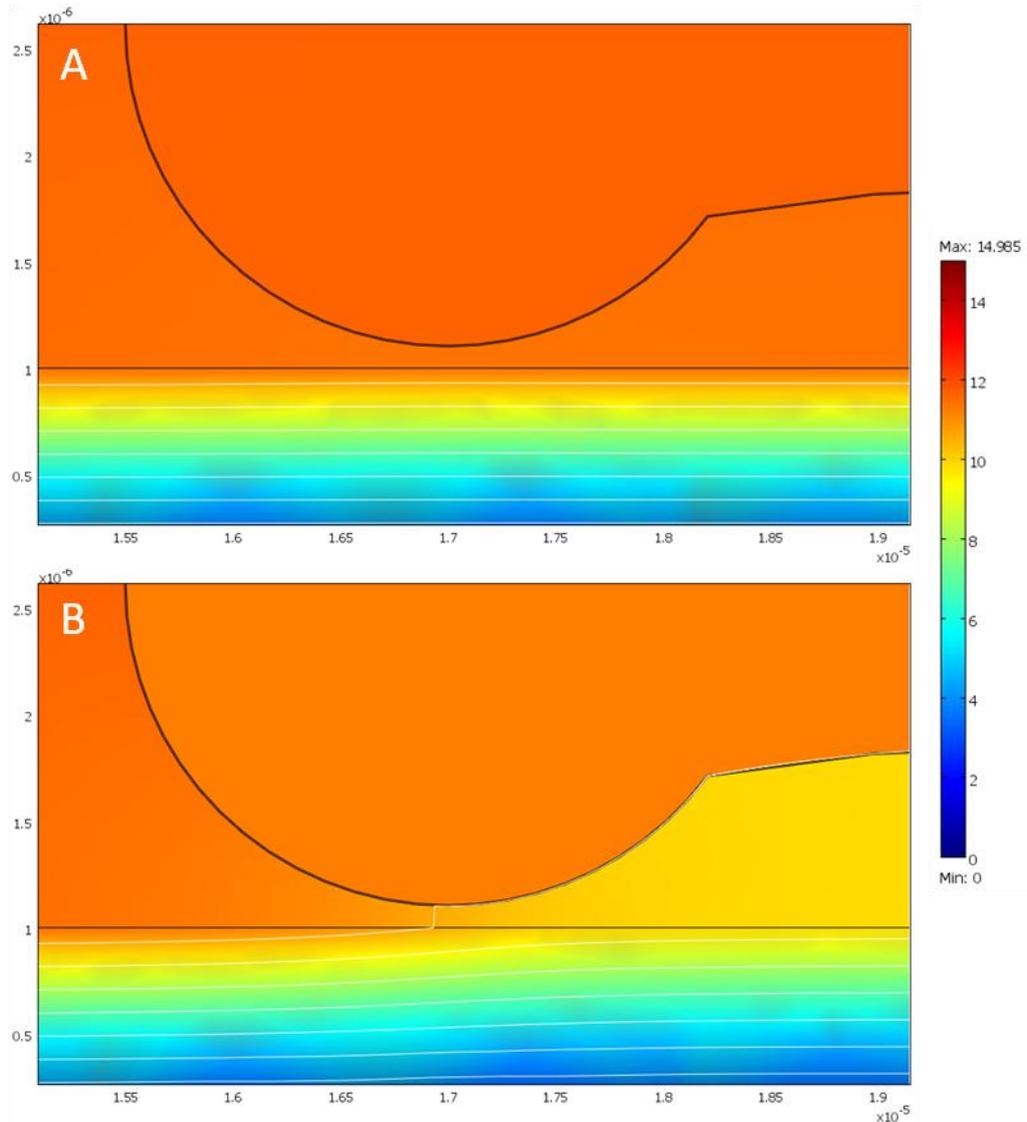
Figure 6-6: Image of a close up of the RBC shown in Figure 6-5. The pictured section is the bottom left corner of the RBC. A) shows the cell at 100 kHz with the equipotential lines being in parallel to the surface of the amorphous silicon. B) shows the cell at 3 kHz, with the electrical shadow being visible under the cell. The equipotential lines are not in parallel and protrude out of the surface and into the cell membrane. This caused a higher voltage to be dropped across the membrane than in A. Colour scale in V, x and y axis in metres.

Figures 6-6 and 6-7 compare in detail how the potential was distributed at the areas where the cell was closest to the a:Si surface for a RBC and a WBC. It can be seen from both examples that for 100 kHz the potential was dropped evenly across the silicon layer and no electric shadow was developing. For a frequency of 3 kHz however, the equipotential lines (in white) can be seen to deform due to the presence of the cell. In each example the difference between two white lines is about 1.2 V. In the case of the RBC the potential lines can be seen 'bending' out of the a:Si layer and into the cellular membrane. The membrane, in effect, becomes part of the silicon layer with regards to the electric

potential. For the white blood cell, however, this effect was much reduced (due to its shape).
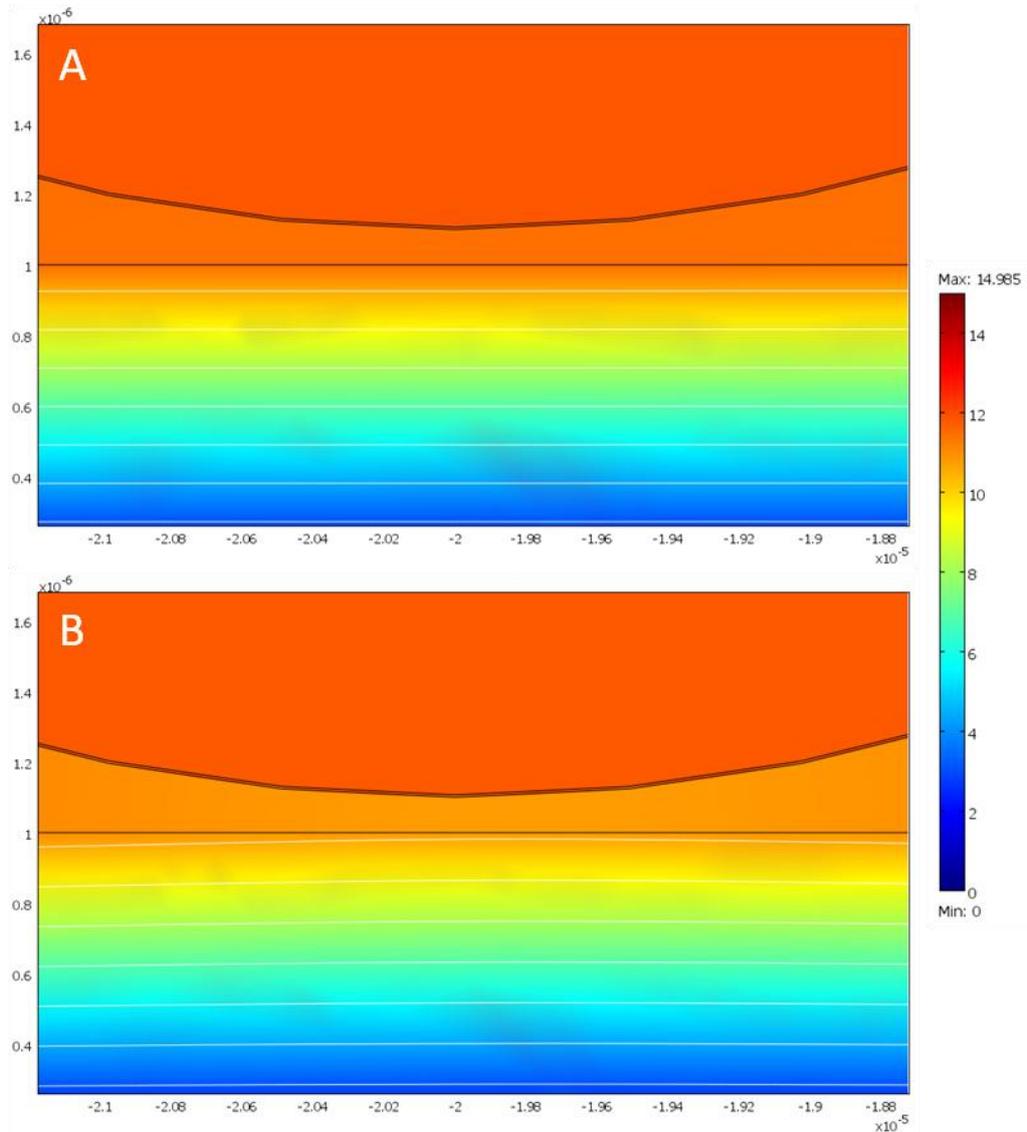
Figure 6-7: Image of a close up of the WBC shown in Figure 6-5 (the pictured section is the bottom of the cell). Similar to Figure 6-6 the distribution of the voltage for 100 kHz (A) and 3 kHz (B) are pictured. The WBC however distorts the potential inside the amorphous silicon to much lesser extent than the red blood cell. Colour scale in V, x and y axis in metres.

To further visualise the shape of the electric shadow and the effect of the shape of the cell causing it, another measurement was plotted in Figure 6-8. Here the voltage distribution along a horizontal line, in parallel to the surface but 100 nm below the surface, was plotted. This represents the voltage distribution inside the silicon layer underneath the cell. As can be seen from Figure 6-8, the voltage under the cell drops and this drop was more pronounced for lower

frequencies. In case of RBCs, the voltage drop inside the silicon for frequencies between 3 and 10 kHz is about 1.3 to 1.4 V (compared to the 'baseline' at 100 kHz where the potential was hardly changed by the cell). This value corresponded well with the induced transmembrane potential determined from the model for these frequencies (see Figure 6-11).

Another observation that can be made here was that not only do RBCs cause a larger drop than WBCs, the voltage was also dropped across a much broader area. The electrical shadow 'cast' by the WBC was much narrower due to the spherical shape of the cell. Another point to note was that the voltage drop underneath WBCs was only approximately 0.5 V while according to the simulation the overall induced TMP is approximately 1 V. This would suggest that the electrical shadow only accounts for about half the TMP for WBCs (the rest is due to its large size) while it accounts for nearly all of the TMP in case of RBCs.
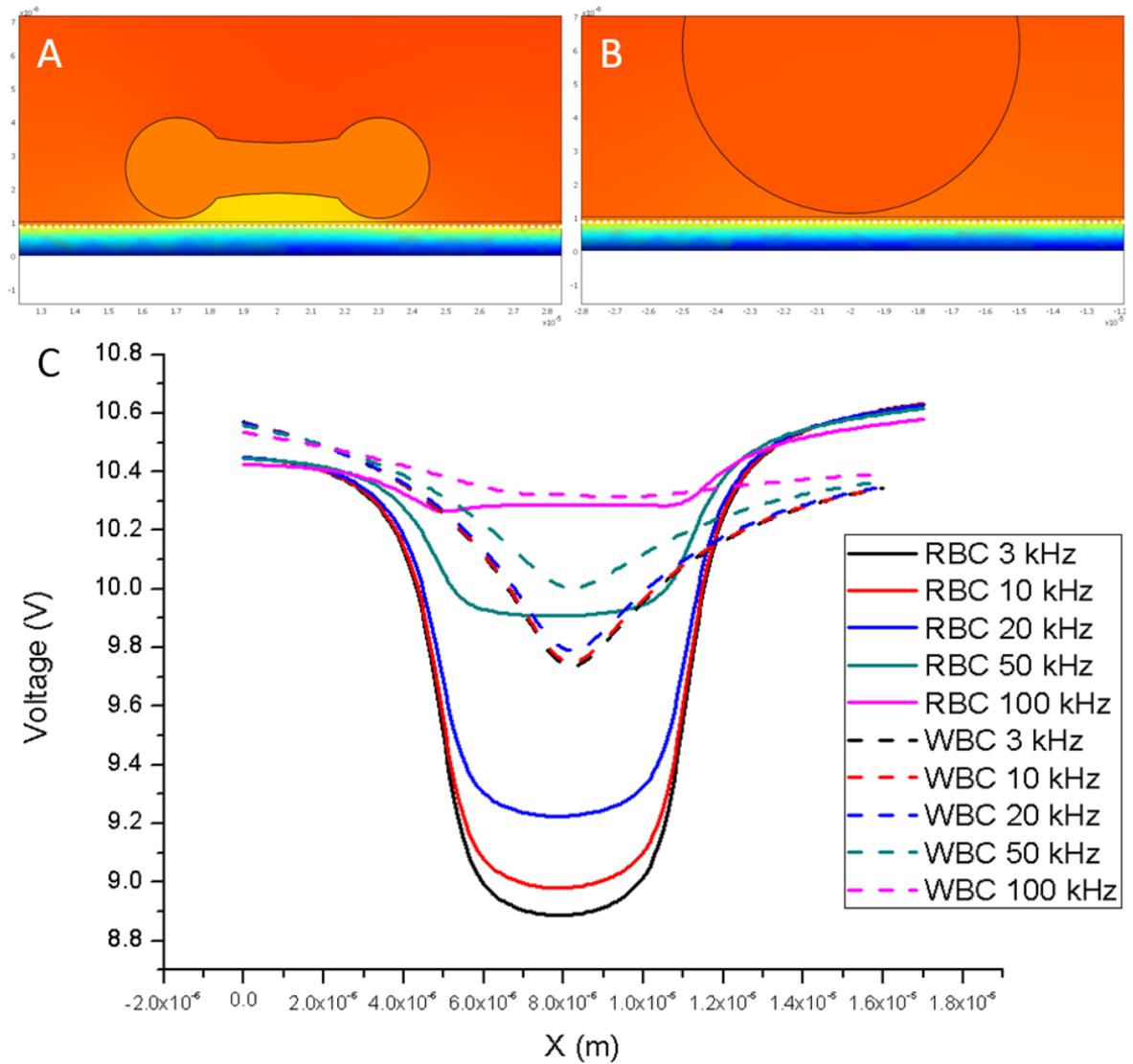
Figure 6-8: Simulation of the shape of the electrical shadow. A) and B) show where the voltage inside the amorphous silicon was measured (white dotted line) 100 nm below the surface. C) The distribution of the voltage under the cell for different frequencies and cells (100 mS/m conductivity). As discussed above, the voltage under the cell was reduced as the potential was dropped across the cell membrane instead. The potential non-uniformity under the red blood cell is much wider due to the shape of the cell. In addition the drop under the RBC is much larger than for the WBC. These two factors combine to cause the induced transmembrane potential of the WBC to be less than for the RBC.

6.2.2 Distance from surface

Attention has to be given to the height of the cell above the silicon layer. For red blood cells resting on a glass surface the height of the cell will change with medium conductivity [97, 98]. This is caused by repulsion of surface charges of RBCs and the glass. The values from the literature for different conductivities (according to Table 6-2) were used in this work for modelling.

Conductivity	Distance
25 mS/m	140 nm
100 mS/m	100 nm
1400 mS/m	10 nm

Table 6-2: Distance of cells from the surface for given conductivities. Values were taken from literature [97, 98].

The height of the cell has a pronounced effect on the induced TMP according to the simulation. Figure 6-9 shows a comparison of different heights of the cell above the surface while keeping conductivity and frequency constant (25 mS/m and 10 kHz respectively).

It can be seen that the induced TMP and the shape of the field differ significantly with height of the cell above the surface. The voltage drop across the silicon layer increased as the distance between the surface and the cell increases. In this case it was increased by 1 volt if the distance of the cell was increased from 10 nm to 2 μm. At the same time, the induced TMP is decreased in this case from 1.4 V to 0.8 V. For a spherical cell that is placed symmetrically between the electrodes, the two TMPs at the top and the bottom of the cell will be equal. This is not the case here as the cell was much closer to the bottom electrode and the field inside the chamber was not uniform. The bottom TMP is higher than the top one and is used for all further evaluations. It should be noted that this discrepancy is becoming less pronounced as the cell is lifted off the surface.
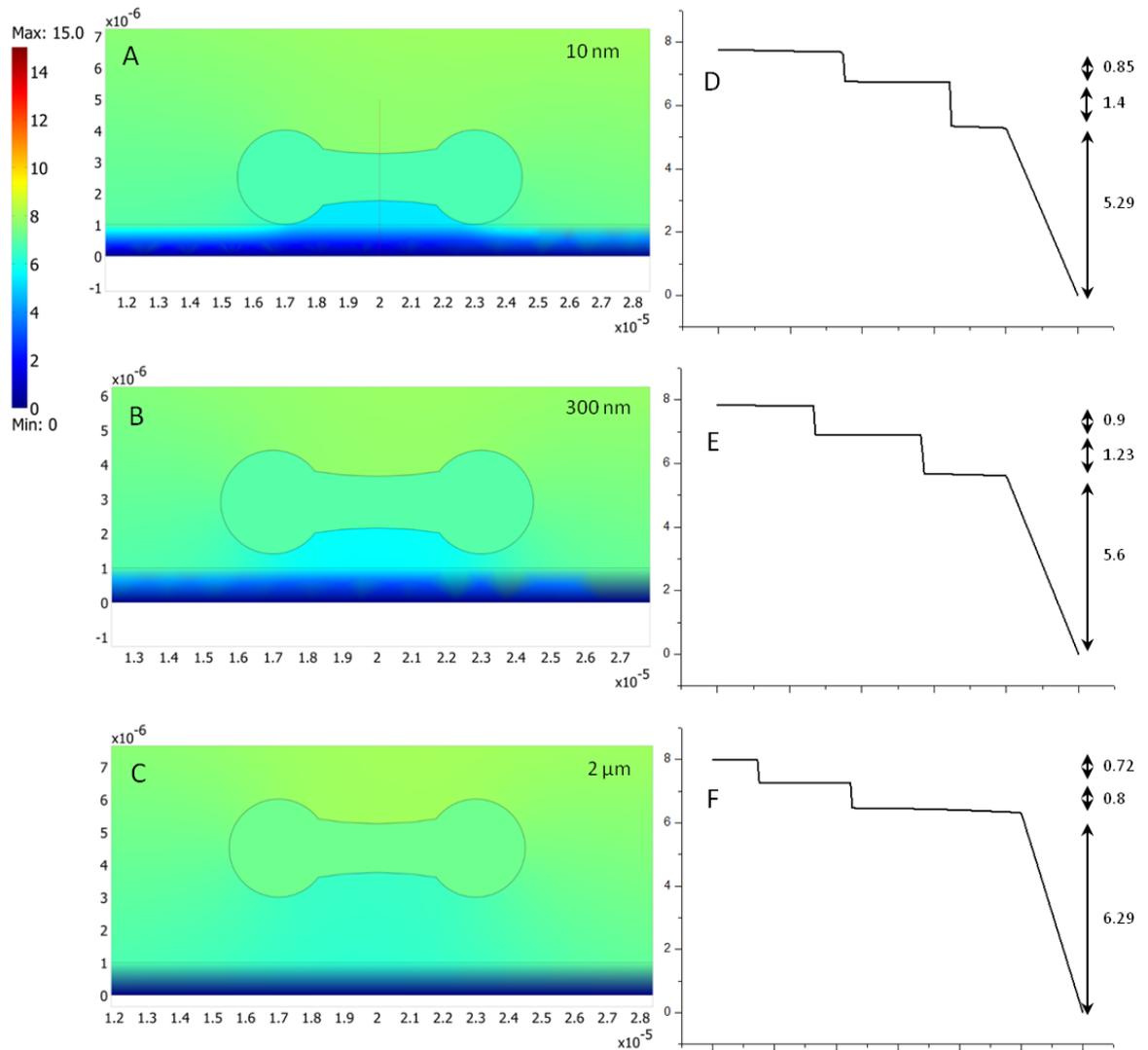
Figure 6-9: Comparison of different heights of the cell above the silicon surface. All simulations were for the same medium conductivity (25ms) and frequency (10kHz). The distance was measured from the two points of the cell that are closest to the silicon. A-C) show COMSOL simulations for three different heights (10, 300 and 2000 nm). Colour scale in V, x and y axis in metres. D-F) show the corresponding voltage drop (in V, y-axis), plotted vs. the distance (mayor tick is 1 µm, x-axis). The voltage drop is measured through the middle of the cell (indicated as the red line in A). The values for the top and bottom TMP as well as the drop across the a:Si layer (indicated by the arrows in the right hand graphs) are given in V.

As discussed above, RBCs have a biconcave shape even when resting on a surface if the conductivity of the medium is low enough that the electrostatic repulsion is not fully shielded [97, 98]. If the conductivity is large, however, the cell appears to be lying flat on the surface and the "pocket" created by the biconcave shape disappears. To account for this change a second morphology for the RBCs at medium conductivities of 1400 mS/m (pure PBS) was used in the model (see Figure 6-10).
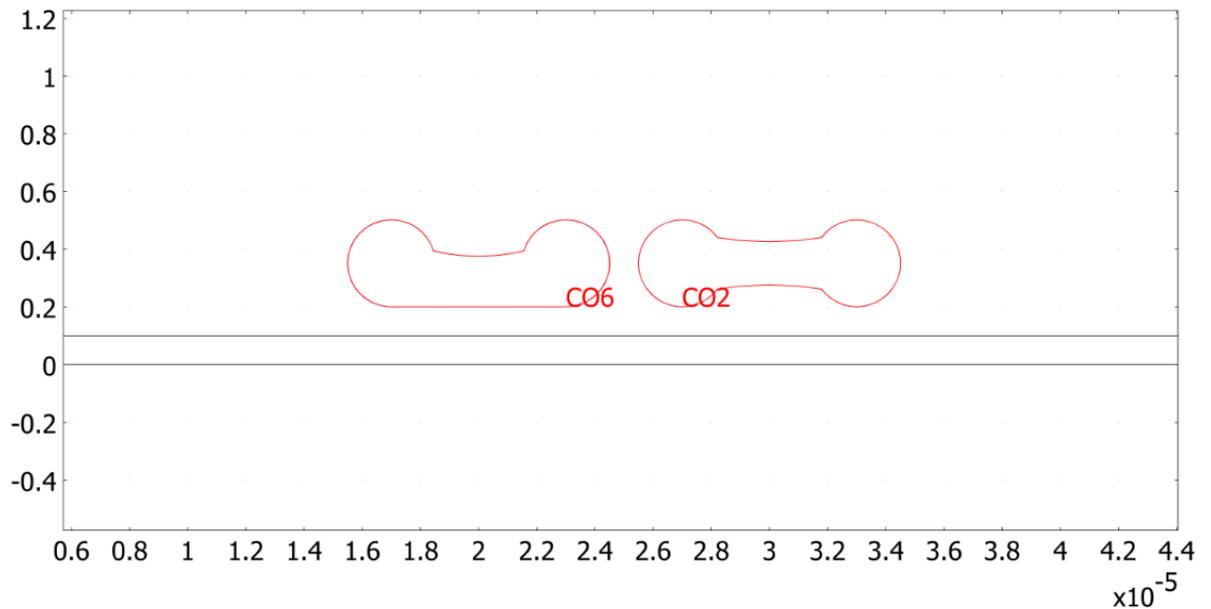
Figure 6-10: Comparison of the biconcave (right, CO2) and flattened biconcave shape (left, CO6) used for the RBCs in the COMSOL simulations. The flattened biconcave shape was used for simulations at a medium conductivity of 1400 mS/m and the cell was placed 10 nm above the surface (in this example the cell is elevated above the surface for clarity). X and y axis in metres.

6.2.3 Induced transmembrane potential

After choosing the distance from the surface, the TMP was modelled for three different conductivities and a range of frequencies. Below is a comparison of induced TMP for RBCs under different conditions (see Figure 6-11).

In order to determine the transmembrane potential, the voltage directly beneath the cellular membrane (on the outside of the cell) was subtracted from the potential inside the cell at the point in the middle of the cell. The point of the membrane where the TMP was measured was the centre of the cell (also see the red line in Figure 6-9 A). The TMP at the top and the bottom of the cell were determined but only the bottom value is plotted in Figure 6-11, since it was the larger of the two values. The smaller TMP at the top of the cell is not of interest for this work since lysis of a cell occurs once a certain threshold is reached.
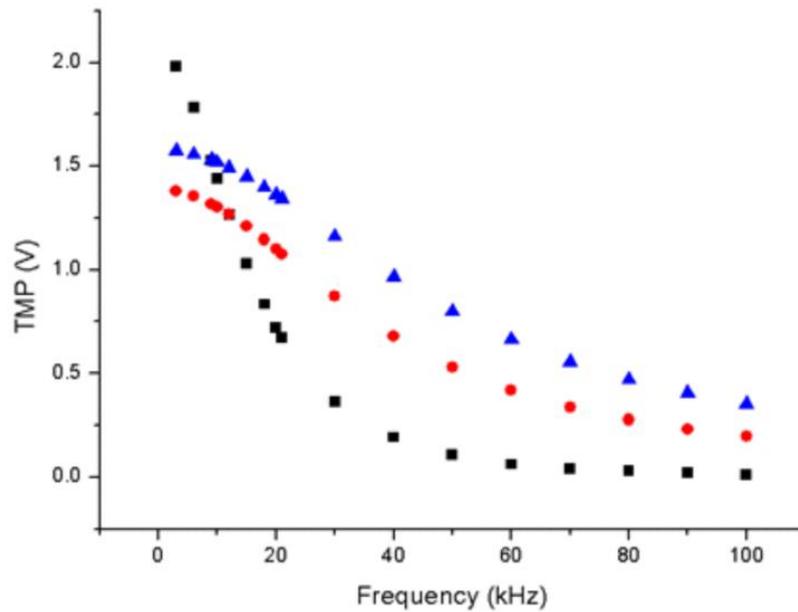
Figure 6-11: Induced TMP from COMSOL simulations as a function of frequency for different values of medium conductivity, black squares 25 mS/m, red circles 100 mS/m, blue triangles 1400 mS/m.

The induced TMP is dependent on frequency. For lower conductivities the induced TMP was higher, although the value drops with increasing frequency. For higher medium conductivities, the initial value was not as high and the drop off is more gradual. While the simulation obviously has several simplifications, it should be noted that for frequencies <10 kHz the induced TMP is in the range of 1 volt in all cases. According to the literature, this value is usually the threshold for irreversible breakdown of the cellular membrane [29].

Since the observed lysis was selective to RBCs over WBCs, the voltage drop across the membrane of a WBC was also determined and is presented in Figure 6-12. The potential was determined in the same way as above for the RBC and also at the centre of the cell (the lowest point of the spherical WBC). For low frequencies, the TMP of the RBC can exceed that of the WBC although it is a much smaller cell (the model used the same height above the surface for both cell types for a given conductivity (see Table 6-2)). Both cells present the same behaviour with regards to frequency but for the WBC the increase with reduced frequency is not as steep. While the transmembrane potential for both cell typesis in the range of 1 V at low frequencies, the TMP of WBCs is only about 70% that of RBCs.
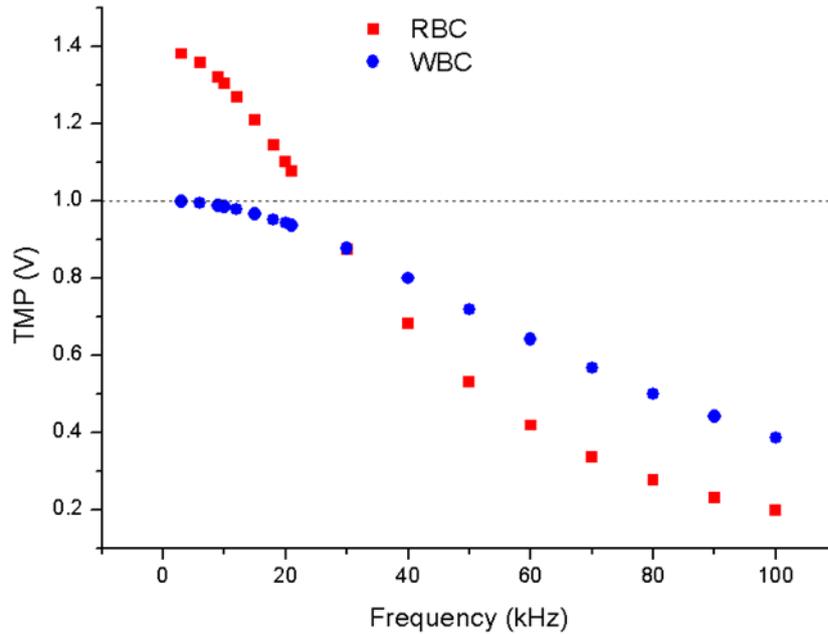
Figure 6-12: Induced transmembrane potential (as a function of frequency) of an erythrocyte (RBC) and leukocyte (WBC) according to the COMSOL model. Values are for cells suspended in a 100 mS/m buffer at 15 Vpk-pk.

An important comparison is that of the virtual electrode in an OET setup and a conventional metal electrode. In the COMSOL model the virtual electrode was created by adding a layer of a:Si (a sub-domain with the electric properties of amorphous silicon, including the conductivity change to simulate a light spot) on top of a boundary under a certain potential (also see Figure 6-1). To simulate a metal electrode, the a:Si layer was removed and the cells were placed at the appropriate distance (see Table 6-2) from the 'naked' boundary. This configuration corresponded to two parallel electrodes of equal size and created a uniform electric field.

In order to account for the effect of the field non-uniformity due to the simulated light spot, another simulation was created. In this case, the boundary conditions at the bottom of the chamber were modified to mirror the case of a metal electrode with a width equal to the width of the saturated region of the simulated light spot (80 μm). In this case the highest transmembrane potential was induced at the top of the red blood cell rather than the bottom of the cell.

The most obvious difference between the two cases is that the boundary conditions at the interface of a conductor are radically different from those of a dielectric. The surface of the conductor is an equipotential line. The electric field lines have to terminate perpendicular to the surface, while they can run more or less in parallel to a dielectric and enter the material at very low angles. Figure 6-13 shows the electric field lines (as red stream lines) going around a red blood cell sitting on top of a layer of amorphous silicon (top) and a metal electrode (bottom). The two simulations were both run at 100 mS/m with a 3 kHz, 15 $V_{pk\text{-}pk}$ AC bias. It can be seen that in both cases the field lines are distorted by the presence of the cell. In the case of the metal electrode, however, the field lines are not constricted as efficiently between the cell membrane and the substrate.
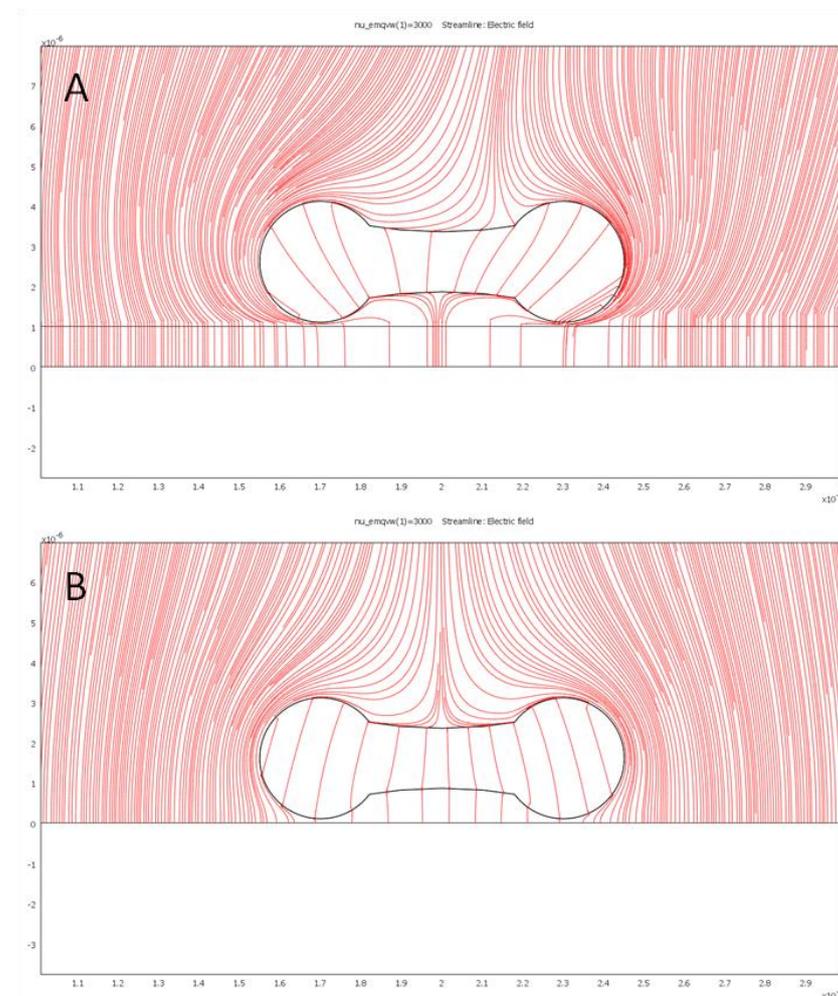
Figure 6-13: Comparison of the electric field lines (in red) going around a RBC for an OET device and a metal conductor. A) Erythrocyte sitting on layer of amorphous silicon. B) Erythrocyte sitting directly on a conductive surface (like a metal electrode). The field lines cannot 'bend' around the cell as well as in A due to the boundary conditions of the conductor. Both simulations were run for a medium conductivity of 100ms/m with an AC bias of 3 kHz at 15 Vpk-pk. Scale is in metres.

In order to verify the effect this difference would have, the values for the induced transmembrane potential (as a function of frequency) of a red blood cell in a 100 mS/m medium, on a conductive surface, were determined. The values for a cell in a uniform electric field and a non-uniform electric field, which mirrors the one from the OET simulations, were generated and compared to the OET values (see Figure 6-14). The TMP was determined in the same way as for Figures 6-11 and 6-12.
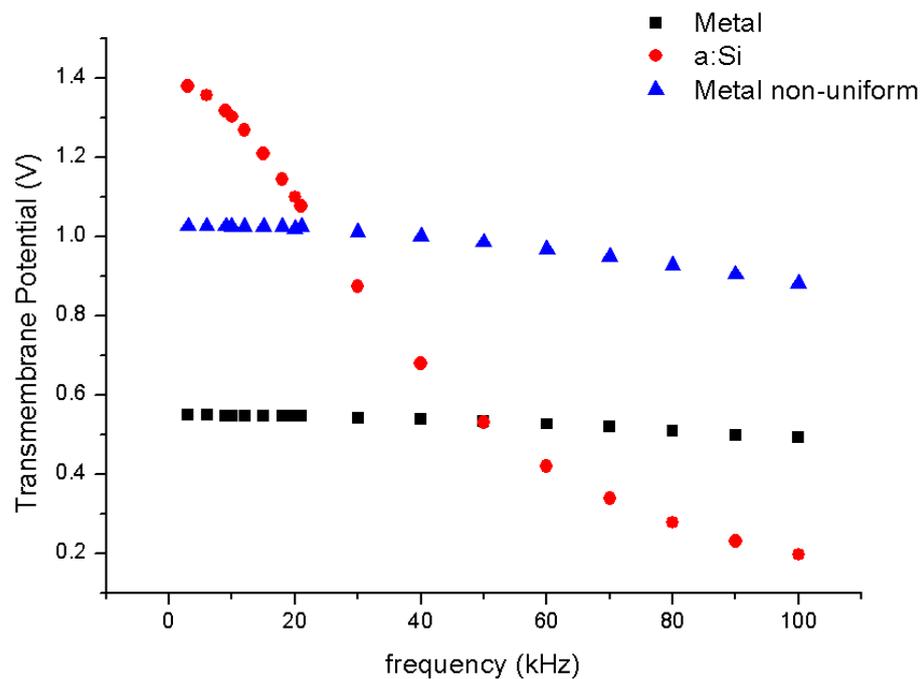
Figure 6-14: Comparison of the induced transmembrane potential of an RBC resting on either a conductor or a layer of a:Si. The TMP of the cell resting on the metal electrode does not exhibit a strong change with frequency. Greater values are observed in the case of a non-uniform electric field, but the values of the TMP are still below those predicted for the OET setup at frequencies below 20 kHz.

Figure 6-14 shows the difference between a conductive surface and a dielectric for a resting cell. As was to be expected the induced TMP shows no significant frequency dependency in the considered regime in the case of metal electrodes. At higher frequencies when the electrical shadow was no longer apparent the value of the TMP in the metal setup far exceeds that of the a:Si case. This was also in good agreement with the fact that the overall voltage drop across the liquid was much higher in this case. In the case of low frequencies however the

increase of the TMP due to the electric shadow effect quickly increases the TMP of the RBC beyond the value of that in the metal electrode setup.

In summary, the results of these simulations show that the induced TMP was increased when the cell was sitting on a layer of amorphous silicon due to the effect referred to herein as the 'electrical shadow'. A number of predictions can be made from these models. An important prediction is that the TMP in small red blood cells might be higher than in the larger WBCs due to their shape. This would enable the selective lysis of smaller cells from larger cells based on shape. According to the simulations, the effect weakens as the frequency increases and disappears completely at frequencies of 100 kHz or more. Furthermore, the effect will also diminish once the cell is elevated off the surface of the a:Si layer. Lastly, the induced TMP in the case of an OET setup is greater than that observed for metal electrodes.

6.2.4 Influence of dielectric parameters

Since the values for the internal conductivity and the membrane permittivity used in this work (0.8 S/m and 12.64 respectively) differ from those found in the literature, it is worth comparing what the simulations would look like with values from the literature. Asami *et al.* [90] reported a internal medium conductivity of 0.62 S/m and a relative permittivity of the membrane of 5.9 for mouse erythrocytes. Gimsa *et al.* [99] reported values of 0.4 S/m and 7.8 respectively for human red blood cells (at frequencies below 15 MHz). Comparisons for the TMP induced on cells in our model using these values can be found in Figure 6-15.
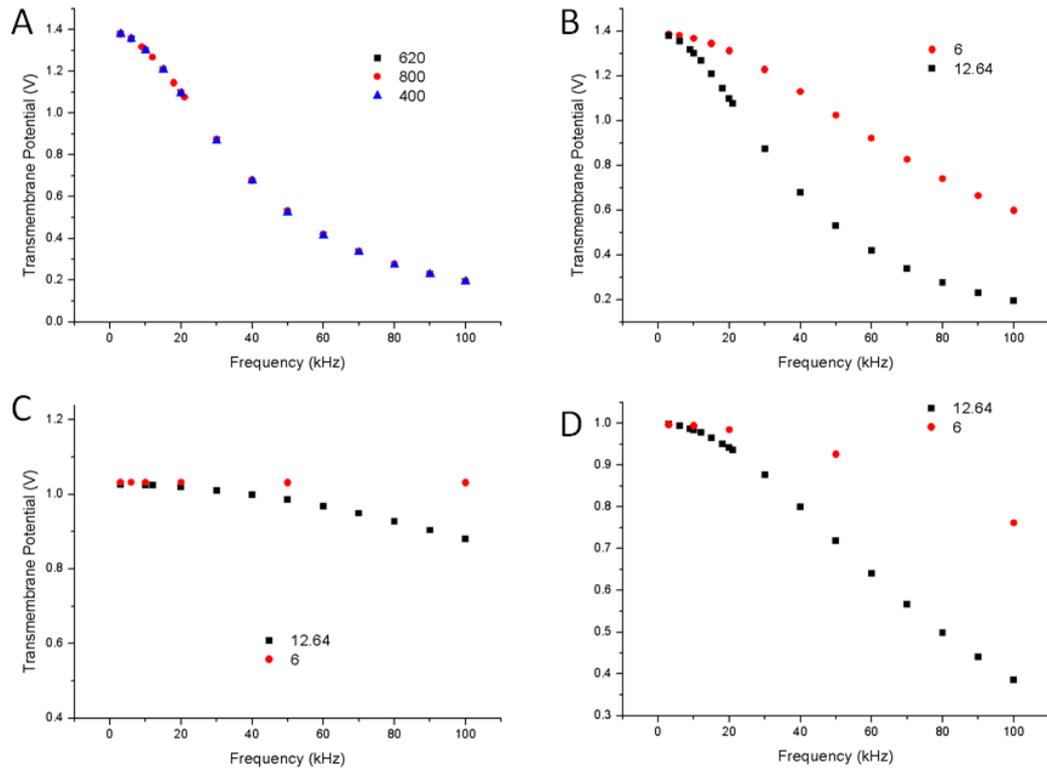
Figure 6-15: Comparison of the induced TMP in the model using different values from the literature (see text). A) Induced TMP for a RBC sitting on a layer of a:Si at an external medium conductivity of 100 mS/m using different values for the conductivity of the intracellular medium (400, 620 and 800 mS/m). No significant change in the induced TMP is observed. B) Induced TMP of a RBC using an internal conductivity of 800 mS/m (and an external conductivity of 100 mS/m) and two different values (12.64 and 6) for the permittivity of the cellular membrane (ε_m). At a lower permittivity the induced TMP drops off more gradually but the overall increase at lower frequencies is still observed. For low frequency values the induced potential is near identical. C) Induced TMP for a red blood cell resting on a conductor (instead of an a:Si surface) with a non-uniform electric field distribution (compare to Figure 6-14). Due to the lower ε value, the TMP displays no change with frequency whatsoever. At low frequencies the induced TMP is identical to the values generated with a higher membrane permittivity. D) Transmembrane potential induced in a white blood cell resting on a layer of amorphous silicon at 100 mS/m conductivity (compare to Figure 6-12) for the two permittivity values. Again, at low frequencies the values for the TMP are unchanged but at higher frequencies the TMP decreases more gradually.

As can be seen from Figure 6-15 a change in conductivity of the intracellular medium has little effect on the induced transmembrane potential under the conditions employed in this model. The difference in membrane permittivity does affect the TMP at higher frequencies. At low frequencies however the values for the potential are changed very little. The major change brought about by the change in permittivity is that the potential drops of more gradual with increased frequency. The values employed in this Chapter, derived from the experimentally determined crossover frequency, however show a better correlation with the experimental values (see Figure 7-15).

6.3 Discussion

To better understand the conditions during an optoelectronic tweezers experiment, a COMSOL model was employed. The model used the same values for the sake of consistency that were employed for the red blood cells when modelling the CM factor (see Chapter 4). The dimensions of the cells were changed to match human erythrocytes. While the models presented here are by necessity simplifications of the actual process found in the experiment, they do present results that allow for interesting comparisons to the experimental observations.

The first interesting observation from the model is that the induced transmembrane potential increases at low frequencies.

The increase of the TMP at lower frequency ranges observed in these simulations is due to the restriction of the electric field by the cell itself. While restriction of an electric field has been described before in order to lyse cells [100, 101] and to promote electrofusion [102], in both of these cases the field is restricted by a non conducting material.

The author now proposes that it is the cell itself that constricts the field at the point of contact with the dielectric material. This constriction is a function of height since a smaller gap between the cell and the semiconducting surface has a larger effect as well as the frequency since the capacitive quality of the cell causes the cell to act as a near perfect insulator only at low frequencies. Hence the field lines are no longer restricted efficiently at high frequencies and the induced TMP drops off rapidly.

As outlined in this Chapter, the presence of a cell creates an electric shadow onto and inside the a:Si layer. The more pronounced this shadow is the more voltage is dropped across the cell instead of the silicon layer. Since the membrane is insulating and in such close proximity to the high resistance layer of silicon (relative to the liquid), the electric field is restricted at the two points where the RBC is closest to the surface (also see Figure 6-13). This restriction causes the cell and the volume of liquid directly underneath it to act as a resistive element. Thus more voltage is dropped across the cell and less voltage

in turn across the silicon layer. This voltage is mostly dropped across the bottom membrane of the cell, with the maximum potential being applied across the section that is directly in the centre of the cell.

The RBC has a large area exposed to the substrate, whilst a WBC has a smaller area of contact. Thus the shape of the cell influences the induced TMP (see Figure 6-8). In this way the shape can offset the effect of the size on the TMP and electrical lysis can be shape selective (rather than size selective).

The voltage drop, implied by the simulations to occur inside the silicon layer, cannot be observed for metals since the material is a conductor. The electrical shadow, however, competes with the fact that the overall voltage drop across the liquid is much reduced in the OET experiments. In a way, the voltage drop across the liquid being reduced is the same as the voltage drop being concentrated into a much smaller layer of a:Si. The cells, courtesy of the constriction of the electric field near the bottom of the chamber, can then effectively become part of this concentrated layer. While the complete voltage is dropped across the liquid in the case of metal electrodes, the distribution of the potential is uniform.

Another point to consider is that the boundary conditions at the interface of a conductor are radically different from those of a dielectric. The surface of the conductor can be represented by an equipotential line. The electric field lines have to terminate perpendicular to the surface, and can therefore not be constricted as effectively between the cell membrane and the metal as they could be between the membrane and another dielectric material (which allow the electric field lines to run in an almost parallel direction to its surface).

This limited ability to restrict the electric field close to the surface combined with the more even distribution of the potential cause the induced TMP to be less for cells on metal electrodes, even though the overall voltage drop across the liquid is higher.

This is however only the case if the cell is resting in close proximity to the surface. In the case of very high conductivity media (pure PBS, 1400 mS/m) the overall voltage drop is so small (less than 0.5 V) across the liquid that the simulations can only account for comparable TMP values (compared to lower conductivity media) if the cell is at a distance of about 10 nm from the surface.

Chapter 7: Electrically induced lysis experimental

7.0 Abstract

In this chapter the experimental results of the work with optoelectronic tweezers (OET) is presented. The work was initially aimed at using traditional DEP for single cellular manipulation, but revealed an interesting phenomenon of shape selective electrically induced lysis. This phenomenon is described in detail and the conditions leading to lysis are quantified and discussed.

7.1 Summary of methods

While initially studying the use of dielectrophoresis as a tool to manipulate blood cells and trypanosomes, OET were also employed. As described in Chapter 1, the use of a photoconductive material, in our case a:Si, allows for the creation of 'virtual' electrodes that can be easily manipulated.

Once the sample is illuminated, the conductivity of the amorphous silicon changes by several orders of magnitude (from approximately 10^4 to 10^6 mS/m [10]). This causes the creation of a non-uniform electric field similar to the work presented in Chapter Four, with the illuminated regions forming the electrodes. This non-uniformity can be used to generate dielectrophoretic forces in the same way as is possible using metal electrodes.

The chip holding the sample was placed on an inverted microscope during experimentation that features a special light path to project the image of a data projector onto the sample (see Chapter 3). During the experiments the sample was recorded with a video camera.

After each experiment the sample was thoroughly cleaned with 70% ethanol and placed in an ultrasonic bath every 4 or 5 of experiments. Since the chamber that holds the sample was made with double sided tape it could be easily disassembled and reassembled for cleaning.

7.2 Results

Initial experiments were conducted with human red blood cells and trypanosomes (*T. cyclops*) and unsurprisingly (see Chapter 5) it was possible to separate out the two cell species (see Figure 7-1). However while performing the experiments, an unusual phenomenon was observed. For certain frequency regimes the red blood cells began to disappear, which under closer observation was revealed as electrically induced lysis.
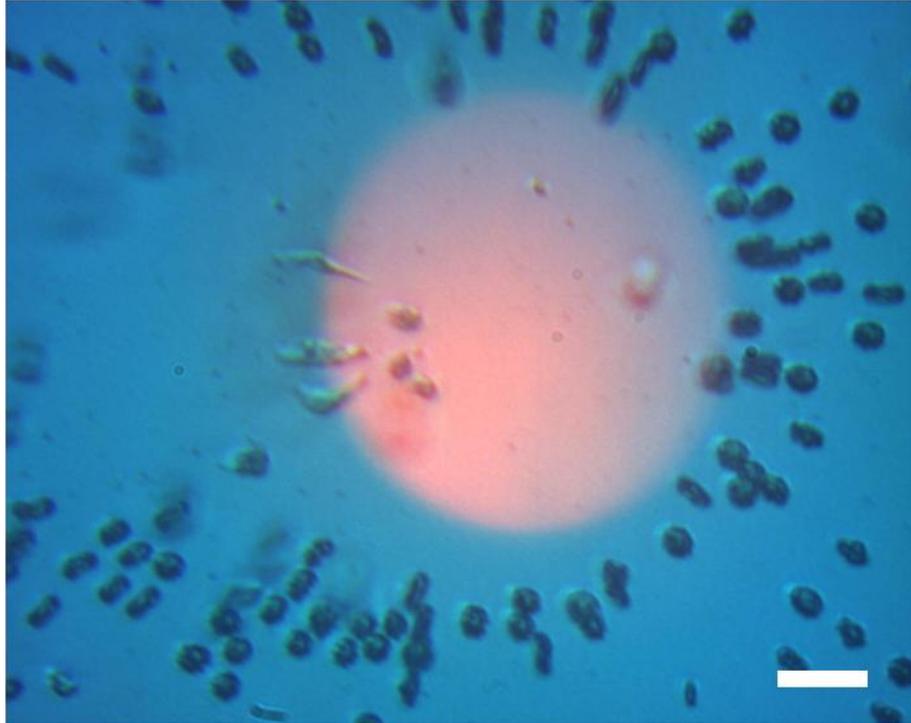
Figure 7-1: Example dielectrophoretic separation of red blood cells and trypanosomes (T. cyclops) using OET. The parasites experience positive DEP and can be moved together with the illuminated region, while the RBCs experience negative DEP and are repelled by the virtual electrode. Scale bar is 20 μm.

When trying to manipulate red blood cells at low frequencies with a high medium conductivity, the cells were observed to 'vanish' instead of being moved through DEP. This process was clearly not levitation, as no shadows could be seen, and changing the focal plane did not reveal cells being levitated above the surface. Figure 7-2 shows the difference between DEP and the observed phenomenon. While in the first experiment the cells were repelled by the area of illumination (high electric field), in the second experiment the effect is only observed within the illuminated area. Cells outside the area were not affected.
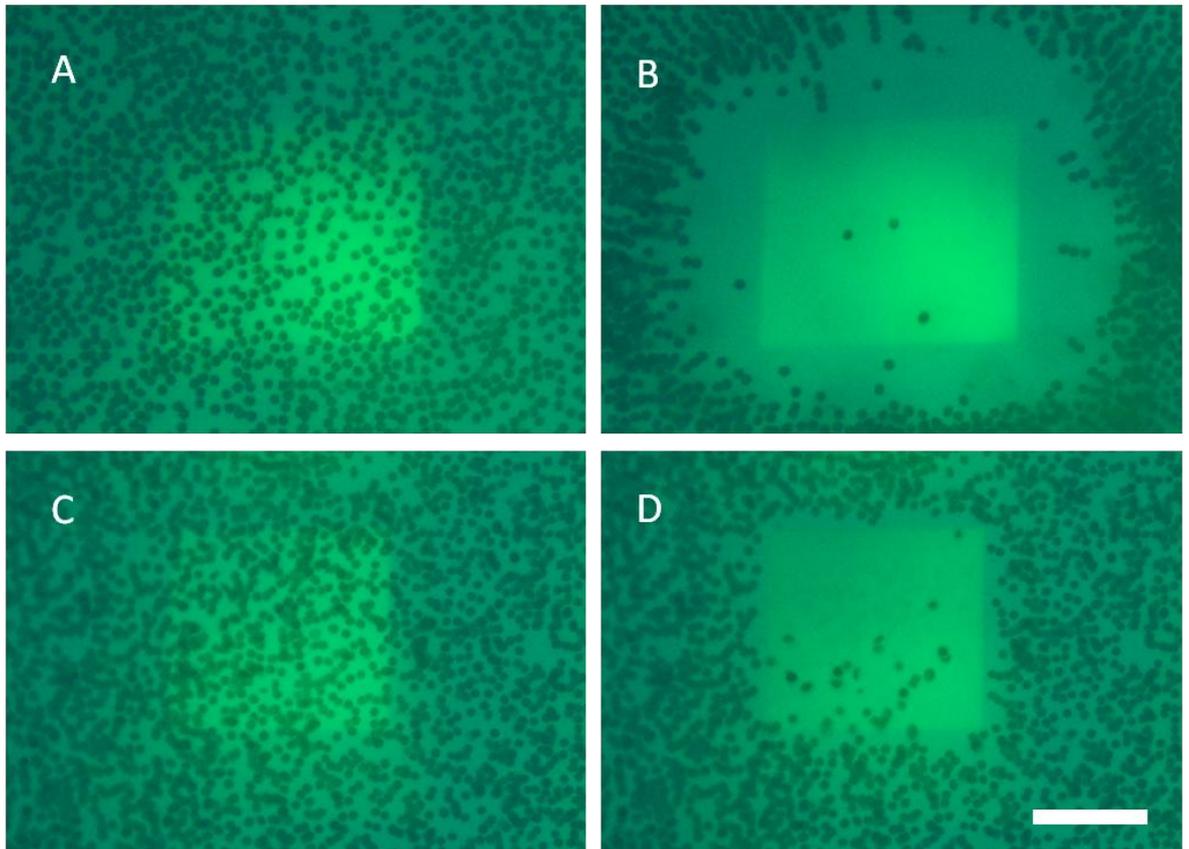
Figure 7-2: Example of lysis of human red blood cells and comparison to dielectrophoretic movement. A-D) show micrographs of RBCs in a OET experiment. A) and B) show negative DEP causing the cells to be repelled from the virtual electrode. Medium conductivity is 16 mS/m and an applied AC bias of 10 kHz at 15 V$_{pk-pk}$. C) and D) show RBCs exposed to the same conditions but at a medium conductivity of 100 mS/m. Due to the increased conductivity, the cells do not undergo negative DEP. Cells not in the illuminated region were not moved and no cells are observed to levitate above the surface during the experiment. Interestingly, the RBCs seem to 'disappear' during the experiment which under closer observation turns out to be electrically induced lysis (see Figure 7-3). Scale bar is 100 µm.

Performing the experiment under larger magnification revealed that the cells were lysed by the electric field (see Figure 7-3). The erythrocytes first undergo swelling and change from a biconcave shape to a spherical shape. This forming of spheroids is well documented in the literature for electrically induced lysis of red blood cells (e.g. [103]). After the cells become spherical, they slowly lose contrast as the intracellular medium diffuses out of the cell. After the process is complete, 'ghost' cells can be seen, the empty remnants of the cells membrane. It took about 20 to 30 seconds until the RBCs seemed to be fully lysed.
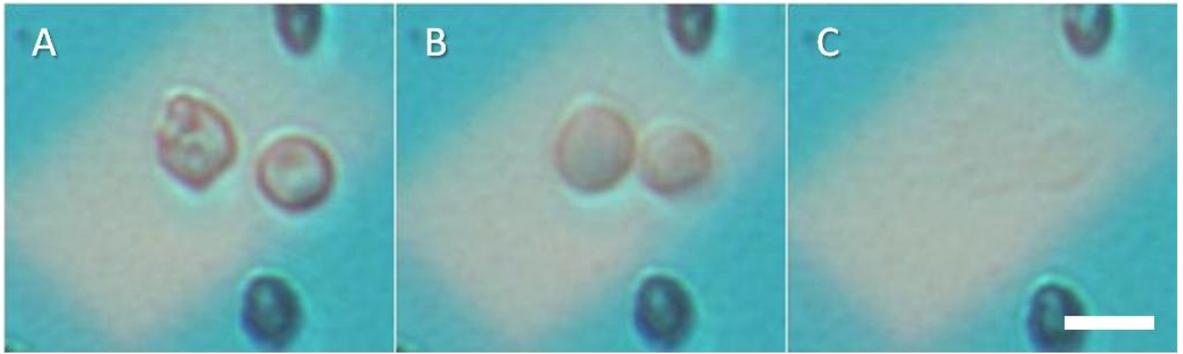
Figure 7-3: Higher magnification micrographs of electrically induced hemolysis in an OET setup. A) Human red blood cells prior to the AC bias being applied. B) 3 seconds after the AC bias has been applied. The erythrocytes become spherical in shape and gradually lose contrast as intracellular medium diffuses out of the cell. C) 20 seconds after the AC bias has been applied. The cells have lost all contrast and are completely lysed. Medium conductivity 100 mS/m, applied bias of 10 kHz with 15 V_{pk-pk}. Scale bar is 10 μm.

Lysis was observed for large areas of illumination. The lysis was not restricted to the edges of the light spot, but was observed across the entire area. An example of large scale lysis of red blood cells is given in Figure 7-4. Here, light patterns in the mm range were created (using a 4x objective lens) where many thousand RBCs were lysed simultaneously.

Furthermore, the phenomenon was only observed for cells lying flat on the surface of the chamber. RBCs that were lifted off the substrate due to DEP or that were observed to stand upright with the field lines (like those in Figure 7-1) did not undergo any lysis, given the setup and conditions used here. In order to confirm this, the cells were also passed over the device using hydrodynamic flow (under conditions where cells lying flat on the surface would lyse). Again, cells that moved over the surface of the silicon instead of lying flat on it were not lysed (see Figure 7-5). In experiments where only some of the erythrocytes underwent DEP, only those that remained on the surface were lysed.
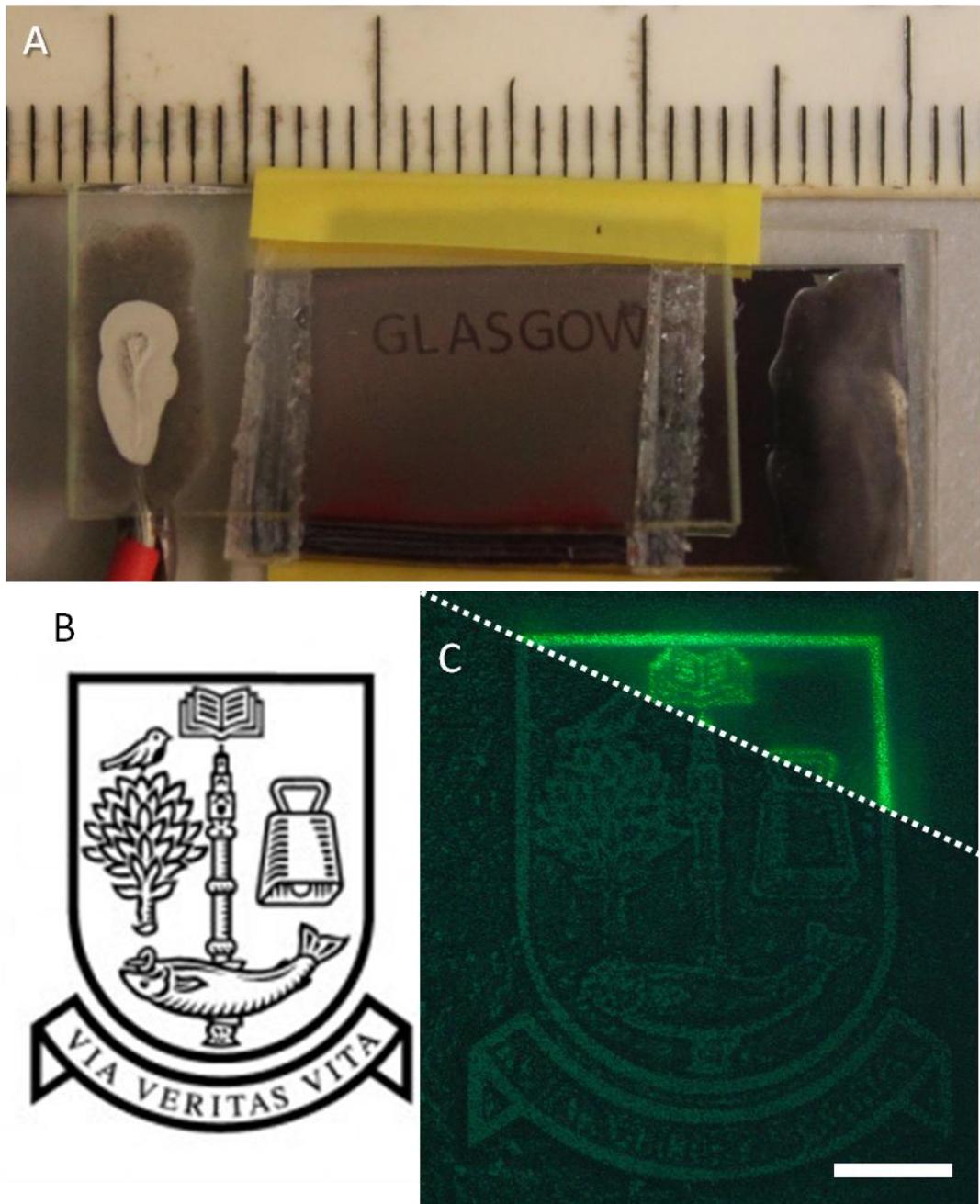
Figure 7-4: Example of massive parallel, large scale lysis of red blood cells using optoelectronic tweezers. A) Photograph of the word GLASGOW lysed into a film of human erythrocytes using a 4x objective. The total length of the word is over one cm and easily readable with the naked eye. B) Picture of the coat of arms of the University of Glasgow. C) Mircograph of the coat of arms being lysed into a film of RBCs. Top right corner shows the sample before the field has been applied, with just the illumination. The bottom of the picture shows the sample after the experiment without the illumination. Scale bar is 200 μm, total height of the lysed pattern is approximately 1 mm. Medium conductivity in both experiments was 100 ms/m with an AC bias of 10 kHz and 15 V$_{pk\text{-}pk}$.
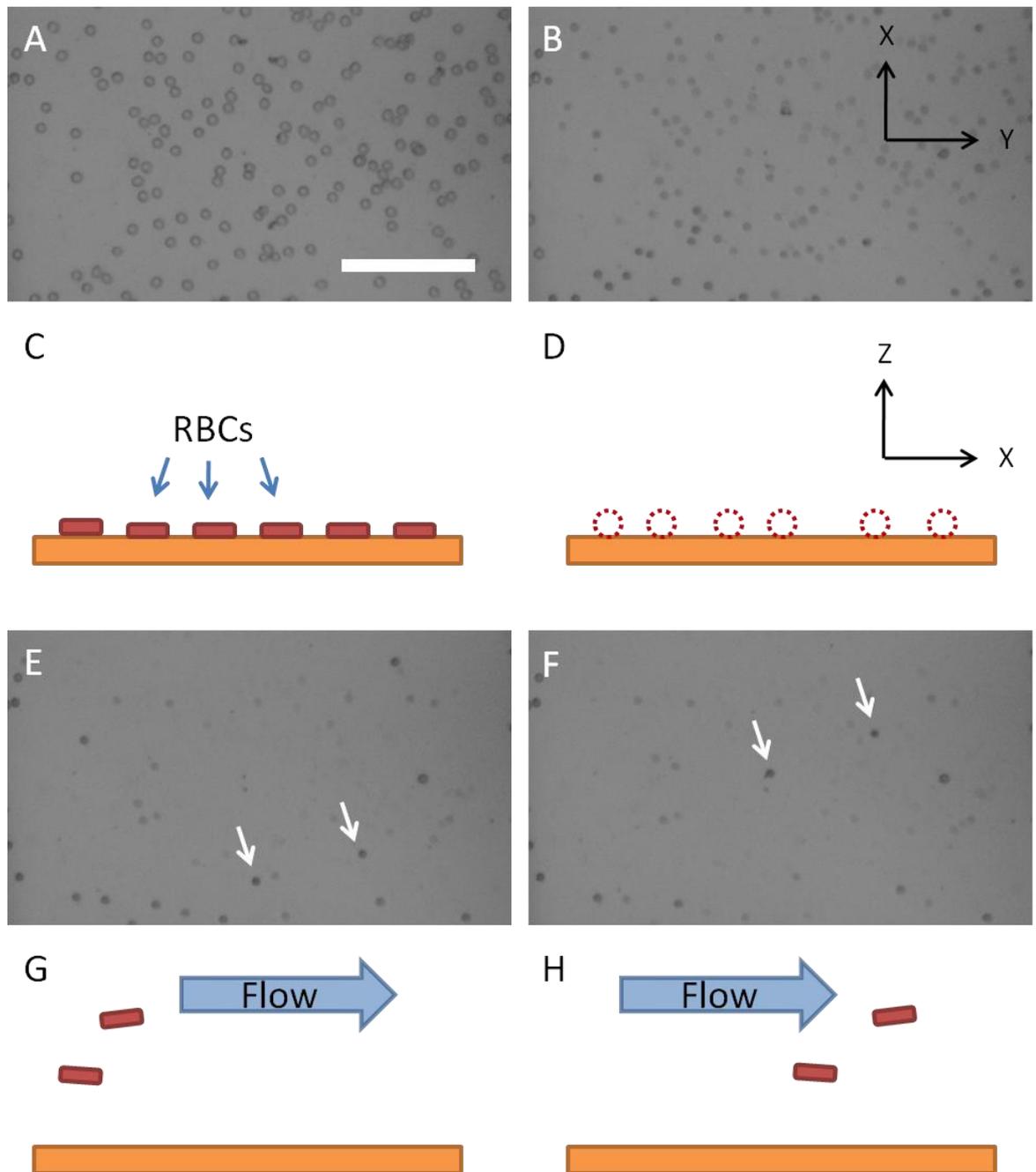
Figure 7-5: Experiment demonstrating the inability to lyse red blood cells that are not resting on the amorphous silicon surface. A) and B) show the lysis of erythrocytes that are resting on the bottom of the OET chamber (top down view). Scale bar is 100 μm. C) and D) show cartoons of a side view of the experiment. E) and F) show the same area after the RBCs have been lysed. Now additional blood cells were passed through the chamber using hydrodynamic flow. These cells were not lysed by the electric field. G) and H) show cartoons of the experiment. Medium conductivity was 100 mS/m with 10 kHz and 15 V$_{pk-pk}$.

Another important observation was the fact that the cells would not lyse when resting on a conductor, given the same conditions used to induce lysis in an OET device. Both metal electrodes, in the form of strips on a glass slide, and indium tin oxide electrodes, as a uniform layer on a glass slide, were used to demonstrate this (Figures 7-6 and 7-7). This observation can be attributed in

part to the fact that, for metal electrodes, the DEP forces were much higher. The reason for these higher forces is mostly due to the fact that the a:Si layer causes the amount of voltage dropped across the liquid to be reduced (when compared to metal electrodes). Thus, for metal electrodes, the cells undergo movement and are levitated away from the electrodes rather than being lysed.

This, however, does not account for all cells as some cells that remain resting on the electrodes were not lysed. No lysis was observed for cells on metal electrodes under certain conditions. It is possible to induce electrical lysis of cells using metal electrodes, but this requires different conditions (higher voltage) than those used to induce lysis with optoelectronic tweezers.

Another interesting observation was that the lysis of cells could be observed over a large range of medium conductivities. While for relatively low conductivities (100 mS/m and below) the voltage drop across the a:Si layer was relatively low (see Figure 6-3), as the conductivity of the medium increases however, so does the potential dropped across the a:Si layer. Lysis was even observed for cells suspended in pure PBS which has a conductivity of 1400 mS/m and was therefore about twice as conductive as the intracellular medium. As can be seen from Figure 6-3, the voltage drop across the medium in which the cells were suspended at these conditions was less than 0.5 volt, according to the simulations.

Lastly, for medium conductivities that are very low (less than 25 mS/m) no lysis was observed, since the cells experienced movement due to dielectrophoretic forces (see Figure 7-2 A and B). These forces were too weak to overcome the adhesion of the RBCs to the silicon surface at higher conductivities.
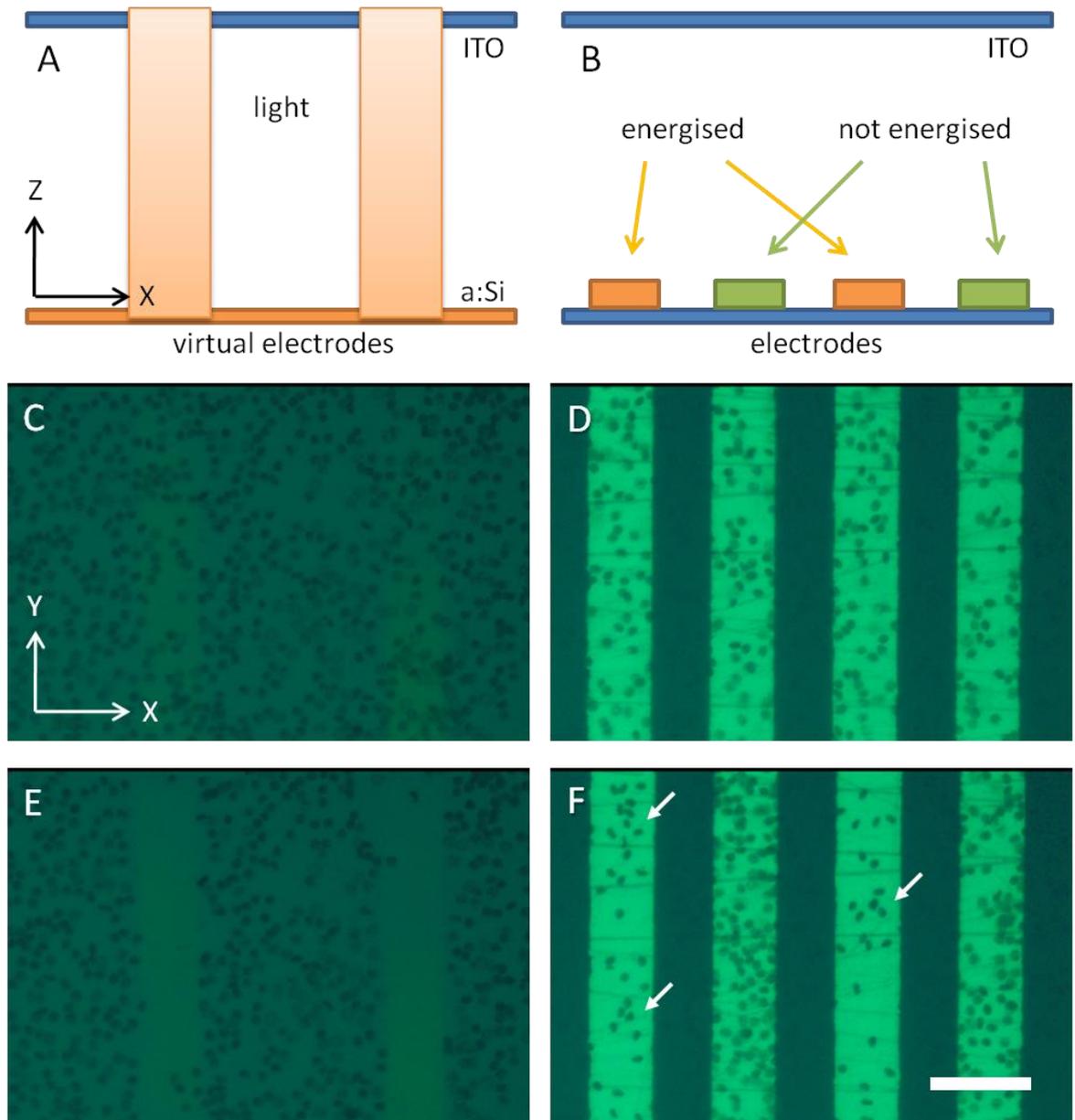
Figure 7-6: Comparison of metal electrodes and OET. A) Schematic of a cross section of the chamber. The two virtual electrodes (30 µm width) were created due to illumination from above, with the electric field going vertically through the chamber. B) Schematic of the metal electrodes used to mimic the conditions in A. While a set of interdigitated electrodes was used (same width as in A) only one set was energised (every other electrode). Instead of applying the potential across the different sets of electrodes at the bottom of the chamber, it was applied vertically across the chamber onto a glass cover coated in ITO. C) and E) show the lysis of human erythrocytes in the OET experiment. D) and F) show an experiment using the same conditions on metal electrodes. Instead of being lysed, some of the RBCs were moved due to DEP forces. The forces were stronger in this case as more voltage was dropped across the liquid. However, even the cells that stayed on the metal surface were not lysed (groups of cells are marked with arrows). Both experiments were performed with the same medium conductivity (100 mS/m) and AC bias (10 kHz, 15 $_{Vpk-pk}$). Scale bar is 50 µm.
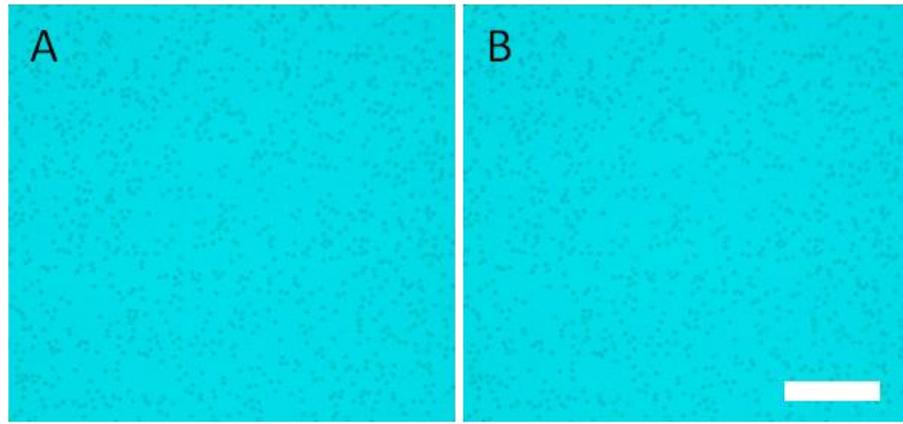
Figure 7-7: Control experiment with bare ITO electrodes. A) and B) show a sample of human blood, suspended in 100 mS/m medium, before and after being exposed to a 10 kHz, 15 V$_{pk-pk}$ AC bias for 30 minutes. No cell lysis was observed. Additional exposure of the cells to illumination patterns from the projector during the experiment did not change the results. Scale bar is 100 µm.

7.2.1 Selective lysis

An important observation that was made while mixing the RBCs with trypanosomes was that the lysis could also be selective. Only the red blood cells were lysed while the motile trypanosomes were not lysed (see Figure 7-8). The trypanosomes remained motile in some cases while in others they seemed to be killed by a short shock (the parasite was observed to undergo a rapid twitching motion and then remained non-motile). This shock seemed to occur only when the parasite was in or came into contact with the surface of the OET chip.
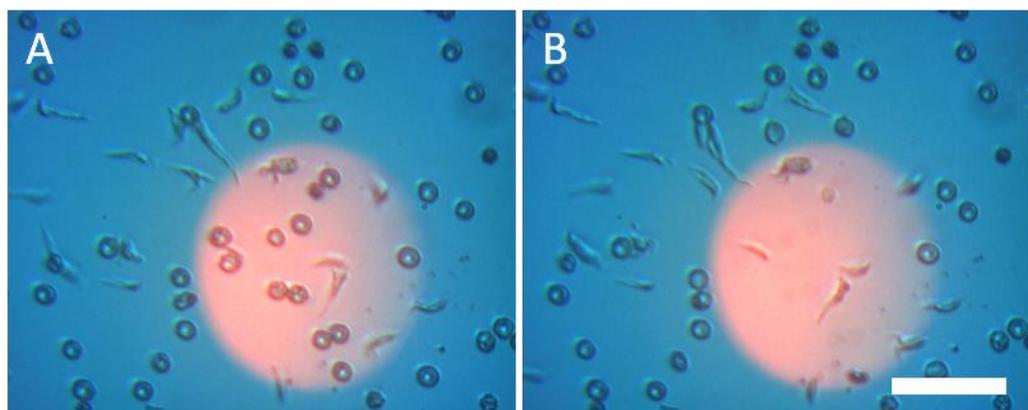
Figure 7-8: Selective electrically induced lysis. A) A mixture of human erythrocytes and trypanosomes (*T. cyclops*), suspended in 100 mS/m medium, just prior to being exposed to a 3 kHz, 14 V$_{pk-pk}$ AC bias. B) While the RBCs underwent lysis, the parasites remained motile and unharmed. Scale bar is 50 µm.

While the parasites were moving and thus not directly in contact with the a:Si, selective lysis was also observed for cells resting on the surface. Red blood cells could be lysed selectively from white blood cells. In Figure 7-9 it can be seen that the RBC (left) underwent sphering (change from a biconcave disk to a sphere) and then lysis while the WBC (right) remained unchanged, even minutes after the lysis of the erythrocyte. The video for Figure 7-9 was taken at 50X magnification, but the same selective lysis was observed for much larger areas containing hundreds of cells.
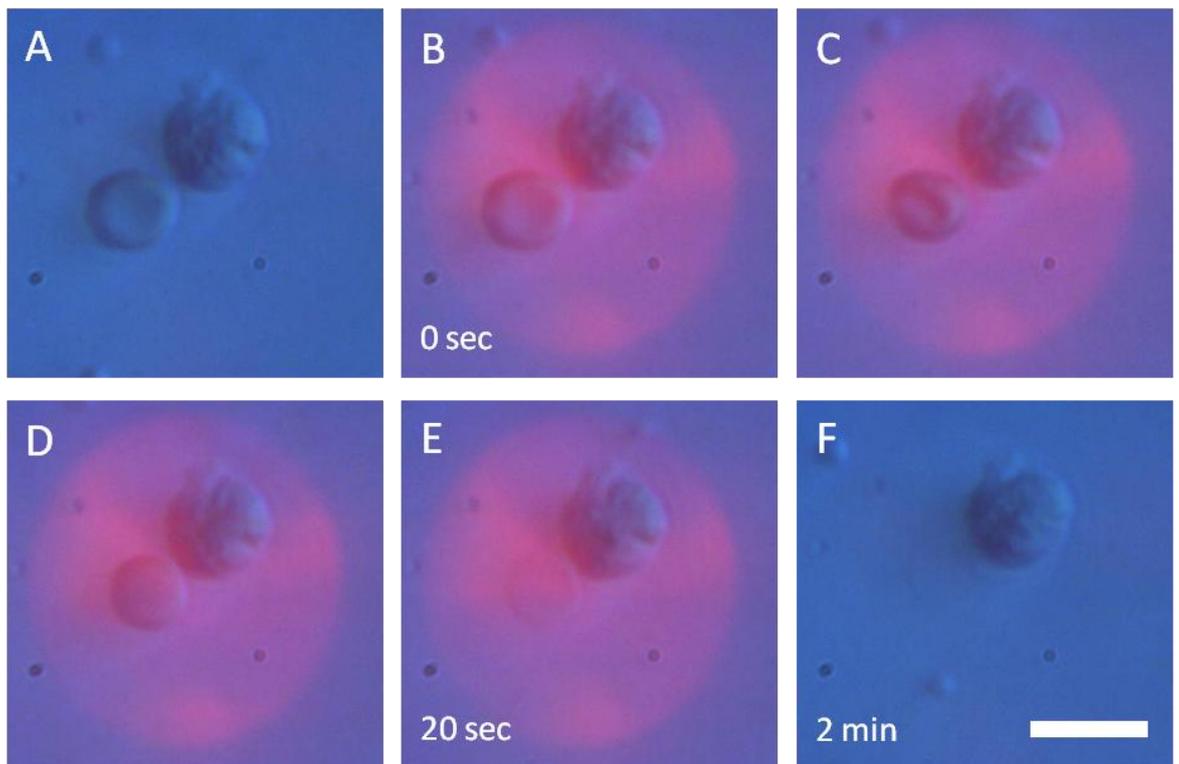
Figure 7-9: Example of selective electrically induced lysis of a red blood cell. A) Human erythrocyte and lymphocyte suspended in 100 mS/m buffer medium. B-E) show the cells after a 5 V_{pkp-pk}, 10 kHz AC bias has been applied. After 20 seconds the red blood cell has been lysed, while the white blood cell was unharmed. F) The WBC remained intact even after several minutes past the end of the experiment. Scale bar is 10 μm.

While it was impossible, with the setup used, to determine whether the WBC was viable through fluorescence, lysis of a leukocyte is usually easy to identify. As seen in Figure 7-10, the cell bursts open and the internal organelles can be seen spilling out of the cell. The remaining cell is clearly visible and a clear difference between a lysed and non-lysed WBC can be observed.
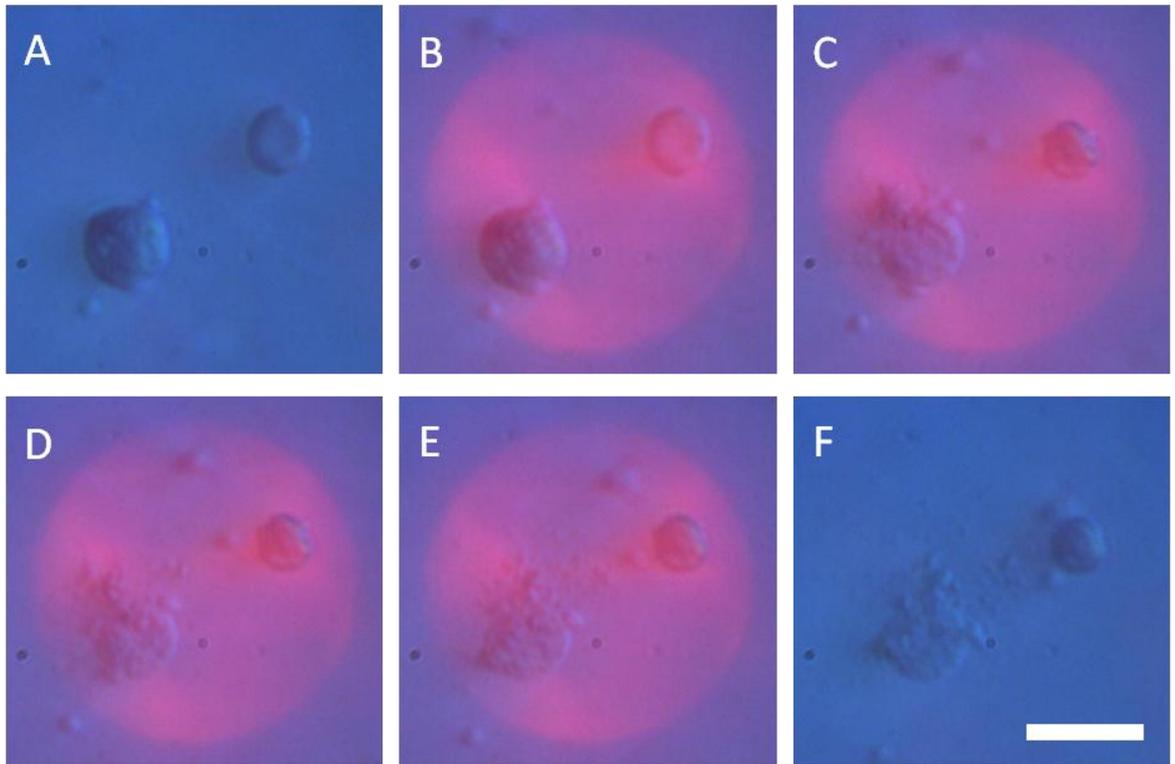
Figure 7-10: Lysis of a white blood cell for comparison. A) shows a human RBC and WBC under the same conditions as in Figure 7-9. B-F) show how in this example the application of an AC bias leads to the lysis and consequent destruction of the WBC. The cell is ruptured by the field and the intracellular content can be seen spilling out of the cell. This violent destruction of the cell is easy to differentiate visually from the result observed in Figure 7-9. Scale bar is 10 μm.

This selective lysis of smaller cells from a mixture with larger cells was not a result that would be expected from traditional electrically induced lysis (see Chapter 1).

To gain a better understanding of the observed phenomena, the percentage of lysed cells for a number of conductivities and frequencies was determined. Initially, these experiments were carried out at a relatively high magnification, using the setup shown in Figure 3-5. The data is presented in Figure 7-11. All videos were evaluated by manually counting the number of lysed cells.
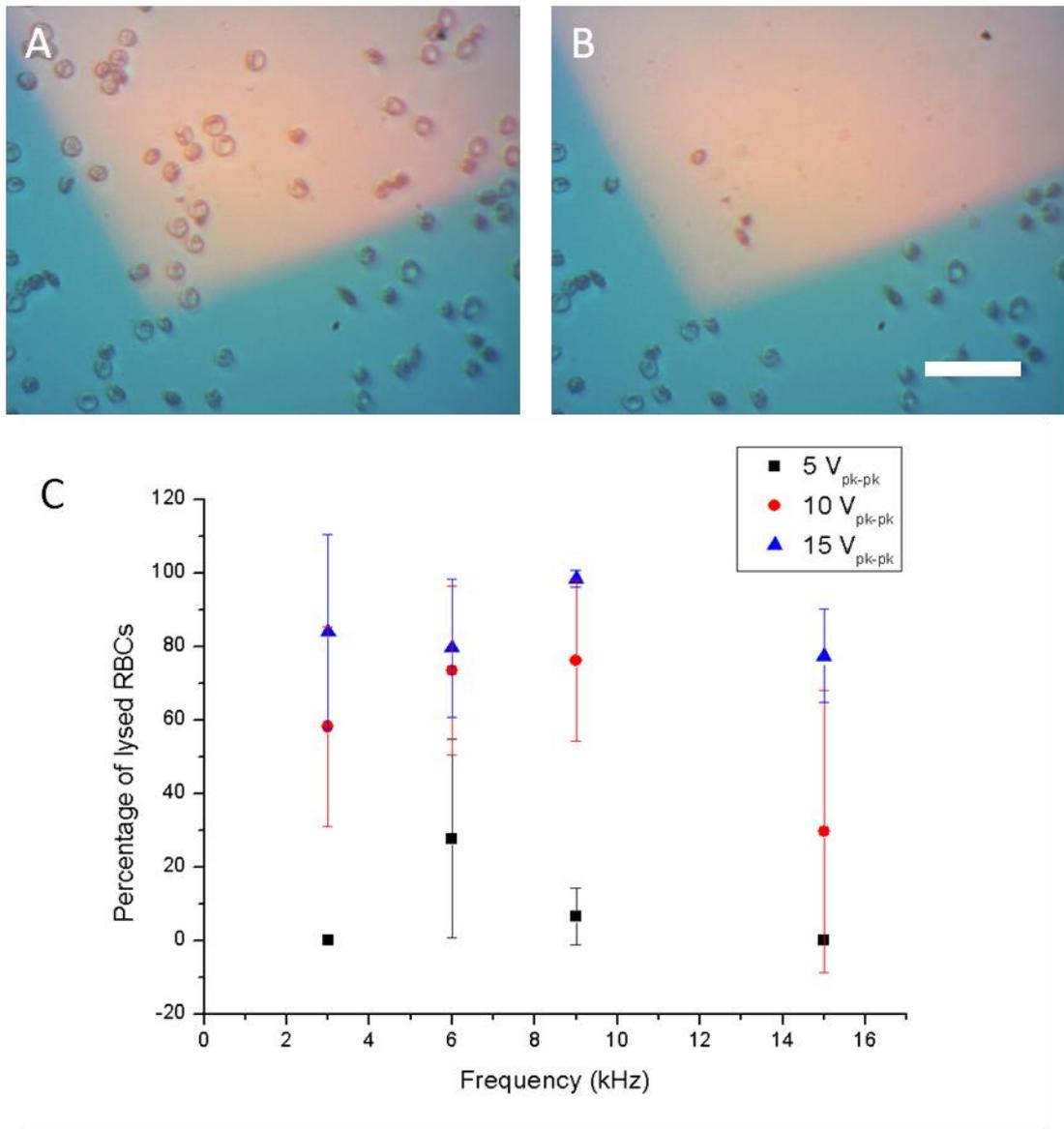
Figure 7-11: Early lysis experiments. A) and B) show a sample of human erythrocytes suspended at a medium conductivity of 100 mS/m before and after the application of a 9 kHz AC bias at 15 V$_{pk-pk}$. C) Early data of the percentage of lysed RBCs as a function of frequency for different voltages. Values are the average of 7 experiments, error is standard deviation. All experiments were performed at a medium conductivity of 100 mS/m using the experimental setup shown in Figure 2-5.

These initial values were variable, likely due in part to the lower number of cells per experiment and to the setup being used. Furthermore, DEP movement was observed more often in this setup than the Olympus setup used for later experiments (Figure 3-4). In Figure 7-11, the percentage of lysed RBCs is observed to decrease at lower frequencies because, for this evaluation, cells that underwent levitation or movement due to DEP were counted as not lysed. In later experiments, DEP forces were much less common and experiments where DEP was predominant were discarded entirely. It should be noted that, due to

the fact that a different projector was used and the optical path was different as well, the values for the TMP determined from the modelling are most likely not applicable in this case (the intensity used to determine the conductivity of the a:Si was measured for the other setup). The data confirmed however that in order to achieve complete lysis of the red blood cells, a potential of 15 volts should be used.

In order to gather reliable data about the percentage of lysed red blood cells, experiments were performed that involved large numbers of red blood cells (using the experimental setup shown in Figure 3-4).

Lysis of red blood cells was observed for different medium conductivities. For each conductivity a number of experiments was conducted to determine the percentage of lysed cells. A large light spot was created containing hundreds of red blood cells and an AC bias of a certain frequency was applied. As outlined in Chapter 3, the videos were evaluated using the Vision Assistant software to count the number of RBCs in the illuminated area before and after the experiment. Experiments where the cells were moved due to DEP were not used for this evaluation. For a medium conductivity of 100 mS/m, DEP was only rarely observed. In this case, the cells were left to settle for a few minutes in order to avoid their movement (the cells become attached to the surface). DEP was much more common at a conductivity of 25 mS/m and any instances where the cells moved were not used for the evaluation. For a medium conductivity of 1400 mS/m (pure PBS) no DEP forces were observed. Between experiments the chamber (Figure 3-6) was disassembled and thoroughly cleaned with 70% ethanol. This cleaning is essential as failure to do so creates areas with residue where no cells will lyse, regardless of frequency or conductivity. The data on the percentage of lysed red blood cells with regard to frequency and conductivity is presented in Figure 7-12.
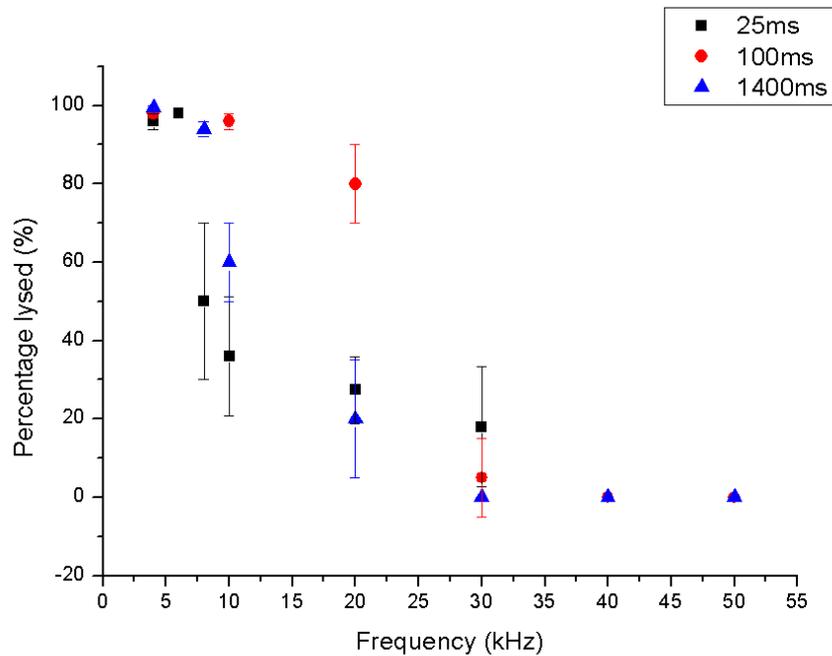
Figure 7-12: Percentage of lysed red blood cells in an OET chip as a function of frequency for 3 different conductivities. Each experiment contained hundreds of cells and at least 8 experiments were counted for each condition. Value is mean and error is standard deviation.

It can be seen that lysis was almost complete at low frequencies (below 10 kHz) regardless of medium conductivity. With higher frequency lysis became less successful and for values above 40 kHz no lysis was observed any more. While the response of cells at 25 mS/m and 1400 mS/m was very similar, the percentage of lysed RBCs stayed above 75 % for a much broader frequency range at 100 mS/m.

Another important factor to quantify was the selective lysis of WBCs and the observed enrichment of these rare cells from RBCs. In order to do this, a number of experiments were performed on a buffy coat sample that were washed and suspended in 100 mS/m buffer medium. In order to prepare a buffy coat, a blood sample is centrifuged at 2500 rpm for 10 minutes and the top layer containing the white blood cells is removed. In this way the concentration of WBCs in the sample is much increased. As outline above, the cells were counted out by hand before and after the experiment, since the software was unable to tell the difference between the two cell species.
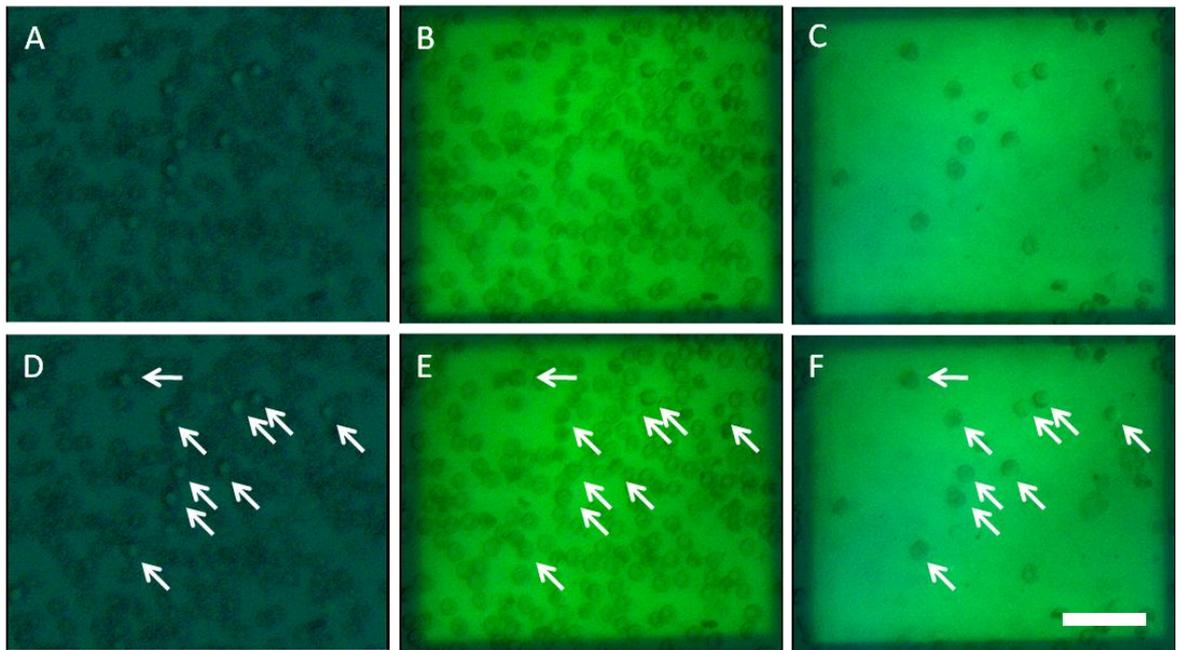
Figure 7-13: Example of selective lysis of RBCs from a mixture of red and white blood cells (medium conductivity of 100 mS/m). A) shows the cells being slightly out of focus. This way the white blood cells are visible as larger bright discs due to their larger spherical shape. B) and C) show 'in focus' images of the cells before and after the application of the AC bias (20 kHz, 15 V$_{pk-pk}$). D-F) show the same pictures but with arrows marking the position of the WBCs for clarity. Scale bar is 50 μm.

In order to identify the WBCs the sample was viewed slightly out of focus with the focal plane above the surface of the chamber (see Figure 7-13). This causes the WBCs to stand out from the RBCs as larger white spots and was used to identify them, since no fluorescence was available. The lysis of both RBCs and WBCs was recorded for different frequencies, but at 30 kHz and above, no lysis was observed. Comparison of this value to Figure 7-12 reveals a discrepancy since for 100 mS/m the reported percentage of lysed cells is not zero (albeit less than 10 percent). This can be attributed to two factors. While all other experiments were performed at a magnification of 10X, the experiments for selective lysis were done at a higher magnification of 20X. This magnification was chosen to make it easier to identify the leukocytes in the images. A change in magnification also changes the intensity of the light forming the electrodes and thus creates slightly different conditions during the experiment. Another factor is that, due to the lower magnification, the experiments for Figure 7-12 involved a higher number of cells. It is possible that with a higher number of repeats, lysis of cells might also be observed for 20X magnification at 30 kHz.

Results of the selective lysis experiments are presented in Figure 7-14. At a frequency of 10 kHz, the vast majority of RBCs were lysed, but the number of lysed WBCs is also significant (nearly 50%). At a frequency of 20 kHz, the number of lysed white blood cells was reduced to less than 20% while still lysing over 90% of RBCs. The enrichment can then be determined from the ratio of the two cell types before and after the experiment. An enrichment of more than 15-fold could be achieved for both 10 kHz and 20 kHz (see Figure 7-14 B).
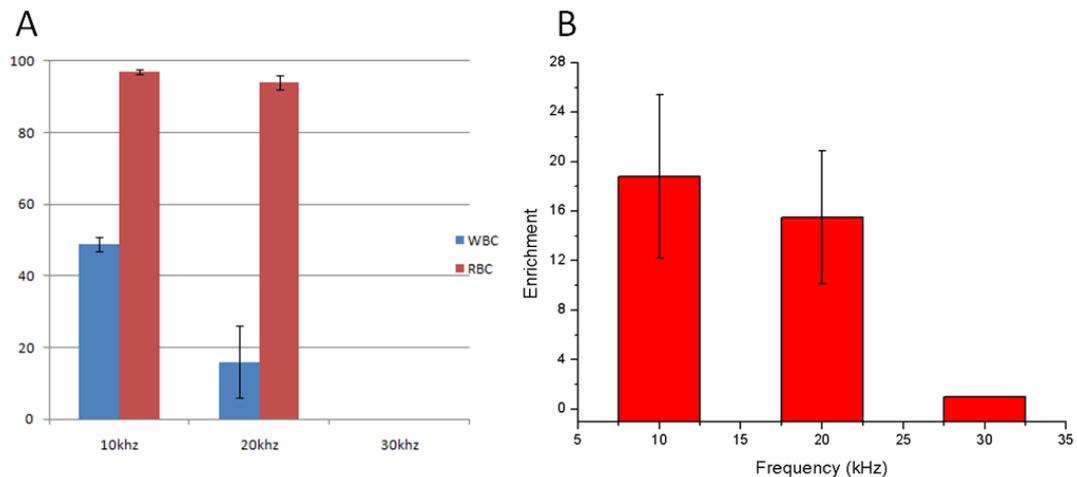
Figure 7-14: Selective lysis of red blood cells from white blood cells and WBC enrichment. A) Percentage of lysed red and white blood cells as a function of frequency. For 30 kHz no lysis was observed. B) Enrichment of WBCs for the same experiments. Each value is the average of six experiments with the error being standard deviation.

As was predicted by the model presented in Chapter 6, cells placed in a optoelectronic tweezers setup and exposed to a low frequency AC bias can undergo electrically induced cell lysis. The induced transmembrane potential exceeds a certain threshold value and the cell is irreversibly destroyed. The interesting predictions from the COMSOL simulations could be largely confirmed in the experiment. This includes selective lysis of cells based on shape rather than size as well as the inability to lyse cells resting on metal electrodes (under the same conditions that induce lysis in an OET setup).

7.3 Discussion

As was pointed out in Chapter 1, optoelectronic tweezers have been reported to induce lysis in cells [38]. However in previous work, this lysis was solely

attributed to the increased potential due to the electric field created by the virtual electrode. However, as has been described in this work, such a classic interpretation of the effect does not correspond with the observations presented here, especially the comparison to conventional electrodes made from conductive material, the frequency regime where the effect is observed and the fact that lysis was observed at very high medium conductivities. Most importantly, the classical model of induced TMP fails to explain the observed selective lysis of smaller from larger cells.

When comparing the experimental results to the modelling done in Chapter 6 it can be observed that the frequency at which the TMP increases in the model corresponds well with the frequency regime in which the number of lysed blood cells increases (see Figure 7-15).
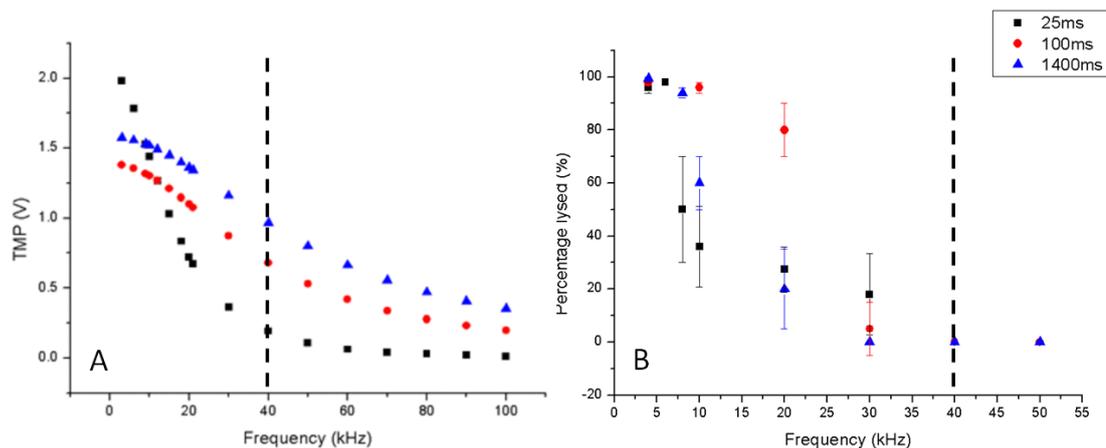
Figure 7-15: Side by side comparison of the induced transmembrane potential according to the simulations (A, also see Figure 6-11) and the experimentally observed lysis (B, also see Figure 7-12) for red blood cells suspended in different conductivity media. No lysis was observed at frequencies of 40 kHz or above and the frequency is marked for convenience in both graphs.

The observed selective lysis of smaller red blood cells from larger white blood cells is an interesting result. Traditionally larger cells experience a larger induced TMP. This would lead to larger cells being lysed under the conditions where smaller cells are lysed. Additionally, Bao *et al*. reported that the threshold voltage for irreversible electrical poration of WBCs was only 400 to 500 V/cm while the threshold for RBCs was 1100 – 1200 V/cm [100]. This makes it hard to explain the observed selective lysis using standard models. The results of

the modelling tie into these observations again, as the proposed electrical shadow effect explains the higher transmembrane potential on the red blood cells.

A particularly puzzling experimental observation was the fact that the lysis was readily observed in the OET setup but, given the same conditions, was absent when working with metal electrodes. This can also be attributed to the electrical shadow causing a larger TMP.

The modelling offers an explanation for the selective lysis in accordance with the observed phenomena. The cells do not lyse when lifted off the surface, as the effect of the shadow can only come to bear for cells resting closely on the substrate. Further, the absence of an electric shadow and the inability to effectively constrict the electric field in the case of a conductive surface can explain the observations made for metal electrodes. Another important observation is that the TMP is in the same order of magnitude, given low frequencies, for a range of medium conductivities (up to 1400 mS/m). Traditionally, electrical lysis would be hard to explain when the voltage drop across the liquid is only 0.5 volt.

It should be noted, however, that the simulations do not match the experimental observations quite as well as in the case of very high medium conductivities. The simulated TMP would suggest a gradual drop off in the percentage of lysed cells. While this observation could be confirmed for a conductivity of 100 mS/m, the behaviour for 1400 mS/m did not follow this pattern (see Figure 7-15). This could be due to an inaccuracy in the shape that was used to model the RBC resting on the surface or in the distance the latter having an especially large effect on the simulated TMP.

Chapter 8: Future Work

8.0 Abstract

In this Chapter the results of this work will be briefly summarised and suggested future work will be presented.

8.1 General Conclusions

The work presented in this thesis focuses on two main points, the enrichment of trypanosomes using TW-DEP and the selective lysis of red blood cells using OET. In both cases a model was presented and discussed that provides a possible explanation of the observed phenomena. For TW-DEP optimal enrichment conditions for mouse RBCs were determined, although human RBCs would require different conditions due to the increased cell size.

As pointed out in the discussion section of Chapter 5, TW-DEP proved to be a good tool to approach enrichment of trypanosomes from blood. The concentration into a small area at a single focal plane is highly advantageous for diagnostic purposes since it speeds up the confirmation of the parasites presence. The concentration technique can be combined with automated detection algorithms [89], which opens up the possibility of a fully automated system.

It is important to compare the technique to the current methods of detection for sleeping sickness. The gold standard for trypanosome detection (mini anion exchange columns) offers a limit of detection at the lowest levels found in the human host (10^2 parasites per ml of whole blood). The presented technique in its current form does not reach this level of sensitivity, but can still be improved upon with further optimisation. In principle, nothing prevents TW-DEP based detection from reaching the same limit of detection. However, it remains to be seen if the necessary tweaking of the technique will increase cost or complexity beyond what is feasible for field use. The cost of the technique is difficult to appraise or compare at this stage. The electrodes can be reused many times, however, provided they are adequately cleaned between experiments. Even the gold electrodes (which are more fragile and prone to scratching than electrodes made from other metals) could be reused dozens of times with careful cleaning.

TW-DEP can provide a much needed new approach to improve diagnostics for sleeping sickness. Although the technique as it is presented in this work is only a proof of principle, the potential exists to develop it further into a practical diagnostic tool.

In the case of selective lysis, the observed phenomenon is highly surprising. The model seems to suggest that an electric shadow is cast by the cell onto the a:Si layer and that this effect is the cause of the shape selective lysis of smaller cells form a population of larger cells.

In conclusion, the lysis of cells observed in optoelectronic tweezers offers a novel way to selectively destroy cells based on their shape. It can be applied to a large number of cells in parallel and enables the selection of rare cells within a sample containing a more abundant population. Of special note is that, unlike the manipulation with TW-DEP, selective lysis can be achieved at very high medium conductivities (negating the need for washing procedures). This technique, has the potential to facilitate downstream analysis of rare cells out of a complex population which could have significant implications (e.g. for cancer diagnostics). The technique also has the potential to be integrated with dielectrophoretic manipulation of living cells, the traditional application of optoelectronic tweezers.

8.2 Future work

Both techniques presented in this work have plenty of areas where one could 'drill deeper', both in terms of theoretical understanding and optimisation of experimental execution.

If the dielectric parameters of the trypanosome could be determined (e.g. through impedance measurements), the modelling could be refined and improved. Besides addressing up-scaling of the device, the sensitivity could also be improved upon. One way would be to use the fact that higher voltages lead to increased enrichment numbers and improved speed of the inward motion, though one would need to modify the central region of the spiral array to avoid lysis of the cells.

Additionally, the procedure could be modified to include an additional dielectrophoretic step in which the cells are just separated in height (opposing two-phase configuration for traditional DEP), before the TW-DEP force is applied. This simple, two step time course procedure would reduce the number of trypanosomes that escape the spiral due to their initial position or due to being displaced by outward moving erythrocytes. Consequently the sensitivity of the operation would increase and the need for up-scaling the device would be lessened. This small step would be able to be implemented without any additional instrumentation or sample preparation.

Furthermore the device could be improved with the aim of constructing a real functional prototype. A hole could be added in the central area of the array in order to remove the incoming trypanosomes and collect them at another part of the device. This way the lysis of the trypanosomes at the central spot could be prevented by placing the tips of the spiral arms further apart and consequently the TW-DEP enrichment could be run at higher voltages. This would in turn speed up the total enrichment (as the trypanosomes enter the central area faster) and increase the sensitivity further.

The OET experiments show interesting experimental results. It would certainly be interesting to further refine the selective lysis process and to extend it to other cell species. Another very interesting approach would be to attempt selective reversible electroporation. Besides the multitude of experimental options, it would be of great interest to further investigate the theoretical background of the observed phenomenon. While the current set of simulations offers a potential explanation, it would greatly benefit from further exploration. One of the most important factors for the current modelling is the shape of the cell and the exact distance of the cell from the surface. While difficult to implement experimentally (due to the opaque layer of amorphous silicon), these factors could be determined to improve future models.

Potential applications for the OET lysis technique might be the study of cells by opening up the intracellular medium for DNA testing. This could be combined with the study of adhesive vs. non adhesive cells in order to study intracellular processes that lead to adhesion.

Obviously the technique could also be applied to enrich rare cells possibly cancer cells from blood or other tissue. Changing the conditions during the experiment would allow for lysis of the cells of interest and combination with further downstream analysis (e.g. of DNA). Every time a new tool (like shape selective lysis) becomes available to researchers the possibilities of applying it in new constructive ways needs to be examined.

References

1. Hughes, M.P., *Nanoelectromechanics in engineering and biology*. Nano- and microscience, engineering, technology, and medicine series. 2003, Boca Raton: CRC Press. 322 p.
2. Jones, T.B., *Electromechanics of Particles* 1995, Cambridge, U.K.: Cambridge Univ. Press.
3. Pethig, R. and S. Smith, *Introductory bioelectronics : for engineers and physical scientists*. 2013, Chichester, West Sussex ; Hoboken: John Wiley & Sons. xvi, 441 p.
4. Turcu, I. and C.M. Lucaciu, *Dielectrophoresis: a spherical shell model*. J. Phys. A: Math. Gen., 1989. **22**.
5. Chung, C., M. Waterfall, S. Pells, A. Menachery, S. Smith, and R. Pethig, *Dielectrophoretic Characterisation of Mammalian Cells above 100 MHz*. J Electr Bioimp,, 2011. **2**.
6. Hagedorn, R., G. Fuhr, T. Muller, and J. Gimsa, *Traveling-wave dielectrophoresis of microparticles*. Electrophoresis, 1992. **13**(1-2): p. 49-54.
7. Wang, X.B., Y. Huang, F.F. Becker, and P.R. Gascoyne, *A unified theory of dielectrophoresis and travelling wave dielectrophoresis*. J. Phys. D: Appl. Phys. , 1994. **27**(7): p. 1571-1574.
8. Gascoyne, P., C. Mahidol, M. Ruchirawat, J. Satayavivad, P. Watcharasit, and F.F. Becker, *Microsample preparation by dielectrophoresis: isolation of malaria*. Lab Chip, 2002. **2**(2): p. 70-5.
9. Becker, F.F., X.-B. Wang, Y. Huang, R. Pethig, J. Vykoukal, and G.P.R. C., *The removal of human leukaemia cells from blood using interdigitated microelectrodes*. J. Phys. D: Appl. Phys., 1994. **27**.
10. Chiou, P.Y., A.T. Ohta, and M.C. Wu, *Massively parallel manipulation of single cells and microparticles using optical images*. Nature, 2005. **436**(7049): p. 370-2.
11. Pohl, H.A., *The Motion and Precipitation of Suspensoids in Divergent Electric Fields*. J. Appl. Phys. , 1951. **22**(7).
12. Pethig, R., *Review Article-Dielectrophoresis: Status of the theory, technology, and applications*. Biomicrofluidics, 2010. **4**(2).
13. Kim, U., C.W. Shu, K.Y. Dane, P.S. Daugherty, J.Y. Wang, and H.T. Soh, *Selection of mammalian cells based on their cell-cycle phase using dielectrophoresis*. Proc Natl Acad Sci U S A, 2007. **104**(52): p. 20708-12.
14. Ho, C.T., R.Z. Lin, W.Y. Chang, H.Y. Chang, and C.H. Liu, *Rapid heterogeneous liver-cell on-chip patterning via the enhanced field-induced dielectrophoresis trap*. Lab Chip, 2006. **6**(6): p. 724-34.
15. Vykoukal, J., D.M. Vykoukal, S. Freyberg, E.U. Alt, and P.R. Gascoyne, *Enrichment of putative stem cells from adipose tissue using dielectrophoretic field-flow fractionation*. Lab Chip, 2008. **8**(8): p. 1386-93.
16. Labeed, F.H., H.M. Coley, H. Thomas, and M.P. Hughes, *Assessment of multidrug resistance reversal using dielectrophoresis and flow cytometry*. Biophys J, 2003. **85**(3): p. 2028-34.
17. Wang, X.B., Y. Huang, X. Wang, F.F. Becker, and P.R. Gascoyne, *Dielectrophoretic manipulation of cells with spiral electrodes*. Biophys J, 1997. **72**(4): p. 1887-99.

18.   Goater, A.D., J.P.H. Burt, and R. Pethig, *A combined travelling wave dielectrophoresis and electrorotation device: applied to the concentration and viability determination of Cryptosporidium.* Journal of Physics D: Applied Physics, 1997. **30**(18).

19.   Pethig, R., M.S. Talary, and R.S. Lee, *Enhancing traveling-wave dielectrophoresis with signal superposition.* IEEE Eng Med Biol Mag, 2003. **22**(6): p. 43-50.

20.   Huang, J.T., G.C. Wang, K.M. Tseng, and S.B. Fang, *A chip for catching, separating, and transporting bio-particles with dielectrophoresis.* J Ind Microbiol Biotechnol, 2008. **35**(11): p. 1551-7.

21.   Hsu, H.Y., A.T. Ohta, P.Y. Chiou, A. Jamshidi, S.L. Neale, and M.C. Wu, *Phototransistor-based optoelectronic tweezers for dynamic cell manipulation in cell culture media.* Lab Chip, 2010. **10**(2): p. 165-72.

22.   Alberts, B., A. Johnson, J. Lewis, M. Raff, K. Roberts, and P. Walter, *Molecular Biology of the Cell, 4th edition.* 2002, New York: Garland Science.

23.   Tsong, T.Y., *Electroporation of cell membranes.* Biophys J, 1991. **60**(2): p. 297-306.

24.   Chen, C., S.W. Smye, M.P. Robinson, and J.A. Evans, *Membrane electroporation theories: a review.* Med Biol Eng Comput, 2006. **44**(1-2): p. 5-14.

25.   Ho, S.Y. and G.S. Mittal, *Electroporation of cell membranes: a review.* Crit Rev Biotechnol, 1996. **16**(4): p. 349-62.

26.   Pucihar, G., D. Miklavcic, and T. Kotnik, *A time-dependent numerical model of transmembrane voltage inducement and electroporation of irregularly shaped cells.* IEEE Trans Biomed Eng, 2009. **56**(5): p. 1491-501.

27.   Grosse, C. and H.P. Schwan, *Cellular membrane potentials induced by alternating fields.* Biophys J, 1992. **63**(6): p. 1632-42.

28.   Gehl, J., *Electroporation: theory and methods, perspectives for drug delivery, gene therapy and research.* Acta Physiol Scand, 2003. **177**(4): p. 437-47.

29.   Zimmermann, U., G. Pilwat, C. Holzapfel, and K. Rosenheck, *Electrical hemolysis of human and bovine red blood cells.* J Membr Biol, 1976. **30**(2): p. 135-52.

30.   Kotnik, T. and D. Miklavcic, *Analytical description of transmembrane voltage induced by electric fields on spheroidal cells.* Biophys J, 2000. **79**(2): p. 670-9.

31.   Mahalanabis, M., H. Al-Muayad, M.D. Kulinski, D. Altman, and C.M. Klapperich, *Cell lysis and DNA extraction of gram-positive and gram-negative bacteria from whole blood in a disposable microfluidic chip.* Lab Chip, 2009. **9**(19): p. 2811-7.

32.   Vandeventer, P.E., K.M. Weigel, J. Salazar, B. Erwin, B. Irvine, R. Doebler, A. Nadim, G.A. Cangelosi, and A. Niemz, *Mechanical disruption of lysis-resistant bacterial cells by use of a miniature, low-power, disposable device.* J Clin Microbiol, 2011. **49**(7): p. 2533-9.

33.   Zarling, J.M., P.A. Moran, L.S. Grosmaire, J. McClure, K. Shriver, and J.A. Ledbetter, *Lysis of cells infected with HIV-1 by human lymphocytes targeted with monoclonal antibody heteroconjugates.* J Immunol, 1988. **140**(8): p. 2609-13.

34.   Nederberg, F., Y. Zhang, J.P. Tan, K. Xu, H. Wang, C. Yang, S. Gao, X.D. Guo, K. Fukushima, L. Li, J.L. Hedrick, and Y.Y. Yang, *Biodegradable nanostructures with selective lysis of microbial membranes.* Nat Chem, 2011. **3**(5): p. 409-14.

35. Parekkadan, B., P. Sethu, D. van Poll, M.L. Yarmush, and M. Toner, *Osmotic selection of human mesenchymal stem/progenitor cells from umbilical cord blood.* Tissue Eng, 2007. **13**(10): p. 2465-73.

36. Bae, C. and P.J. Butler, *Automated single-cell electroporation.* Biotechniques, 2006. **41**(4): p. 399-400, 402.

37. Lai, H.H., P.A. Quinto-Su, C.E. Sims, M. Bachman, G.P. Li, V. Venugopalan, and N.L. Allbritton, *Characterization and use of laser-based lysis for cell analysis on-chip.* J R Soc Interface, 2008. **5 Suppl 2**: p. S113-21.

38. Valley, J.K., S. Neale, H.Y. Hsu, A.T. Ohta, A. Jamshidi, and M.C. Wu, *Parallel single-cell light-induced electroporation and dielectrophoretic manipulation.* Lab Chip, 2009. **9**(12): p. 1714-20.

39. Lin, Y.-H. and G.-B. Lee, *An optically induced cell lysis device using dielectrophoresis.* Appl. Phys. Lett., 2009. **94**.

40. Coster, H.G., *A quantitative analysis of the voltage-current relationships of fixed charge membranes and the associated property of "punch-through".* Biophys J, 1965. **5**(5): p. 669-86.

41. Coster, H.G., *Discovery of "punch-through" or membrane electrical breakdown and electroporation.* Eur Biophys J, 2009. **39**(1): p. 185-9.

42. Pauly, H. and H.P. Schwan, *[Impendance of a suspension of ball-shaped particles with a shell; a model for the dielectric behavior of cell suspensions and protein solutions].* Z Naturforsch B, 1959. **14B**(2): p. 125-31.

43. Marszalek, P., D.S. Liu, and T.Y. Tsong, *Schwan equation and transmembrane potential induced by alternating electric field.* Biophys J, 1990. **58**(4): p. 1053-8.

44. Gimsa, J. and D. Wachner, *Analytical description of the transmembrane voltage induced on arbitrarily oriented ellipsoidal and cylindrical cells.* Biophysical Journal, 2001. **81**(4): p. 1888-1896.

45. Barrett, M.P., R.J. Burchmore, A. Stich, J.O. Lazzari, A.C. Frasch, J.J. Cazzulo, and S. Krishna, *The trypanosomiases.* Lancet, 2003. **362**(9394): p. 1469-80.

46. Brun, R., J. Blum, F. Chappuis, and C. Burri, *Human African trypanosomiasis.* Lancet, 2010. **375**(9709): p. 148-59.

47. Barrett, M.P., D.W. Boykin, R. Brun, and R.R. Tidwell, *Human African trypanosomiasis: pharmacological re-engagement with a neglected disease.* Br J Pharmacol, 2007. **152**(8): p. 1155-71.

48. Stich, A., P.M. Abel, and S. Krishna, *Human African trypanosomiasis.* BMJ, 2002. **325**(7357): p. 203-6.

49. Steverding, D., *The history of African trypanosomiasis.* Parasit Vectors, 2008. **1**(1): p. 3.

50. Schlitzer, M., *[Agents for the treatment of African sleeping sickness. Those developed in the last century].* Pharm Unserer Zeit, 2009. **38**(6): p. 552-8.

51. Chappuis, F., L. Loutan, P. Simarro, V. Lejon, and P. Buscher, *Options for field diagnosis of human african trypanosomiasis.* Clin Microbiol Rev, 2005. **18**(1): p. 133-46.

52. WHO. *Human African Trypanosomiasis: Number of new reported cases (T.b. gambiense) by country.* 2012 7.6.2013]; Available from: http://apps.who.int/gho/data/node.main.A1636.

53. WHO_Media_Centre, *Trypanosomiasis, Human Africa (sleeping sickness) - Fact Sheet N°259.* 2012.

54.   Pepin, J. and H.A. Meda, *The epidemiology and control of human African trypanosomiasis.* Adv Parasitol, 2001. **49**: p. 71-132.

55.   Vanhollebeke, B. and E. Pays, *The trypanolytic factor of human serum: many ways to enter the parasite, a single way to kill.* Mol Microbiol, 2010. **76**(4): p. 806-14.

56.   Stich, A., M.P. Barrett, and S. Krishna, *Waking up to sleeping sickness.* Trends Parasitol, 2003. **19**(5): p. 195-7.

57.   Cecchi, G., F. Courtin, M. Paone, A. Diarra, J.R. Franco, R.C. Mattioli, and P.P. Simarro, *Mapping sleeping sickness in Western Africa in a context of demographic transition and climate change.* Parasite, 2009. **16**(2): p. 99-106.

58.   Njiokou, F., C. Laveissiere, G. Simo, S. Nkinin, P. Grebaut, G. Cuny, and S. Herder, *Wild fauna as a probable animal reservoir for Trypanosoma brucei gambiense in Cameroon.* Infect Genet Evol, 2006. **6**(2): p. 147-53.

59.   Welburn, S.C., K. Picozzi, E.M. Fevre, P.G. Coleman, M. Odiit, M. Carrington, and I. Maudlin, *Identification of human-infective trypanosomes in animal reservoir of sleeping sickness in Uganda by means of serum-resistance-associated (SRA) gene.* Lancet, 2001. **358**(9298): p. 2017-9.

60.   Sharma, R., E. Gluenz, L. Peacock, W. Gibson, K. Gull, and M. Carrington, *The heart of darkness: growth and form of Trypanosoma brucei in the tsetse fly.* Trends Parasitol, 2009. **25**(11): p. 517-24.

61.   Abubakar, L.U., W.D. Bulimo, F.J. Mulaa, and E.O. Osir, *Molecular characterization of a tsetse fly midgut proteolytic lectin that mediates differentiation of African trypanosomes.* Insect Biochem Mol Biol, 2006. **36**(4): p. 344-52.

62.   Masocha, W., M.E. Rottenberg, and K. Kristensson, *Migration of African trypanosomes across the blood-brain barrier.* Physiol Behav, 2007. **92**(1-2): p. 110-4.

63.   Stich, A., *[African sleeping sickness. An ancient threat returns].* Pharm Unserer Zeit, 2009. **38**(6): p. 546-50.

64.   [cited 2013 4.3.2013]; Available from: httpwww.accuratereloading.com/hr20071.html.

65.   Pays, E., *The variant surface glycoprotein as a tool for adaptation in African trypanosomes.* Microbes Infect, 2006. **8**(3): p. 930-7.

66.   Taylor, J.E. and G. Rudenko, *Switching trypanosome coats: what's in the wardrobe?* Trends Genet, 2006. **22**(11): p. 614-20.

67.   Engstler, M., T. Pfohl, S. Herminghaus, M. Boshart, G. Wiegertjes, N. Heddergott, and P. Overath, *Hydrodynamic flow-mediated protein sorting on the cell surface of trypanosomes.* Cell, 2007. **131**(3): p. 505-15.

68.   Magez, S. and M. Radwanska, *African trypanosomiasis and antibodies: implications for vaccination, therapy and diagnosis.* Future Microbiol, 2009. **4**: p. 1075-87.

69.   Welburn, S.C., I. Maudlin, and P.P. Simarro, *Controlling sleeping sickness - a review.* Parasitology, 2009. **136**(14): p. 1943-9.

70.   Tshimungu, K., B.B. Kalambayi, M. Kiyombo, L.N. Okenge, and P.D. Mol, *Knowledge, behaviours, practices and beliefs regarding Human African Trypanosomiasis (HAT) among inhabitants of Kinshasa (Democratic Republic of Congo).* Sante, 2008. **18**(3): p. 141-7.

71.   Kennedy, P.G., *Human African trypanosomiasis-neurological aspects.* J Neurol, 2006. **253**(4): p. 411-6.

72.   Magnus, E., T. Vervoort, and N. Van Meirvenne, *A card-agglutination test with stained trypanosomes (C.A.T.T.) for the serological diagnosis of T.*

B. gambiense trypanosomiasis. Ann Soc Belg Med Trop, 1978. **58**(3): p. 169-76.

73. Magnus, E., N. Van Meirvenne, T. Vervoort, D. Le Ray, and M. Wery, *Use of freeze-dried trypanosomes in the indirect fluorescent antibody test for the serodiagnosis of sleeping sickness.* Ann Soc Belg Med Trop, 1978. **58**(2): p. 103-9.

74. Noireau, F., J.P. Gouteux, and J.P. Duteurtre, *[Diagnostic value of a card agglutination test (Testryp CATT) in the mass screening of human trypanosomiasis in the Congo].* Bull Soc Pathol Exot Filiales, 1987. **80**(5): p. 797-803.

75. WHO, *Trypanosomiasis control manual.* 1983, Geneva, Switzerland: World Health Organization.

76. Souto-Padron, T., *The surface charge of trypanosomatids.* An Acad Bras Cienc, 2002. **74**(4): p. 649-75.

77. Lumsden, W.H., C.D. Kimber, and M. Strange, *Trypanosoma brucei: detection of low parasitaemias in mice by a miniature anion-exchanger/centrifugation technique.* Trans R Soc Trop Med Hyg, 1977. **71**(5): p. 421-4.

78. Lumsden, W.H., C.D. Kimber, D.A. Evans, and S.J. Doig, *Trypanosoma brucei: Miniature anion-exchange centrifugation technique for detection of low parasitaemias: Adaptation for field use.* Trans R Soc Trop Med Hyg, 1979. **73**(3): p. 312-7.

79. Sachs, R., *The superiority of the miniature Anion-Exchange Centrifugation Technique for detecting low grade trypanosome parasitaemias.* Trans R Soc Trop Med Hyg, 1984. **78**(5): p. 694-6.

80. FIND.   [cited 2013 7.6.2013]; Available from: http://www.finddiagnostics.org/.

81. Asonganyi, T., F. Doua, S.N. Kibona, Y.M. Nyasulu, R. Masake, and F. Kuzoe, *A multi-centre evaluation of the card indirect agglutination test for trypanosomiasis (TrypTect CIATT).* Ann Trop Med Parasitol, 1998. **92**(8): p. 837-44.

82. Holm, S.H., J.P. Beech, M.P. Barrett, and J.O. Tegenfeldt, *Separation of parasites from human blood using deterministic lateral displacement.* Lab Chip, 2011. **11**(7): p. 1326-32.

83. Njiru, Z.K., A.S. Mikosza, E. Matovu, J.C. Enyaru, J.O. Ouma, S.N. Kibona, R.C. Thompson, and J.M. Ndung'u, *African trypanosomiasis: sensitive and rapid detection of the sub-genus Trypanozoon by loop-mediated isothermal amplification (LAMP) of parasite DNA.* Int J Parasitol, 2008. **38**(5): p. 589-99.

84. Menachery, A. and R. Pethig, *Controlling cell destruction using dielectrophoretic forces.* IEE Proc.-Nanobiotechnol., 2005. **152**(4).

85. Huang, Y., R. Holzel, R. Pethig, and X.B. Wang, *Differences in the AC electrodynamics of viable and non-viable yeast cells determined through combined dielectrophoresis and electrorotation studies.* Phys Med Biol, 1992. **37**(7): p. 1499-517.

86. Gimsa, J., *A comprehensive approach to electro-orientation, electrodeformation, dielectrophoresis, and electrorotation of ellipsoidal particles and biological cells.* Bioelectrochemistry, 2001. **54**(1): p. 23-31.

87. Pethig, R., L.M. Jakubek, R.H. Sanger, E. Heart, E.D. Corson, and P.J. Smith, *Electrokinetic measurements of membrane capacitance and conductance for pancreatic beta-cells.* IEE Proc Nanobiotechnol, 2005. **152**(6): p. 189-93.

88.   Green, N.G., A. Ramos, and H. Morgan, *Numerical solution of the dielectrophoretic and travelling wave forces for interdigitated electrode arrays using the finite element method.* Journal of Electrostatics 2002. **56**(2): p. 235-254.

89.   Menachery, A., C. Kremer, P.E. Wong, A. Carlsson, S.L. Neale, M.P. Barrett, and J.M. Cooper, *Counterflow dielectrophoresis for trypanosome enrichment and detection in blood.* Sci Rep, 2012. **2**: p. 775.

90.   Asami, K., Y. Takahashi, and S. Takashima, *Dielectric properties of mouse lymphocytes and erythrocytes.* Biochim Biophys Acta, 1989. **1010**(1): p. 49-55.

91.   Pauly, H. and H.P. Schwan, *Dielectric properties and ion mobility in erythrocytes.* Biophys J, 1966. **6**(5): p. 621-39.

92.   Gimsa, J., T. Schnelle, G. Zechel, and R. Glaser, *Dielectric spectroscopy of human erythrocytes: investigations under the influence of nystatin.* Biophys J, 1994. **66**(4): p. 1244-53.

93.   Rodriguez, J.A., M.A. Lopez, M.C. Thayer, Y. Zhao, M. Oberholzer, D.D. Chang, N.K. Kisalu, M.L. Penichet, G. Helguera, R. Bruinsma, K.L. Hill, and J. Miao, *Propulsion of African trypanosomes is driven by bihelical waves with alternating chirality separated by kinks.* Proc Natl Acad Sci U S A, 2009. **106**(46): p. 19322-7.

94.   Valley, J.K., A. Jamshidi, A.T. Ohta, H.Y. Hsu, and M.C. Wu, *Operational Regimes and Physics Present in Optoelectronic Tweezers.* J Microelectromech Syst, 2008. **17**(2): p. 342-350.

95.   Canham, P.B., *The Minimum Energy of Bending as a Possible Explanation of the Biconcave Shape of the Human Red Blood Cell.* J. Theoret. Biol., 1970. **26**.

96.   Fischer, T.M., *Shape memory of human red blood cells.* Biophys J, 2004. **86**(5): p. 3304-13.

97.   Gingell, D. and I. Todd, *Red blood cell adhesion. II. Interferometric examination of the interaction with hydrocarbon oil and glass.* J Cell Sci, 1980. **41**: p. 135-49.

98.   Trommler, A., D. Gingell, and H. Wolf, *Red blood cells experience electrostatic repulsion but make molecular adhesions with glass.* Biophys J, 1985. **48**(5): p. 835-41.

99.   Gimsa, J., T. Muller, T. Schnelle, and G. Fuhr, *Dielectric spectroscopy of single human erythrocytes at physiological ionic strength: dispersion of the cytoplasm.* Biophys J, 1996. **71**(1): p. 495-506.

100.   Bao, N., T.T. Le, J.X. Cheng, and C. Lu, *Microfluidic electroporation of tumor and blood cells: observation of nucleus expansion and implications on selective analysis and purging of circulating tumor cells.* Integr Biol (Camb), 2010. **2**(2-3): p. 113-20.

101.   Wang, H.Y., A.K. Bhunia, and C. Lu, *A microfluidic flow-through device for high throughput electrical lysis of bacterial cells based on continuous dc voltage.* Biosens Bioelectron, 2006. **22**(5): p. 582-8.

102.   Techaumnat, B., K. Tsuda, O. Kurosawa, G. Murat, H. Oana, and M. Washizu, *High-yield electrofusion of biological cells based on field tailoring by microfabricated structures.* IET Nanobiotechnol, 2008. **2**(4): p. 93-9.

103.   Chang, D.C. and T.S. Reese, *Changes in membrane structure induced by electroporation as revealed by rapid-freezing electron microscopy.* Biophys J, 1990. **58**.

Appendix

HM1 - 9 Medium, Recipe

Components	g/L
CaCl2	0.165
KCl	0.33
KNO3	0.000076
MgSO4	0.098
NaCl	4.5
NaHCO3	3.020
NaH2PO4.H2O	0.125
Na2SeO3.5H2O	0.000017
Glucose	4.5
Phenol Red	0.015
HEPES	5.960
Mercaptoethanol	0.015
Bathocuproine disulfonate.Na2	0.028
DL-alanine	0.025
L-arginine.HCl	0.084
L-asparagine. H2O	0.025
L-aspartic acid	0.030
L-cysteine	0.182
L-cystine	0.091
L-glutamic acid	0.075
L-glutamine	0.584
glycine	0.030
L-histidine.HCl.H2O	0.042
DL-isoleucine	0.105
L-leucine	0.105
L-lysine.HCl	0.146
DL-methionine	0.030
L-phenylalanine	0.066
L-proline	0.040
DL-serine	0.042
DL-threonine	0.095
L-tryptophane	0.016
L-tyrosine	0.104
DL-valine	0.094
B12	0.000013
Biotin	0.000013
D-Ca pantothenate	0.004
Choline chloride	0.004
Folic acid	0.004
i-Inositol	0.0072
Niacinamide	0.004
Pyridoxal HCl	0.004
Riboflavin	0.0004

Cunninghams Medium, Recipe

Components	g/L
$CaCl_2.2 H_2O$	0.15
KCl	2.98
$NaH_2PO_4.H_2O$	0.53
$MgSO_4.7 H_2O$	3.7
$MgCl_2.6 H_2O$	3.04
Glucose	0.7
D-Fructose	0.4
Sucrose	0.4
Phenol Red	0.015
β-alanine	2
DL-alanine	1.09
L-arginine.HCl	0.44
L-asparagine. H2O	0.024
L-aspartic acid	0.11
L-cysteine	0.08
L-cystine	0.03
L-glutamic acid	0.25
L-glutamine	1.64
glycine	0.12
L-histidine	0.16
DL-isoleucine	0.09
L-leucine	0.09
L-lysine	0.15
DL-methionine	0.20
L-phenylalanine	0.20
L-proline	6.90
DL-serine	0.20
DL-threonine	0.10
L-tryptophane	0.10
L-tyrosine	0.20
DL-valine	0.21
BME vitamins (100X)	2 mL
Pyruvate Na	0.114
L-malic	0.67
α-ketoglutaric	0.37
Fumaric	0.055
Succinic	0.06
Cis-aconitic acid	0.522

Publications resulting from this work

Journal Publications:

Menachery, A., C. Kremer, P.E. Wong, A. Carlsson, S.L. Neale, M.P. Barrett, and J.M. Cooper, *Counterflow dielectrophoresis for trypanosome enrichment and detection in blood.* Sci Rep, 2012. **2**: p. 775.

Shape-Dependent Cell lysis . Clemens Kremer, Christian Witte, Steven L. Neale, Julien Rebound, Michael P. Barrett , Jonathan M. Cooper ; Angewandte Chemie – 2014 Accepted for publication

Conference Publications:

25 – 29 June 2012
Kenya Workshop, Nairobi Institute of Primate Research, Nairobi, Kenya
Oral presentation: *Developing Diagnostics for the Developing World*

21 – 26 January 2012
SPIE Photonics West 2012, Moscone Center, San Francisco, USA
Oral presentation: *Optoelectronic tweezers for medical diagnostics*

7. November 2011
Changing the World: A conference for early career researchers, University of Glasgow, Glasgow, UK
Oral presentation: *Diagnostics for sleeping sickness*

14 – 16 August 2011
IEEE EMBS PGBiomed-2011, IET Teacher Building, Glasgow, UK
Oral presentation: *Improved diagnostics for Human African Trypanosomiasis*